# SYNTHESIS AND CHARACTERIZATION OF LOW-DIMENSIONAL MOLECULAR MAGNETIC MATERIALS

By

CHEN LIU

A DISSERTATION PRESENTED TO THE GRADUATE SCHOOL
OF THE UNIVERSITY OF FLORIDA IN PARTIAL FULFILLMENT
OF THE REQUIREMENTS FOR THE DEGREE OF
DOCTOR OF PHILOSOPHY

UNIVERSITY OF FLORIDA

2004

Copyright 2004

by

Chen Liu

To my parents, my sister, and my grandmother.

ACKNOWLEDGMENTS

The research presented in this dissertation is the result of the collaboration of many diligent individuals. Among them, I would like to thank my research advisor, Professor Daniel R. Talham. Dr. Talham is an excellent researcher, mentor, and a great person to work with. I am very grateful to Dr. Talham for accepting me into his group and I am very fortunate to have the opportunity to learn from him. During the course of my research, Dr. Talham has taught me how to define and thoughtfully formulate an approach to solve problems, which has deeply influenced me. I thank Dr. Talham for his encouragement, support, and exceptional guidance both in my research and in my personal development. I am also thankful to Professor Mark Meisel and his graduate students Ju-Hyun Park, Diktys Stratakis; and to postdoctoral fellow Dr. Erik Cizmar in the Physics Department for performing all the magnetic measurements and discussing magnetic data. Ju-Hyun and Erik are wonderful colleagues and I greatly appreciate their work. I would very much like to express my gratitude to Dr. Khalil Abboud and the students working in his lab, Alex Oblezov and Bob Shelton, for characterizing and discussing the crystal structures of my compounds.

I was fortunate to have worked with some very talented students. Dr. Jeff Culp, a former member in Dr. Talham's group, is a person who is always able to see a bigger picture and never loses his sight of the simplest truth. I enjoyed and learned a lot from many inspiring late-night conversations with him on research. I also want to thank another previous group member, Dr. Melissa Petruska, for her efforts of helping me to

get started on synthesis and for teaching me many synthetic skills. I have also benefited a lot from all kinds of help from other members in the Talham group, postdoctoral fellow Dr. Renal Backov; former student Dr. Jonathan Woodward; and, Eduardo Perez-Cordero who has a lot of experience on chemistry and physics, and is always willing to pass along his knowledge to his peers. I also want to thank members in Professor Boncella's group, both past and present, Dr. Tim Foley, Dr. Tom Cameron, and Elon Ison for their generous help in teaching me synthetic skills and the usage and maintenance of lab equipments. They are great people to work with. I also appreciate the work performed by the staff in the NMR lab, the Mass Spectrometry and Elemental Analysis labs, the General and Chemical Stockrooms, and the Cryogenic facility. I want to thank the Chemistry Department for providing me a graduate assistantship to support my education.

Finally, I want to thank my family, my loving parents, my sister, and my grandmother, who have shown tremendous understanding and offered me the most important support. They endured the unimaginable suffering of having to be separated from me for so many years. For that, I am forever in debt to them, and for their sacrifices, I give my deepest thanks.

TABLE OF CONTENTS

page

ACKNOWLEDGMENTS ..... iv

LIST OF TABLES ..... x

LIST OF FIGURES ..... xii

ABSTRACT ..... xvi

CHAPTER

1 INTRODUCTION ..... 1

Scope of the Dissertation ..... 1
Magnetic Phenomena in Molecular Materials ..... 2
Noninteracting Systems ..... 4
The Van Vleck Equation ..... 4
Diamagnetic and Paramagnetic Susceptibility and the Curie Law ..... 6
Zero-Field Splitting and Single-Ion Anisotropy ..... 9
Interacting Systems ..... 13
The Curie-Weiss Law ..... 13
Magnetic Exchange ..... 15
Magnetic Ordering ..... 21
Synthesis and Structural Aspects of Low-Dimensional Coordination Polymers ..... 22
Spin-Ladder Systems ..... 29

2 SYNTHESIS, STRUCTURE AND MAGNETIC PROPERTIES OF A CHARGE TRANSFER SALT, FERRICENYL(III)TRIS(FERROCENYL(II))BORATE, REVISITING AN OLD CASE ..... 36

Introduction to Molecular Magnets Based on Ferrocene and Its Derivatives ..... 36
Background Information on Ferricenyl(III)tris(ferrocenyl(II))borate ..... 43
Experimental Section ..... 46
Materials ..... 46
Synthesis of Chloromercuriferrocene ..... 46
Synthesis of 1-Bromoferrocene ..... 47
Synthesis of Ferricenyl(III)tris(ferrocenyl(II))borate ($Fc_4B$), **1** ..... 47
EPR Measurements ..... 48
Magnetic Measurements ..... 48

Results and Discussion ..... 49
Synthesis of $Fc_4B$ ..... 49
Description of the Structure of $Fc_4B$ ..... 50
Magnetic Properties of $Fc_4B$ ..... 50
Conclusion ..... 54

3 STRUCTURE AND MAGNETIC PROPERTIES OF $Cu_2Cl_4(CH_3CN)_2$ ..... 55

Magnetism in Dimeric Systems ..... 55
Magneto-structural Correlations in Cu(II) Dimers ..... 58
Experimental Section ..... 62
Materials ..... 62
Synthesis of $Cu_2Cl_4(CH_3CN)_2$, **2** ..... 63
EPR Measurements ..... 63
Magnetic Measurements ..... 63
Results and Discussion ..... 64
Description of the Structure ..... 64
EPR Measurements ..... 64
Magnetic Properties of $Cu_2Cl_4(CH_3CN)_2$ ..... 64
Conclusion ..... 70

4 SYNTHESIS, STRUCTURE AND MAGNETISM OF LADDER-LIKE STRUCTURES $[Co(NO_3)_2(4,4'\text{-BIPYRIDINE})_{1.5}(MeCN)]_n$ AND $Ni_2(2,6\text{-PYRIDINEDICARBOXYLIC ACID})_2(H_2O)_4(PYRAZINE)$ ..... 71

Coordination Polymers with Ladder-like Structures ..... 71
A Strategy for Synthesizing Ladder-like Structures ..... 74
Experimental Section ..... 76
Materials ..... 76
Synthesis of $[Co(NO_3)_2(4,4'\text{-bipyridine})_{1.5}(MeCN)]_n$, **3** ..... 76
Synthesis of $Ni_2(dpa)_2(pyz)(H_2O)_4$, **4** ..... 77
X-ray Diffraction experiment on $Ni_2(dpa)_2(pyz)(H_2O)_4$ ..... 77
Magnetic Measurements on $[Co(NO_3)_2(4,4'\text{-bipyridine})_{1.5}(MeCN)]_n$ ..... 78
Magnetic Measurements on $Ni_2(dpa)_2(pyz)(H_2O)_4$ ..... 79
Results and Discussion ..... 79
Structure Description of $[Co(NO_3)_2(4,4'\text{-bipyridine})_{1.5}(MeCN)]_n$ ..... 79
Structure Description of $Ni_2(dpa)_2(pyz)(H_2O)_4$ ..... 80
Magnetic Properties of $[Co(NO_3)_2(4,4'\text{-bipyridine})_{1.5}(MeCN)]_n$ ..... 83
Magnetic Properties of $Ni_2(dpa)_2(pyz)(H_2O)_4$ ..... 85
Conclusion ..... 89

5 STRATEGIES FOR THE SYNTHESIS OF PRUSSIAN BLUE ANALOGUES WITH LADDER-LIKE STRUCTURES ..... 90

Synthesis and Structures of Low-Dimensional Prussian Blue Analogues ..... 91
Zero-Dimensional Systems ..... 93
One-Dimensional Systems ..... 94

Ladder-like Systems ..... 96
Two-Dimensional Systems ..... 97
Strategies for Synthesizing PB Analogues with Ladder-like Structures ..... 99
Experimental Section ..... 104
Materials ..... 104
Synthesis of $Ni(dpa)(H_2O)_3$ ..... 104
Synthesis of 4'-Phenyl-2,2':6',2''-terpyridine (Ph-terpy) ..... 105
Synthesis of $[Fe^{III}(Ph\text{-}terpy)]Cl_3$ ..... 106
Synthesis of $[Fe^{III}(terpy)]Cl_3$ ..... 106
Synthesis of $[Ni^{II}(CN)_4]_3[Fe^{III}(terpy)]_2$ ..... 106
Synthesis of $[Fe(MeCN)_6](CF_3SO_3)_2$ ..... 107
Synthesis of $[Fe(cyclam)(MeCN)_2](PF_6)_2$ ..... 107
Synthesis of $[Fe(cyclam)](CN)_2$ ..... 107
Results and Discussion ..... 108
Conclusion ..... 109

6 SYNTHESES, STRUCTURES AND MAGNETISM OF $Cu_2(C_2O_4)(HISTAMINE)_2(N_3)_2$, $Cu_2(C_2O_4)(HISTAMINE)_2[N(CN)_2]_2$, $[Cu_4(4,4'\text{-}BIPYRIMIDINE)_2(N_3)_8]_n$, AND $[Cu(TEREPHTHALATO)(H_2O)_2{\bullet}H_2O]_n$ ..... 111

Introduction ..... 111
Experimental Section ..... 113
Materials ..... 113
Synthesis of $Cu_2(C_2O_4)(histamine)_2[N(CN)_2]_2$, **5** ..... 113
Synthesis of $Cu_2(C_2O_4)(histamine)_2(N_3)_2$, **6** ..... 114
Synthesis of $[Cu_4(2,2'\text{-bipyrimidine})_2(N_3)_8]_n$, **7** ..... 114
Synthesis of $[Cu(terephthalato)(H_2O)_2{\bullet}H_2O]_n$, **8** ..... 114
X-ray Diffraction Experiments ..... 115
EPR Measurements ..... 116
Magnetic Measurements ..... 116
Results and Discussion ..... 117
Description of the Structure of $Cu_2(C_2O_4)(histamine)_2[N(CN)_2]_2$. ..... 117
Description of the Structure of $Cu_2(C_2O_4)(histamine)_2(N_3)_2$ ..... 119
Description of the Structure of $[Cu_4(2,2'\text{-bipyrimidine})_2(N_3)_8]_n$. ..... 121
Description of the Structure of $[Cu(terephthalato)(H_2O)_2{\bullet}H_2O]_n$ ..... 123
EPR Measurements ..... 125
Magnetic Properties of $Cu_2(C_2O_4)(histamine)_2[N(CN)_2]_2$ ..... 128
Magnetic Properties of $Cu_2(C_2O_4)(histamine)_2(N_3)_2$ ..... 129
Magnetic Properties of $[Cu(terephthalato)(H_2O)_2{\bullet}H_2O]_n$ ..... 131
Conclusion ..... 138

7 EPILOGUE ..... 140

APPENDIX

A CRYSTAL STRUCTURAL DATA FOR COMPOUND **4** ..... 145

B CRYSTAL STRUCTURAL DATA FOR COMPOUND **5** ..... 149

C CRYSTAL STRUCTURAL DATA FOR COMPOUND **6** ..... 153

D CRYSTAL STRUCTURAL DATA FOR COMPOUND **7** ..... 157

E CRYSTAL STRUCTURAL DATA FOR COMPOUND **8** ..... 160

LIST OF REFERENCES ..... 163

BIOGRAPHICAL SKETCH ..... 173

LIST OF TABLES

Table page

4-1. Fitting results for the molar susceptibility *vs* temperature plot of $Ni_2(dpa)_2(pyz)(H_2O)_4$ fitted to Equation 4-1. ....88

6-1. Fitting results for the molar susceptibility *vs* temperature plot of $Cu_2(C_2O_4)(histamine)_2[N(CN)_2]_2$. ....129

6-2. Fitting results for the molar susceptibility *vs* temperature plot of $Cu_2(C_2O_4)(histamine)_2(N_3)_2$. ....130

6-3. Fitting results for the molar susceptibility *vs* temperature plot of $[Cu(terephthalato)(H_2O)_2 \cdot H_2O]_n$. ....135

A-1. Atomic coordinates and equivalent isotropic displacement parameters for **4** ....145

A-2. Bond lengths and angles for **4**. ....146

A-3. Hydrogen coordinates and isotropic displacement parameters for **4** ....148

A-4. Hydrogen bond lengths and angles for **4** ....148

B-1. Atomic coordinates and equivalent isotropic displacement parameters for **5**. ....149

B-2. Bond lengths and angles for **5**. ....150

B-3. Hydrogen coordinates and isotropic displacement parameters for **5**. ....152

C-1. Atomic coordinates and equivalent isotropic displacement parameters for **6** ....153

C-2. Bond lengths and angles for **6**. ....154

C-3. Hydrogen coordinates and isotropic displacement parameters for **6**. ....156

C-4. Hydrogen bond lengths and angles for **6** ....156

D-1. Atomic coordinates and equivalent isotropic displacement parameters for **7** ....157

D-2. Bond lengths and angles for **7**. ....158

D-3. Hydrogen coordinates and isotropic displacement parameters for **7**. ....159

E-1. Atomic coordinates and equivalent isotropic displacement parameters for **8**.....160

E-2. Bond lengths and angles for **8**.....161

E-3. Hydrogen coordinates and isotropic displacement parameters for **8**. .....162

E-4. Hydrogen bond lengths and angles for **8**.....162

LIST OF FIGURES

Figure page

1-1. Zero-field splitting effect on an $S = 3/2$ state ..... 9

1-2. Anisotropic splitting of the ground state of Ni(II) ..... 10

1-3. Zero-field splitting of the ground state and the first excited state for an Ni(II) ion in a trigonally distorted octahedral environment ..... 11

1-4. Plots of Curie and Curie-Weiss behaviors of an $S = 1/2$ system ..... 16

1-5. Spin angular momentum vectors ..... 20

1-6. Various topologies obtained using bifunctional ligands and spacers ..... 25

1-7. Ladder-like structure and spin gap ..... 30

1-8. Structure of a superconducting cuprate, $(Sr, Ca)_{14}Cu_{24}O_{41}$ ..... 32

1-9. Crystal structure and of the exchange pathways in BPCB. ..... 33

1-10. Plots of $\chi$ *vs* $T$ and $M$ *vs* $H$ for a powder sample of BPCB. ..... 33

1-11. Structure of $[Cu^{II}(opba)]^{2-}$, a bisbidentate molecular building block ..... 34

1-12. Ladder-like structure of $Gd^{III}_2$ $[Cu^{II}(opba)]_3 \cdot 6DMSO \cdot 4H_2O$ ..... 35

2-1. Chains of $[Fe(Me_5C_5)_2][TCNE] \cdot MeCN$ ..... 37

2-2. Magnetic properties of $[Fe(Me_5C_5)_2][TCNE]$ ..... 38

2-3. Magnetization hysteresis of $[Fe(Me_5C_5)_2][TCNE]$ at 2 K ..... 39

2-4. Molecular structure of $Fc_4B$ ..... 43

2-5. Plots of $\chi T$ *vs* $T$ and $\chi^{-1}$ *vs* $T$ for $Fc_4B$ under various magnetic fields ..... 45

2-6. Synthetic route for $Fc_4B$ ..... 49

2-7. Packing diagram of $Fc_4B$ ..... 51

2-8. Selected distances between iron(III) ions in $Fc_4B$ ..... 51

2-9. Room-temperature EPR spectrum of $Fc_4B$ ..... 52

2-10. Plot of $\chi T$ *vs* $T$ for $Fc_4B$ obtained with 20 G and 100 G measuring field ..... 52

2-11. Plot of $\chi^{-1}$ *vs* $T$ for $Fc_4B$ obtained with 20 G and 100 G measuring field ..... 53

3-1. Splitting of the magnetic energy levels in an $S = 1/2$ dimer ..... 57

3-2. General structure of planar Cu(II) dimer complex ..... 58

3-3. Distortions in copper(II) dimers ..... 58

3-4. Molecular orbitals for di-$\mu$-hydroxo bridged copper(II) dimers ..... 60

3-5. Exchange energy, $J/k$, as a function of bridging angle, $\varphi$, for a series of copper(II) chloride salts ..... 62

3-6. Structure of $Cu_2Cl_4(CH_3CN)_2$ ..... 65

3-7. The X-band EPR spectra of a polycrystalline sample of $Cu_2Cl_4(CH_3CN)_2$ at various temperatures ..... 65

3-8. Plot of $\chi T$ *vs* $T$ for $Cu_2Cl_4(CH_3CN)_2$ ..... 67

3-9. Magnetization as a function of field obtained at 2 K for $Cu_2Cl_4(CH_3CN)_2$ ..... 67

3-10. Comparison of the exchange parameter of $Cu_2Cl_4(CH_3CN)_2$ with other isostructural Cu(II) dimers containing different types of terminal ligands ..... 69

4-1. Structure of $Ni(4,4'\text{-bipyridine})_{2.5}(H_2O)_2(ClO_4)_2 \cdot 1.5(4,4'\text{-bipyridine}) \cdot 2H_2O$ ..... 71

4-2. Structure of 1,4-bis(4-pyrodylmethyl)benzene and of [Cd(1,4-bis(4-pyrodylmethyl)benzene)$_{1.5}$][$NO_3$]$_2$ ladders ..... 72

4-3. Ladder-like structure of $[Cu_2(bpm)(dca)_4]_n$ ..... 73

4-4. Proposed methodology for the synthesis of coordination polymers with a ladder-like structure ..... 74

4-5. Repeating unit of a ladder-like structure ..... 75

4-6. Structure of 2,2':6',2"–terpyridine (terpy) and 2,6-pyridinedicarboxylic acid (dpa) dianion ..... 76

4-7. Synthetic scheme for $[Co(NO_3)_2(4,4'\text{-bipyridine})_{1.5}(solv)]_n$ ..... 80

4-8. Ladder-like structure of $[Co(NO_3)_2(4,4'\text{-bipyridine})_{1.5}(solv)]_n$ ..... 80

4-9. The structural repeating unit and selected bond lengths of $Ni_2(dpa)_2(pyz)(H_2O)_4$.....81

4-10. Ladder-like structure in $Ni_2(dpa)_2(pyz)(H_2O)_4$.....82

4-11. Plots of *M vs H* and $\chi T$ *vs* T for $[Co(NO_3)_2(4,4'\text{-bipyridine})_{1.5}(MeCN)]_n$ at 2 K .....84

4-12. Fine-structure splitting of the lowest levels of Co(II) under the combined action of an octahedral field and spin orbital coupling .....84

4-13. Coordination modes around Co(II) in $[Co(NO_3)_2(4,4'\text{-bipyridine})_{1.5}(MeCN)]_n$ .....85

4-14. Magnetization measured as a function of field at 2 K, 5 K, and 10 K, respectively, for $Ni_2(dpa)_2(pyz)(H_2O)_4$.....86

4-15. Susceptibility plotted as a function of temperature for $Ni_2(dpa)_2(pyz)(H_2O)_4$.....87

5-1. Idealized structure of Prussian Blue .....92

5-2. Structures of the $M(Me_3TACN)L_3$ ($L = CN^-$ or $H_2O$) molecular building block and $[(Me_3TACN)_8Cr_8Ni_6(CN)_{24}]^{12+}$cluster .....93

5-3. Three $PPh_4[Ni(pn)_2][Fe(CN)_6]\bullet H_2O$ 1-D chains .....95

5-4. Chain structure of $[Fe^{III}(cyclam)][Fe^{III}(CN)_6]\bullet 6H_2O$ .....95

5-5. Structural repeating unit and ladder structure in $[Ni^{II}(en)_2]_3[Co^{III}(CN)_6]_2\bullet 2H_2O$ .....97

5-6. Top view of the 2-D $[Ni^{II}(N\text{-}men)_2]_3[Fe^{III}(CN)_6]_2\bullet nH_2O$ network.....98

5-7. Structure of the 2-D $[Ni^{II}(1,1\text{-}dmen)_2]_2[Fe^{III}(CN)_6]N_3\bullet 4H_2O$ network .....98

5-8. Structural repeating unit of a ladder-like PB analogue.....102

5-9. Structure of a metal ion coordinated to a cyclam molecule .....104

6-1. The dimeric structural repeating unit of $Cu_2(C_2O_4)(histamine)_2[N(CN)_2]_2$. .....118

6-2. Top view of the 2-D sheet of $Cu_2(C_2O_4)(histamine)_2[N(CN)_2]_2$ .....119

6-3. Side view of $Cu_2(C_2O_4)(histamine)_2[N(CN)_2]_2$. .....119

6-4. Structural repeating unit of $Cu_2(C_2O_4)(histamine)_2(N_3)_2$ .....120

6-5. Side view of one 2-D sheet of $Cu_2(C_2O_4)(histamine)_2(N_3)_2$.....120

6-6. Side view of $Cu_2(C_2O_4)(histamine)_2(N_3)_2$ stacking along the *a* axis. .....121

6-7. Anticipated ladder-like structure of $[Cu_4(2,2'\text{-bipyrimidine})_2(N_3)_8]_n$.....122

6-8. The 2-D network of $[Cu_4(2,2'\text{-bipyrimidine})_2(N_3)_8]_n$ ..... 123

6-9. Side view of the 2-D sheet of $[Cu_4(2,2'\text{-bipyrimidine})_2(N_3)_8]_n$. ..... 123

6-10. Coordination modes of terephthalate dianion..... 124

6-11. A top view of the chain structure of $[Cu(terephthalato)(H_2O)_2{\bullet}H_2O]_n$ ..... 124

6-12. A view along the chain (*c*-axis) of $[Cu(terephthalato)(H_2O)_2{\bullet}H_2O]_n$..... 125

6-13. Packing diagram of seven chains of $[Cu(terephthalato)(H_2O)_2{\bullet}H_2O]_n$ ..... 125

6-14. Room-temperature X-band EPR spectrum of $Cu_2(C_2O_4)(histamine)_2[N(CN)_2]_2$...126

6-15. Room-temperature X-band EPR spectrum of $Cu_2(C_2O_4)(histamine)_2(N_3)_2$. ..... 127

6-16. Room-temperature X-band EPR spectrum of $[Cu(terephthalato)(H_2O)_2{\bullet}H_2O]_n$.... 127

6-17. Magnetic susceptibility for per mole of $Cu_2(C_2O_4)(histamine)_2[N(CN)_2]_2$..... 128

6-18. Magnetic susceptibility for per mole of $Cu_2(C_2O_4)(histamine)_2(N_3)_2$ ..... 130

6-19. Plot of $\chi T$ *vs* $T$ for $[Cu(terephthalato)(H_2O)_2{\bullet}H_2O]_n$ fitted to the Bonner Fisher expression for an $S = 1/2$ chain..... 131

6-20. Plot of inverse susceptibility as a function of temperature for $[Cu(terephthalato)(H_2O)_2{\bullet}H_2O]_n$ ..... 133

6-21. Spin canting along the chain (*c* axis) of $[Cu(terephthalato)(H_2O)_2{\bullet}H_2O]_n$..... 134

6-22. Plot of $\chi T$ *vs* $T$ for $[Cu(terephthalato)(H_2O)_2{\bullet}H_2O]_n$ fitted to a modified bonner Fisher expression..... 136

6-23. Plot of molar magnetization of $[Cu(terephthalato)(H_2O)_2{\bullet}H_2O]_n$ as a function of field at 2 K and 5 K, respectively..... 136

6-24. Magnetic couplings in $[Cu(terephthalato)(H_2O)_2{\bullet}H_2O]_n$..... 137

Abstract of Dissertation Presented to the Graduate School
of the University of Florida in Partial Fulfillment of the
Requirements for the Degree of Doctor of Philosophy

SYNTHESIS AND CHARACTERIZATION OF LOW-DIMENSIONAL MOLECULAR MAGNETIC MATERIALS

By

Chen Liu

May 2004

Chair: Daniel R. Talham
Department: Chemistry

This dissertation presents experimental results from the synthesis and structural, magnetic characterization of representative low-dimensional molecule-based magnetic materials. Most of the materials reported in this dissertation, both coordination polymers and cuprate, are obtained as the result of synthesizing and characterizing spin ladder systems; except the material studied in Chapter 2, ferricenyl(III)trisferrocenyl(II)borate, which is not related to the spin ladder project. The interest in spin ladder systems is due to the discovery of high-temperature superconductivity in doped cuprates possessing ladder-like structures, and it is hoped that investigation of the magnetic behavior of ladder-like structures will help us understand the mechanism of high-temperature superconductivity.

Chapter 1 reviews fundamental knowledge of molecular magnetism, general synthetic strategies for low-dimensional coordination polymers, and a brief introduction to the current status of research on spin ladder systems.

Chapter 2 presents a modified synthetic procedure of a previously known monomeric complex, ferricenyl(III)trisferrocenyl(II)borate, **1**. Its magnetic properties were characterized and previous results have been disproved.

Chapter 3 investigates the magnetism of $[CuCl_2(CH_3CN)]_2$, **2**, a cuprate whose structure consists of isolated noninterpenetrating ladders formed by the stacking of Cu(II) dimers. This material presents an unexpected ferromagnetic interaction both within the dimeric units and between the dimers, and this behavior has been rationalized based on the effect of its terminal nonbridging ligands.

In Chapter 4, the synthesis and magnetism of two ladder-like coordination polymers, $[Co(NO_3)_2(4,4'\text{-bipyridine})_{1.5}(MeCN)]_n$, **3**, and $Ni_2$(2,6-pyridinedicarboxylic acid)$_2(H_2O)_4$(pyrazine), **4**, are reported. Compound **3** possesses a covalent one-dimensional ladder structure in which Co(II) ions are bridged through bipyridine molecules. But, it is essentially a paramagnetic system because twisting between the two pyridine rings magnetically isolates the Co(II) ions.The ladder-like structure of **4** is formed by stacking Ni(II) dimers through hydrogen bonding and $\pi$-$\pi$ interaction. Individual ladders are also linked *via* an extensive hydrogen-bonding network. This material presents weak antiferromagnetic exchange coupling both within the Ni(II) dimers and between dimers, as well as a strong zero-field splitting effect.

Compared to the materials discussed in Chapter 3 and Chapter 4, Chapter 5 presents a strategy of synthesizing ladder-like structures in a distinctively different system, bimetallic cyanide-bridged Prussian Blue analogs. Calculations are designed and carried out to identify two potentially successful model structures which are subsequently attempted synthetically. The two model structures are $[Ni^{II}(CN)_4]_3[Fe^{III}(terpy)]_2$

and $[Fe^{II}(cyclam)_2]_3[Ni^{II}(dpa)]_2(CN)_6$.

Finally, in Chapter 6, four Cu(II)-based low-dimensional materials are reported. Two of them, $Cu_2(C_2O_4)(histamine)_2[N(CN)_2]_2$, **5**, and $Cu_2(C_2O_4)(histamine)_2(N_3)_2$, **6**, consist of dimeric structural units that assemble into two-dimensional sheets. Magnetically, both behave as an isolated dimer system. On the other hand, compound **7**, $[Cu_4(4,4'\text{-bipyrimidine})_2(N_3)_8]_n$, has a two-dimensional covalent network structure that can be viewed as being formed by covalently bridging one-dimensional ladders. $[Cu(terephthalato)(H_2O)_2{\bullet}H_2O]_n$, **8**, consists of one-dimensional chains of equally spaced Cu(II) ions bridged by the carboxylate groups of terephthalic acid dianion. Antiferromagnetic coupling within chains with weak spin canting is observed at elevated temperatures. As temperature is lowered, net magnetic moments within the chains start coupling ferromagnetically to form magnetic two-dimensional sheets that are coupled antiferromagnetically as temperature is lowered further.

# CHAPTER 1
# INTRODUCTION

## Scope of the Dissertation

Most of the materials presented in this dissertation are obtained from the efforts of synthesizing and characterizing magnetic properties of spin-ladders, except the material studied in Chapter 2, ferricenyl(III)trisferrocenyl(II)borate, ($Fc_4B$), which is not related to the spin-ladder project. The spin carriers in these compounds are first-row transition-metal ions instead of free radicals or rare earth ions.

The motivation of the spin-ladder project originated from the observation of high-temperature superconductivity in 1986 among some highly doped cuprates.[1] Although the mechanism of such behavior is still unclear at this point, it has been related to antiferromagnetic coupling between the Cu(II) ions in the two-dimensional copper oxide network containing ladder-like structures.[2] The observed superconductivity in the doped cuprates very much resembles the theoretical predictions made for doped ladder-like structures.[3,4] Therefore, it is hoped that research on the magnetic properties of spin-ladder systems will improve our understanding of the mechanism of high-temperature superconductivity. Thus, the purpose of the spin-ladder project is first to characterize the magnetism of some of the known cuprates in search of spin-ladder behavior, and, in light of recent developments in the field of crystal engineering, to also synthesize new examples of coordination polymers possessing ladder-like structures and then investigate their magnetic properties.

At the time this dissertation was written, several ladder-like structures, both cuprates and coordination polymers, had been synthesized and magnetically characterized. However, no spin-ladder behavior was observed.

The chapters are organized according to the dimensionalities of the materials synthesized and investigated, starting with a zero-dimensional monomer, moving on to a Cu(II)-based dimer and two ladder-like structures, and, finally, two-dimensional sheets. Chapter 1 contains fundamental knowledge of molecular magnetism, the synthetic and structural aspects of coordination polymers, and general remarks on spin-ladder systems. In Chapter 2, the synthesis and magnetism of a monomeric complex, ferricenyl(III)trisferrocenyl(II)borate, is reported. Chapter 3 presents the magnetic behavior of a cuprate, $Cu_2Cl_4(CH_3CN)_2$, possessing a ladder-like structure. In Chapter 4, the synthesis and magnetic properties of two ladder-like structures based on Ni(II) and Co(II) are presented. In Chapter 5, synthetic strategies are discussed regarding the construction of Prussian Blue analogues with ladder-like structures. Experimental results based on the proposed strategies are also presented. The last chapter, Chapter 6, presents the synthesis and magnetic properties of three examples of Cu(II)-based two-dimensional structures.

## Magnetic Phenomena in Molecular Materials

Although the magnetic phenomena in molecules had been studied by chemists and physicists for decades,[5-7] magnetic materials had traditionally been iron metal and iron oxides until 1986 when the first molecule-based material, $[Fe(C_5Me_5)_2]^+[TCNE]^-$, where TCNE is tetracyanoethenide, prepared by conventional synthetic methodology was discovered to show long-range ferromagnetic ordering.[8] Research activities in the field of molecular magnetism in the past decade or so have created a large number of new

materials that display a variety of magnetic phenomena due to the unique characteristics attributed to the molecular nature of the materials.[9-12] The quest for room-temperature molecule-based magnets is just one of the many research directions in this field. Research in single-molecule magnets is aimed at producing information-storage devices with ever-smaller size and much larger memory.[13, 14] Photo-induced magnetization[15-19] and molecular bistability[20-24] are obviously of technological importance. Molecular magnetism of low-dimensional systems is especially important for the understanding of quantum mechanics.[25-29] Many theoretical predictions of low-dimensional properties can now be tested on real materials, and it is hoped that research concerning the magnetism of ladder-like systems, an interdimensional structure between 1-D and 2-D, can shine some light on the mechanism of high-temperature superconductivity. Thus, molecular magnetism is naturally an interdisciplinary field involving chemistry, physics, and material and biological sciences.

Magnetism is primarily due to the magnetic moments arising from the angular momenta of the intrinsic quantum mechanical phenomena of spin of electrons, since the permanent dipole moments of some atomic nuclei are too small to produce significant effects even at extremely low temperatures (a few milliKelvin). Any theory must therefore first address the electronic structure of the atoms and ions involved in the magnetic material. However it is beyond the scope of this dissertation to enter into the theory of the electronic structure of ions and molecules. In the following sections, some fundamental concepts of basic importance to the understanding of magnetic phenomena in solids are considered. First, the magnetism of discrete noninteracting magnetic ions characterized by the Curie Law is discussed. Then, magnetism of interacting magnetic

systems where magnetic centers couple to each other is presented. Magnetic anisotropy is also an important issue that frequently leads to peculiar magnetic phenomena. This will be discussed for both zero-field splitting and anisotropic-exchange mechanisms.

## Noninteracting Systems

The presence of magnetic moments is the only necessary condition required for a material to exhibit magnetic behavior. Magnetic behavior is typically detected by a material's attraction or repulsion to a magnet. Fields of a few Tesla, as attainable in most laboratories, change the energy of the system by some few wavenumbers. Spin-orbital coupling energy is rarely lower than 30 to 50 $cm^{-1}$ and crystal field and molecular orbital energies are of the order of $10^4$ $cm^{-1}$. We will therefore assume that the ion or molecule is in its ground state with a resultant orbital, spin, and total angular momentum, $\boldsymbol{L}$, $\boldsymbol{S}$, and $\boldsymbol{J}$, respectively, and treat spin-orbital coupling and external magnetic field as perturbations to the ground state.

### The Van Vleck Equation

In a magnetic field $\boldsymbol{B}$, a sample of 1 mol of a molecular compound acquires a molar magnetization $\boldsymbol{M}$ which is related to $\boldsymbol{B}$ as [11]

$$\boldsymbol{\chi} = \partial \boldsymbol{M} / \partial \boldsymbol{B} \tag{1-1}$$

where $\boldsymbol{\chi}$ is the molar magnetic susceptibility. $\boldsymbol{M}$, the molar magnetic moment, is a vector. $\boldsymbol{B}$ is an axial vector and $\boldsymbol{\chi}$ is a second rank tensor. The molar paramagnetic susceptibility characterizes how an applied magnetic field $\boldsymbol{B}$ interacts with the angular momenta associated with the thermally populated states of a molecule.[11] It is always possible to choose reference axes so that $\boldsymbol{\chi}$ can be diagonalized to afford the principal values, $\chi_x$, $\chi_y$, $\chi_z$. If the sample is magnetically isotropic, $\boldsymbol{\chi}$ becomes a scalar, $\chi$ ($\chi_x = \chi_y = \chi_z = \chi$). When

the magnetic field is weak enough and homogeneous, to a good approximation, $\chi$ can be treated as being independent of $B$ as

$$\chi = M / B \tag{1-2}$$

According to classical mechanics, the magnetization the sample acquires is related to its energy variation as

$$M = - \partial E / \partial B \tag{1-3}$$

Similarly, when we consider a molecule with an energy spectrum $E_n$ ( $n = 1, 2, \ldots$ ) in an external magnetic field $B$, a microscopic magnetization $\mu_n$ is acquired for each energy level as

$$\mu_n = - \partial E_n / \partial B \tag{1-4}$$

At thermal equilibrium, according to the Boltzmann distribution law, the macroscopic molar magnetization $M$ is a weighted sum of the microscopic magnetizations

$$M = \frac{N \Sigma_n (-\partial E_n / \partial B) exp(-E_n / kT)}{\Sigma_n exp(-E_n / kT)} \tag{1-5}$$

where $N$ is Avogadro's number and the denominator is the partition function, $Z$. Equation 1-5 can be simplified based on a few assumptions so that information on $E_n = f(B)$ is no longer required. The first approximation is that $E_n$ can be expanded as

$$E_n = E_n^{(0)} + E_n^{(1)} B + E_n^{(2)} B^2 + \ldots \tag{1-6}$$

where $E_n^{(0)}$ is the energy of level $n$ in zero field. $E_n^{(1)}$ and $E_n^{(2)}$ are the first- and second-order Zeeman coefficients, respectively. When $B$ is not too large and $T$ is not too small, the exponential in Equation 1-5 can be written as

$$exp(-E_n / kT) = exp(-E_n^{(0)} / kT)(1 - E_n^{(1)} B / kT) \tag{1-7}$$

Then Equation 1-5 can be transformed into

$$M = \frac{N\Sigma_n(-E_n^{(1)} - 2E_n^{(2)}B)(1 - E_n^{(1)}B/kT)\exp(-E_n^{(0)}/kT)}{\Sigma_n(1 - E_n^{(1)}B/kT)\exp(-E_n^{(0)}/kT)} \tag{1-8}$$

The third assumption is that the magnetization is zero in zero field

$$\Sigma_n E_n^{(1)} \exp(-E_n^{(0)}/kT) = 0 \tag{1-9}$$

Substituting Equation 1-9 into 1-8 and only retain the terms linear in $B$ results

$$M = \frac{NB\Sigma_n(E_n^{(1)2}/kT - 2E_n^{(2)})\exp(-E_n^{(0)}/kT)}{\Sigma_n \exp(-E_n^{(0)}/kT)} \tag{1-10}$$

and, since $\chi = M/B$, we have

$$\chi = \frac{N\Sigma_n(E_n^{(1)2}/kT - 2E_n^{(2)})\exp(-E_n^{(0)}/kT)}{\Sigma_n \exp(-E_n^{(0)}/kT)} \tag{1-11}$$

Equation 1-11 is the Van Vleck equation. We only need to know the quantities of $E_n^{(0)}$, $E_n^{(1)}$, and $E_n^{(2)}$ to apply this equation. It is no longer necessary to calculate the derivatives $\partial E_n / \partial B$. When all energies $E_n$ are linear in $B$, the second-order Zeeman coefficient $E_n^{(2)}$ vanishes and Equation 1-11 becomes

$$\chi = \frac{N\Sigma_n E_n^{(1)2}\exp(-E_n^{(0)}/kT)}{kT\Sigma_n \exp(-E_n^{(0)}/kT)} \tag{1-12}$$

**Diamagnetic and Paramagnetic Susceptibility and the Curie Law**

The total molar magnetic susceptibility can be regarded as the sum of two contributions associated with diamagnetism and paramagnetism, respectively.[11]

$$\chi_T = \chi_{dia} + \chi_{para} \tag{1-13}$$

Diamagnetism is a property of all matter because it arises from completely filled electronic shells, that is, from paired spins. Since transition-metal ions with unpaired

spins also have filled shells, they too have a diamagnetic contribution to their total susceptibility. When a diamagnetic substance, a substance that does not contain unpaired spins, is placed in a magnetic field, the density of the magnetic lines of force within the sample is reduced. Since this is equivalent to the substance producing a flux opposing the field, it follows that the substance will tend to move to regions of lower field, or to be repelled out of the field.[11] The molar susceptibility of a diamagnetic material is negative and very small, on the order of $-1$ to $-10^4$ emu/mol. Diamagnetic susceptibility is independent of temperature and the strength of applied field. It normally only serves as a correction of a measured susceptibility in order to obtain paramagnetic susceptibility. Paramagnetic susceptibility can be observed only with materials possessing unpaired spins which interact with an external field to cause the lines of force within a paramagnetic sample to concentrate. In a system where paramagnetic centers do not interact with each other, the paramagnetic susceptibility of the system varies inversely with temperature according to the Curie law: [11]

$$\chi_{para} = C / T \tag{1-14}$$

where $C$ is the Curie constant and $T$ is the absolute temperature. The Curie law can be derived quite simply as follows. Consider an orbital singlet with $2S + 1$ spin degeneracy. The external magnetic field resolves the degeneracy of the $M_s$ states according to the magnetic quantum numbers $M_s$ and the energy of each sublevel is

$$E_n = M_s g \beta B \tag{1-15}$$

where $\beta$ is the Bohr magneton. Since the zero of energy can be taken as the level of the lowest energy in the magnetic field and energies $E_n$ are linear in $B$, it is possible to use the simplified form of the Van Vleck equation, Equation 1-12, provided that $B / kT$ is small,

with $E_n^{(0)} = E_n^{(2)} = 0$ and $E_n^{(1)} = M_s g\beta$, $M_s = -S, -S+1, \ldots, S-1, S$. Equation 1-12 then transforms into

$$\chi = \frac{N g^2 \beta^2}{k T} \cdot \frac{(-S)^2 + (-S+1)^2 + \ldots + (+S)^2}{2S+1} \tag{1-16}$$

which leads to

$$\chi = \frac{N g^2 \beta^2}{3 k T} S(S+1) \tag{1-17}$$

Equation 1-17 is the Curie law in which the Curie constant $C$ depends on the spin multiplicity of the ground state. The molar magnetization for one mole of paramagnetic sample can be derived by rewriting Equation 1-5 using the partition function, $Z$

$$Z = \Sigma_n \exp(-E_n / kT) \tag{1-18}$$

$$= \Sigma_{Ms} \exp(-M_s g \beta B / kT) \tag{1-19}$$

$$= \sinh[(2S+1)x/2] / \sinh(x/2) \tag{1-20}$$

where

$$x = g \beta B / kT \tag{1-21}$$

We can then write

$$\partial \ln Z / \partial B = (1/kT) \frac{\Sigma_n (-\partial E_n / \partial B) \exp(-E_n / kT)}{\Sigma_n \exp(-E_n / kT)} \tag{1-22}$$

$$= (g\beta/2kT)\{(2S+1)\coth[(2S+1)y/2S] - \coth(y/2S)\} \tag{1-23}$$

where $y = g\beta SB / kT$, and Equation 1-5 takes the form of

$$M = NkT(\partial \ln Z / \partial B) \tag{1-24}$$

$$= Ng\beta S B_s(y) \tag{1-25}$$

where $B_s(y)$ is the Brillouin function [11]

$$B_S(y) = y\,(S+1)/3S + terms\ in\ y^3 + \ldots \qquad (1\text{-}26)$$

when $B/kT$ is not too large.

**Zero-Field Splitting and Single-Ion Anisotropy**

There are situations in which the magnetic behavior of a paramagnetic sample deviates from the Curie law. One important source of the deviation is the zero-field splitting effect which is a single-ion event and a central issue in paramagnetism. In general, zero-field splitting refers to the removal of the spin microstate (the Zeeman components, $M_s$) degeneracy for $S > 1/2$ systems in the absence of an external magnetic field. It causes magnetic anisotropy and, as a consequence, the deviation from the Curie law. To illustrate zero-field splitting, we can use an example of $L = 0$ and $S = 3/2$ system for convenience. Its energy-level diagram is shown in Figure 1-1.[29] In an axial ligand field, the degeneracy between $S = \pm 1/2$ states and $S = \pm 3/2$ states is resolved before an external magnetic field is applied. The $S = \pm 3/2$ states are separated by $2D$ from the $S = \pm 1/2$ states. The population of levels depends on the value of the zero-filed splitting parameter $D$ and the thermal energy, $kT$. When the $S = \pm 3/2$ states have higher energy, $D > 0$; if the $S = \pm 3/2$ states have lower energy, $D < 0$.

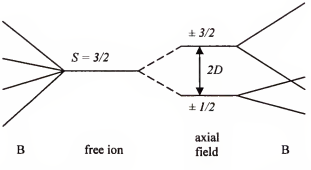


Figure 1-1. Zero-field splitting effect on an $S = 3/2$ state. On the left is the usual Zeeman effect. On the right, the spin degeneracy of the ground state is partially removed before a magnetic field is applied.

When a transition-metal ion is placed in an axial ligand field capable of causing the zero-field splitting effect, the ligand field establishes a molecular axis. So, when an external magnetic field is applied, it is important to specify if the molecular axis is parallel, perpendicular, or at some intermediate direction with respect to the direction of the external magnetic field. The parallel situation is often noted by a subscript *z (or //)*, and the perpendicular situation is designated by a subscript of *x (or ⊥)* . Figure 1-2 shows the anisotropic effect of zero-field splitting.[11]

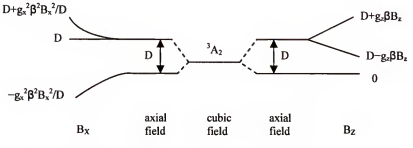


Figure 1-2. Anisotropic splitting of the ground state of Ni(II).

With zero-field splitting, the energy separation between different states ($m_s$) is no longer uniform as the situation shown in Equation 1-15, and different splitting patterns are obtained depending on the orientation of the external field with respect to the ligand field direction. It is then obvious that applying the Van Vleck equation will afford different results, $\chi_{//}$ and $\chi_{\perp}$, when the external field is applied parallel and perpendicular to the molecular axis, respectively. When $D$ is positive, $\chi_{//}$ ($\chi_z$) tends to zero, while $\chi_{\perp}$ ($\chi_x$) approaches to a finite nonzero value. When $D$ is negative, $\chi_{//}$ ($\chi_z$) becomes infinity, and $\chi_{\perp}$ ($\chi_x$) tends to a small but finite value. The average susceptibility thus obtained for a polycrystalline or powder sample is the average [11] of $\chi_{//}$ and $\chi_{\perp}$ according to

$$\langle\chi\rangle = (\chi_{//} + 2\chi_{\perp})/3 \qquad (1\text{-}27)$$

Although other mechanisms exist, zero-field splitting effect is primarily a consequence of spin-orbit coupling and/or the distortion of ligand field (the lowering of ligand field symmetry) that change the electronic structure of the ground state and low-lying excited states. As mentioned earlier, the splitting due to ligand field distortion is a much stronger effect than that caused by spin-orbit coupling. A state without first-order orbital angular momentum is isotropic since only the orbital component of the wavefunction can "feel" the difference between different spatial orientations. Since spin-orbit coupling is an anisotropic event, zero-field splitting causes anisotropy of the system. When the ground state is orbitally degenerate, such as the $T$ state in $O_h$ symmetry, the spin-orbit coupling operator that transforms as rotation splits the degenerate spin microstates and the zero field splitting effect is large. If the ground state is orbitally nondegenerate, spin-orbit coupling working in concert with distortion of ligand field mixes orbitally degenerate excited state into the ground state. Thus, the components arising from the ground state are stabilized through the ground-state/excited-state interactions. The above discussion is shown in Figure 1-3.[11]

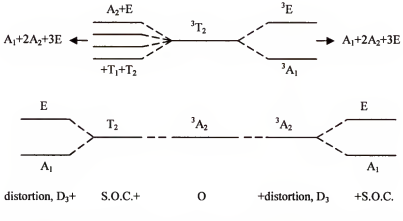


Figure 1-3. Zero-field splitting of the ground state and the first excited state for an Ni(II) ion in a trigonally distorted octahedral environment. S.O.C. is spin-orbit coupling.

If the system has an odd number of unpaired electrons, the spin degeneracy cannot be completely removed in zero magnetic field. If the crystal field symmetry is low enough, every level will retain at least two-fold spin degeneracy called Kramers doublets that can be further resolved by an external magnetic field. For a system with an even number of unpaired electrons, the spin degeneracy may be completely removed by a low-symmetry ligand field so that only singlet levels remain with the ground state being $J = 0$. Then the energy separations may be so large that EPR transitions would not be observed in the microwave region. The zero-field splitting is expressed by the phenomenological Hamiltonian [11]

$$\boldsymbol{H}_{ZFS} = \boldsymbol{S}\cdot\boldsymbol{D}\cdot\boldsymbol{S} \tag{1-28}$$

where $\boldsymbol{D}$ is the zero-field splitting parameter and is a symmetric and traceless tensor. The total Hamiltonian that describes the single-ion behavior can be written as [11]

$$\begin{aligned}\boldsymbol{H} &= \beta\boldsymbol{S}\cdot\boldsymbol{g}B + \boldsymbol{S}\cdot\boldsymbol{D}\cdot\boldsymbol{S} \\ &= g_u\beta\boldsymbol{S}_uB_u + D[\boldsymbol{S}_z^2 - S(S+1)/3] + E(\boldsymbol{S}_x^2 - \boldsymbol{S}_y^2)\end{aligned} \tag{1-29}$$

if the $\boldsymbol{D}$-tensor and the $\boldsymbol{g}$-tensor are assumed to have the same principal axes. The first term on the right of Equation 1-29 is the Zeeman term.The index $u$ notes the direction of the applied magnetic field; $g_u$ is the value of $\boldsymbol{g}$ and $\boldsymbol{S}_u$ is the component of $\boldsymbol{S}$ along this direction. $D$ and $E$ are the axial and rhombic zero-field splitting parameters, respectively. In axially distorted systems, the rhombic term $E$ is zero.

In conclusion, single-ion anisotropy which is responsible for the deviation from the Curie law in a paramagnetic system may be caused by zero-field splitting or $g$-value anisotropy, both are consequences of one or a combination of more than one of the following factors: spin-orbital coupling, distortion of ligand field, low-symmetry lattice,

or thermal contraction on cooling, *etc*. These factors change the electronic structure of the magnetic ground state, and, in some cases, also introduce orbital angular momentum into the ground state so that the magnetic moment arising from the ground state is no longer a spin-only state.

## Interacting Systems

### The Curie-Weiss Law

In genuine paramagnetic system, magnetic moments do not interact even at $T = 0$ *K*. Such a system is the analogue of an ideal gas system and the Curie law that describes the magnetic behavior of such a system in the entire temperature range is the equivalence of the ideal gas law. However, in some systems, when the linear approximation ($B/kT$ is small) for the Curie law is violated; that is, when temperature is low or the field is high, magnetic moments on the neighboring ions start to interact with each other and the magnetic behavior of the sample begins to deviate from the Curie law. That is, the high-temperature magnetic behavior of such systems no longer obeys the Curie law, but a modified version called the Curie-Weiss law. This type of deviation from the Curie law is fundamentally different from that caused by the zero-field splitting effect. The mechanism of such interaction is called magnetic exchange and will be introduced in the next section. Magnetic exchange may or may not lead to a long range magnetic ordering, a three-dimensional magnetic phase transition. The deviation of the magnetically interacting systems from the Curie law at high temperatures can be described by the Curie-Weiss law as

$$\chi = C / (T-\theta) \tag{1-30}$$

where $\theta$ is the Weiss temperature. When $\theta$ is positive, the coupling between paramagnetic ions is ferromagnetic which corresponds to the parallel alignment of the

magnetic moments. If $\theta$ is negative, the coupling is antiferromagnetic and the magnetic moments are aligned antiparallel to each other. The magnetic interaction between paramagnetic ions can be treated as a perturbation added on to the Zeeman term. The total spin Hamiltonian with isotropic $\boldsymbol{g}$-tensor is [11]

$$\boldsymbol{H} = g\beta\boldsymbol{S}B - zJ\langle S\rangle\boldsymbol{S} \tag{1-31}$$

The first term on the right of Equation 1-31 is the Zeeman Hamiltonian and the second term accounts for the weak intermolecular interactions in which $\langle S\rangle$ is the mean value of $\boldsymbol{S}$, $J$ is the interaction parameter between two nearest neighbors, and $z$ is the number of the nearest neighbors for a given paramagnetic ion. The eigenvalues of Equation 1-31 are

$$E(S,M_s) = M_s(g\beta B - zJ\langle S\rangle) \tag{1-32}$$

where $\langle S\rangle$ is given by the Boltzmann distribution law

$$\langle S\rangle = \frac{\Sigma_{Ms} M_s \exp[-E(S,M_s)/kT]}{\Sigma_{Ms} \exp[-E(S,M_s)/kT]} \tag{1-33}$$

where the summation spans from $+S$ to $-S$. Using Equations 1-32 and 1-33, we can then write

$$\langle S\rangle = \frac{\Sigma_{Ms} M_s[1 - M_s(g\beta B - zJ\langle S\rangle)/kT]}{\Sigma_{Ms}[1 - M_s(g\beta B - zJ\langle S\rangle)/kT]} \tag{1-34}$$

where the summation runs from $+S$ to $-S$ and the exponential has been expanded to the first order. It follows that

$$\langle S\rangle = -S(S+1)(g\beta B - zJ\langle S\rangle)/3kT \tag{1-35}$$

$$= -[S(S+1)g\beta B]/[3kT - zJS(S+1)] \tag{1-36}$$

The magnetic moment for an electron with spin $s$ is

$$m = -g_e\beta s \tag{1-37}$$

For a polyatomic molecule, the magnetization may be expressed as

$$M = -Ng\beta\langle S\rangle \tag{1-38}$$

Such that the magnetic susceptibility can be expressed by using $\partial M / \partial B$

$$\chi = \frac{Ng^2\beta^2 S(S+1)}{3kT - zJS(S+1)} \tag{1-39}$$

and $\chi$ may be rewritten as

$$\chi = C / (T - \theta) \tag{1-40}$$

which is the form of the Curie-Weiss law introduced earlier with the Weiss temperature $\theta$ defined as

$$\theta = zJS(S+1)/3k \tag{1-41}$$

The comparison of the Curie law and the Curie-Weiss law are compared in Figure 1-4. When the magnetic interactions are weak, in order to make it easier to visualize the interactions, the magnetic susceptibility *vs.* temperature plot is frequently converted to plots of inverse susceptibility *vs.* temperature or plots of the product of susceptibility and temperature as a function of temperature. The type and strength of the interaction are reflected by the sign and the value of the Weiss temperature obtained from the inverse susceptibility *vs.* temperature plot as the intercept with the temperature axis.

**Magnetic Exchange**

The process through which magnetic ions interact with each other is called magnetic exchange interaction, or, simply, exchange. Exchange interaction is electrostatic in nature and the effect is essentially the formation of weak bond between interacting magnetic moments, an intermediate situation between bonding and nonbonding.

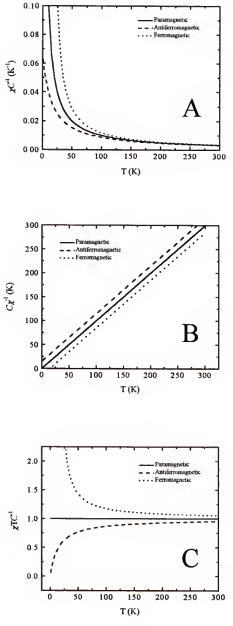


Figure 1-4. Plots of Curie (solid line) and Curie-Weiss behaviors of an $S = 1/2$ system. (A) $\chi / C$ vs. $T$, (B) $C / \chi$ vs. $T$, and (C) $\chi T / C$ vs. $T$. The dotted lines represent ferromagnetic coupling ($\theta = 15$ K) and the dashed lines represent antiferromagnetic coupling ($\theta = -15$ K). The susceptibility is normalized by division by the Curie constant, $C$.

Possible origins of magnetic exchange process include (1) the overlap of orthogonal orbitals, which obeys the Hund's rule and leads to ferromagnetic

Interactions; (2) intramolecular or intermolecular configuration interaction leading to ferromagnetic or antiferromagnetic interactions depending on the orbitals involved; and (3) the through-space dipole-dipole interaction leading to ferromagnetic or antiferromagnetic interactions depending on the geometrical relationship of the interacting magnetic ions. Although exchange refers to interactions among the nearest neighbors, the interactions may spread over quite a long distance in a crystalline lattice to induce magnetic ordering. The exchange interaction can be anisotropic since zero-field splitting also operates in concert with exchange in a magnetically interacting system. The anisotropy of individual ions is retained in cooperative exchange interactions. It leads to anisotropic magnetization, and determines whether or not long-range ordering is possible. Exchange has its quantum mechanical origin in the electronic repulsion and the Pauli principle.

Let's consider the simplest situation in which two atoms each having one unpaired spin form a bond. If the bonding is strong, the possibility of having the two electrons with parallel spins is very low. The result is a spin-singlet state corresponding to the pairing of the spins on the two electrons to satisfy the Pauli principle. The excited state refers to the promotion of one electron into a higher energy level and is a spin-triplet state based on the Hund's rule. The singlet/triplet energy separation is much larger than the thermal energy $kT$ at room temperature. However, when the bonding is weak, the energy separation between the singlet and the triplet states decreases, and eventually becomes comparable to the magnitude of $kT$. When two metal ions interact through a bridge, the local spins $S_A$ and $S_B$ are no longer good quantum numbers. The spin states of the pair should now be defined by the total spin quantum number $S$ according to

$$\left| S_A - S_B \right| \leq S \leq S_A + S_B \tag{1-42}$$

According to the Clebsch-Gordon series, total spin quantum number can be obtained for situations where multiple spins are present on each magnetic ion. There are basically two types of exchange interactions; direct exchange and indirect exchange. Direct exchange refers to the situation in which the coupled spins on two ions or molecules are very close and there is a significant overlap between their wavefunctions. Indirect exchange operates when the coupled spins are separated over a large distance and interact only through a nonmagnetic intermediary. As far as our studies are concerned, the nonmagnetic intermediary can be an atom, an ion, or a molecule, and the coupling is known as superexchange which is the most important interaction mechanism for transition metal complexes. In the simplest case of two coupling magnetic ions each having only one unpaired electron *i.e.*, a spin-only doublet ground state without first order orbital angular momentum, the totally isotropic interaction that involves all three components of the interacting spin angular momenta $\boldsymbol{S_A}$, and $\boldsymbol{S_B}$, is often described by the phenomenological HDVV (Heisenberg-Dirac-Van Vleck) Hamiltonian [11]

$$\boldsymbol{H} = -J\,\boldsymbol{S_A}\cdot\boldsymbol{S_B} \tag{1-43}$$

where $J$ is the isotropic exchange parameter and its absolute value is the energy separation between the singlet state ($S=0$) and the triplet state ($S=1$). Possible perturbations to this Hamiltonian are spin-orbit coupling and antisymmetric exchange among others. Equation (1-43) is a simplified form of a more general expression of isotropic-magnetic exchange interaction

$$\boldsymbol{H} = -\Sigma J_{ij}\,\boldsymbol{S_i}\cdot\boldsymbol{S_j} \tag{1-44}$$

where the sum is taken over all pair-wise interactions of spins *i* and *j* in a lattice. There are different conventions regarding the sign and the value of *J*. As written in Equation 1-43, negative *J* represents antiferromagnetic coupling, and positive *J* indicates ferromagnetic coupling. If there is no negative sign in front of *J* in Equation 1-43, the interpretation is then reversed. Sometimes, different forms of the Hamiltonian are used with or without a coefficient of *2* in front of *J*. Figure 1-5 shows several types of interactions between magnetic moments in a lattice.

Paramagnetism refers to the situation in which all the magnetic moments are oriented randomly to each other so that all the moments cancel each other and result in zero net moment. Ferromagnetism is the basis for any practically useful magnet in which all the moments are parallel to each other and point to the same direction. A net magnetic moment is then obtained. Both ferrimagnetism and canted antiferromagnetism (weak ferromagnetism) are special cases of antiferromagnetism.

Antiferromagnetism arises when all the moments are parallel to each other but each pointing to the opposite direction with respect to all its neighboring moments. The result is zero net moment. However, if the antiferromagnetically coupled moments have different magnitudes, the magnetic moments can not completely cancel each other out and a net magnetic moment is obtained. This situation is called ferrimagnetism. Another scenario is when the individual moments form an angle between each other (spin canting) rather than being perfectly parallel to each other. In this case, magnetic moments again do not cancel completely and a weak net moment is possible. This is called canted antiferromagnetism or weak ferromagnetism.

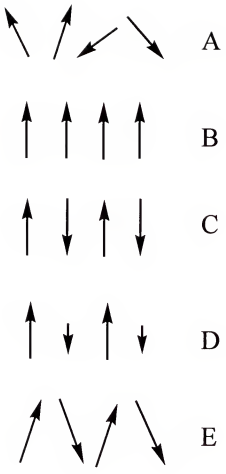


Figure 1-5. Spin angular momentum vectors. The interactions between the magnetic moments are (A) paramagnetic, (B) ferromagnetic, (C) antiferromagnetic, (D) ferrimagnetic, and (E) canted antiferromagnetic (weak ferromagnetic).

The exchange interaction described by Equation 1-44 is isotropic in which all the spin components are involved in exchange. As a consequence of single-ion anisotropy, there are situations where not all spin components participate in exchange. We use the concept of spin dimensionality to indicate the number of spin components that participate in exchange interactions. This can be conveniently explained by using the following Hamiltonian [11]

$$\boldsymbol{H} = -J\Sigma\,[a\,\boldsymbol{S}_i^z\,\boldsymbol{S}_j^z + b(\boldsymbol{S}_i^x\,\boldsymbol{S}_j^x + \boldsymbol{S}_i^y\,\boldsymbol{S}_j^y)] \qquad (1\text{-}45)$$

where the sum extends over all nearest neighboring spins with $i \neq j$ and $J$ is the exchange parameter. When $a = b = 1$, the interaction is fully isotropic and all spin components participate in the exchange interactions. This is called the Heisenberg model. If $a = 1$ and $b = 0$, the resulting Hamiltonian is the Ising model in which only spin component along one particular direction is involved in exchange. When $a = 0$ and $b = 1$, the result is the XY model with the exchange interaction being constrained in a given plane. So the spin dimensionality of the Heisenberg, the XY, and the Ising model is 3, 2, and 1, respectively.

**Magnetic Ordering**

It is necessary to distinguish exchange interaction from magnetic ordering. As stated earlier, although exchange is the basis for any possible long-range magnetic ordering, exchange only refers to short range interactions and does not necessarily lead to magnetic ordering which is a three-dimensional magnetic phase transition characterized by distinctive specific-heat behavior. In magnetically ordered systems, the coupling of magnetic ions must extend over a relatively long distance. This distance is called correlation length and it tends to infinity at the critical temperature obtained from the specific-heat measurement. A true magnetic ordering is a thermodynamically spontaneous process. In the case of ferromagnetic ordering, as temperature is lowered, magnetic moments are spontaneously aligned parallel to their nearest-neighbors as a result of exchange and many small magnetic domains start to form in the sample. The magnetic moments within each domain are parallel to each other and give rise to a nonzero net magnetic moment. This is called spontaneous magnetization. However, dipole-dipole interactions orient different domains in a random fashion so that the magnetic moments arising from all the domains cancel out with each other, and the net

moment of the entire sample is zero. The boundary between domains is known as the domain wall. To align all the domains to the same direction, an external magnetic field is needed. This field is frequently weak and has little impact on the spontaneous magnetization inside each domain. However, as a field is applied, the domains whose moments are parallel with the field will grow at the expense of a neighboring domain as the spins within the domain wall gradually align with the field. This alignment with the field propagates in the domain wall from one spin to another, and the domain wall gradually disappears and all the small domains eventually combine into one large domain. The entire sample is then magnetized and the magnetization acquired is the saturation magnetization. The description of the magnetic domains also applies to antiferromagnetic ordering. However, in antiferromagnetic ordering, there is no spontaneous magnetization since the spins in each domain are antiparallel to each other and the net moment is zero. Antiferromagnetic ordering can be viewed as two identical interpenetrating ferromagnetic sublattices with the same magnetization but opposite directions.[29] The magnetic susceptibility of a single crystal in antiferromagnetic state is highly anisotropic. That is, magnetization obtained when an external field is applied parallel to the sublattices' magnetic moments is different from the one obtained when the field is applied perpendicular to the sublattices' magnetic moments.

**Synthesis and Structural Aspects of Low-Dimensional Coordination Polymers**

Coordination polymer, also known as metal-organic coordination networks or metal-organic frameworks, are metal-organic compounds that extend infinitely into one, two or three dimensions *via* covalent metal-ligand bonding.[30-33] In the solid state, the extended polymeric structures, whether they are one-dimensional chains,

two-dimensional sheets, or interdimensional structures such as ladders, are held together by intermolecular forces, such as hydrogen-bonding, Van der Waals forces, and $\pi$-$\pi$ stacking interactions. These intermolecular forces generally have weaker strength compared to the covalent bonding within the extended networks. Both the covalent linkages provided by various multifunctional organic ligands and the intermolecular forces can propagate magnetic exchange interactions between paramagnetic transition metal ions. This is an important point because it determines the temperature range where true low dimensional magnetic properties may be observed. At high temperatures, only the exchange pathways that strongly couple the metal ions are important. As temperature is lowered, weaker magnetic couplings between individual clusters, chains, sheets, or ladders propagated through intermolecular forces also become important and compete with the magnetic couplings within the extended networks, leading the magnetism toward three-dimensional behaviors. However, depending on the nature and the relative orientations of the orbitals involved, a stronger covalent linkage is not necessarily a more efficient pathway of transmitting magnetic coupling than a weaker intermolecular interaction. In true low-dimensional magnetism, only the short-range magnetic coupling within the nearest-neighbors is important, magnetic long-range ordering is impossible or observed only at 0 K depending on the lattice dimensionality of the structure and the spin dimensionality of the transition-metal ions involved.

Making a supermolecule is like constructing a building, which starts with bricks as subunits, and cement as a linker. These two components are put together first to form a wall, and eventually to an entire building. In chemistry, the synthesis of coordination polymers is a major task in the field of crystal engineering. The general principle of

crystal engineering is that the driving force for the crystal formation is self-organization. Coordination polymers are currently synthesized based on the self-assembly principle in which individual molecular building blocks are dissolved in solution phase, and, *via* the connections provided by organic linker molecules, self-assemble into targeted extended structures. Chemists have only very limited understanding of the mechanism of the self-assembling process. The state-of-art in 1988 was described by J. S. Maddox [34] as: " it remains one of the continuing scandals in the physical sciences that it remains impossible to predict crystalline architecture from a knowledge of chemical composition." This statement remains largely true today. Nonetheless, the self-assembling process has perfected in nature where simple molecular building blocks self-assemble with lock-and-key precision into complicated structures such as proteins, enzymes, cell membranes, and eventually, life. Despite the difficulties, more and more knowledge has been accumulated to better control the structures of the final synthetic results. There are three strategies [31] that have thus far been successfully applied: (1) a simple extension of transition-metal or metal-cluster coordination geometry by exploiting linear bifunctional ligands. The metal moiety acts as a node which defines the overall network geometry of the coordination polymer. Such a strategy would be expected to afford any of the architectures illustrated in Figure 1-6 and all these motifs have now been realized;[31] (2) use of exodentate multitopic ligands which also act as nodes in the architecture of the resulting coordination polymers; (3) use exodentate ligands as nodes and metal ions as spacers. This model is limited by the small number of transition metal ions that can adopt linear coordination geometry.

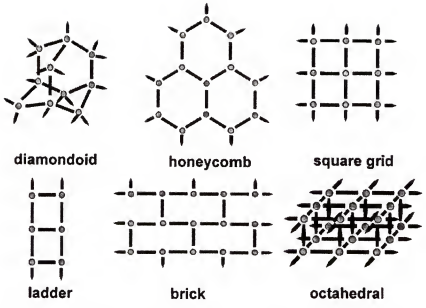


Figure 1-6. Various topologies obtained using bifunctional ligands and spacers. The metal ions are the nodes of the resulting network. The dots represent metal complexes (nodes) and the sticks represent bridging ligands which can be organic molecules or transition metal complexes.

The molecular building blocks are prepared by reacting selected transition-metal ions with multidentate organic ligands so that certain coordination sites on the metal ion are blocked while others remain open for subsequent reactions with the bridging ligands. The geometry of so produced molecular building blocks determines how the supramolecular structure is going to extend. The most commonly used organic bridging ligands (spacers) are simple organic molecules based on bifunctional exodentate nitrogen donors such as pyrazine, 4,4'-bipyridine, and 2,2'-bipyrimidine, among others. Some blocking ligands can also simultaneously serve as bridging ligands. The number of organic ligands that can be used as blocking and/or bridging ligands is, practically speaking, unlimited. Organic molecules designed for specific blocking and/or bridging coordination modes can always be synthesized as needed.

Many possible structures can be synthesized by polymerizing the metallic

centers (nodes) and bridging motifs. Several factors can be used to control the outcome. The importance of the node to spacer stoichiometry in determining the architecture is crucial. The coordination geometry at the metal centers can vary significantly, but, if the stoichiometry remains constant, the architecture of the final coordination polymer is likely to remain unchanged. For example, one-dimensional polymers can be observed for nodes of any of the following geometries: linear, T-shaped, square planar, trigonal bipyramidal, or even octahedral. Indeed, even geometries like trigonal and tetrahedral are capable of one-dimensional chains. The key requirement for the formation of one-dimensional structures is quite simple: the ratio of the metal to the bifunctional bridging ligand should be 1:1. Lower ratios afford discrete clusters (0-D), while higher ratios afford higher dimensional structures. However, a given stoichiometry can afford different types of extended structures. This is called polymorphorism.[31] For example, a metal to ligand ratio of 1:1.5 may not always give rise to ladder-like structures, brick wall and herringbone structures are also possible. Another very important factor that affects the formation of a particular polymeric structure is the choice of guest molecule. In the extended supramolecular structures, there is frequently empty space inside and between the covalent networks. Most of the structures require such void space be occupied by guest molecules in order to crystallize. If the guest molecules of the right size and shape are not available to match the empty space in a targeted extended structure, that structure may not form. The guest molecules can be solvent molecules if the network is neutral. If the network is charged, then counter ions are required to balance the charge. In this case, the counter ions are the guests. The commonly used counter ions include cations such as tetraphenylphosphonium $PPh_4^+$, tetramethylammonium and its analogues, anions such as

halides, $NO_3^-$, $ClO_4^-$, $BF_4^-$, $PF_6^-$, $CF_3SO_3^-$, $N_3^-$, *etc.* The guest molecules or ions reside inside the cavities within the networks, or situate themselves in between the chains, sheets, or ladders in the crystal structure. In some structures, the guest molecules can move in and out the structure while the integrity of the network structure is retained. This important behavior makes these structures especially suited for hydrogen storage and catalysis because the surface area provided by the void space can be enormously large and the efficiency of storage and catalysis may be very high. As far as magnetism is concerned, the presence or absence of guest, and the type of guest molecules can determine how the extended networks pack themselves in the crystals, and this may affect the magnetic exchange interactions.

Experimentally, besides the organic and organometallic syntheses that provide the basic ingredients for the synthesis of extended coordination polymers, the final self-assembling process, or the crystallization, is crucial. In the most ideal scenario, prefabricated molecular building blocks and the bridging molecules can both be dissolved in the same solvent or in different but miscible solvents, then the solutions are mixed together, and the extended structure slowly forms and crystallizes out as single crystals. However, since the final products have polymeric structures, the solubility is low in most solvents. Frequently, as the individual solutions of the starting materials are mixed together, the polymeric product immediately precipitates out as powder, making it impossible to extract structural information through X-ray diffraction experiments. Carefully choosing the right solvent may solve this problem. However, sometimes the powder precipitation is a result of the lack of balance between the kinetics of the chemical reaction and the kinetics of the crystallization process. Polymerization reaction

occurs too fast before the product can crystallize. If the formation of the extended structure can be slowed down and becomes comparable with the crystallization process, single crystals may be obtained. To solve this problem, a useful method is to let the solutions of the starting materials slowly diffuse into each other. A typical way to do this is to use a U-shaped tube with openings at both ends. Then, the solutions of the two reactants are added separately from the two ends. Normally, before the solutions are added, the tube is already filled with a pure solvent or agar serving as the intermediary to dilute the reactant solutions. At the interface where the solutions meet, the concentration of the reactants would be so low that no immediate precipitation would occur, and over the time crystals slowly form as the polymerization reaction proceeds very slowly. The limitation of such method is that at the interface the original stoichiometry is lost and the synthesis can no longer be motivated toward the designed structure by the stoichiometry. Also, the relative concentrations of the two reactants at different locations inside the U-tube are different due to different diffusion rate of the different molecules. The result is the formation of crystals of different identities in the U-tube, which are sometimes difficult to separate. The situation is worse if more than two reactants are used. Opposite situations also exist where the solvent dissolves the extended structure very well and no crystals can be obtained. In this case, the solution containing the reactants may be layered on top of a solvent that poorly dissolves the coordination polymer, such as hexane, so that single crystals would start growing at the interface and extend into the lower phase.

Finally, an invaluable and inexhaustible information source for the design and analysis of crystal structures is the Cambridge Crystallographic Data Center (CCDC). This database currently contains more than 290,000 crystal structures that include all

known organic structures and most of the inorganic structures. It enables structures to be visualized and examined in detail for structural and functional features.

**Spin-Ladder Systems**

A spin-ladder is a system having dimensionality between 1-D and 2-D. It is named ladder because the unique pattern of the magnetic couplings in such a structure can be visualized to resemble the shape of a ladder. Structurally, a ladder-like system as shown in Figure 1-6 may be viewed as two one-dimensional chains joined together through linear bidentate ligands that provide the rungs of the ladder, or viewed as a series of dimeric structures stacked on top of each other through either covalent linkages or intermolecular forces. Of course, other synthetic routes toward a ladder also exist. The spin carriers in the structure are transition-metal ions located at the intersections (nodes) of the legs and the rungs. Only the spin-ladders in which all the spin carriers are coupled antiferromagnetically are of interest in our study due to their potential implication to the mechanism of high-temperature superconductivity. From a physical point of view, a spin- ladder is a system where the magnetic couplings between the spin carriers along the legs ($J_{//}$) and along the rungs ($J_{\perp}$) are of comparable magnitudes, $0.1 \leq J_{\perp}/J_{//} \leq 10$, and the magnetic interactions between ladders should be negligiblecompared to those within individual ladders.[35] This criterion demands that in the solid state the individual ladders should be isolated from each other and no interpenetration between ladders should occur because, otherwise, interladder magnetic interactions interfere with those within individual ladders and spin-ladder behavior may not be observed. However, as can be seen later, this criterion is difficult to fulfill since it is natural for interpenetration to occur in the solid state so that empty space in the crystal lattice can be minimized. Also, in a spin-ladder system, a finite amount of energy is required to promote the system from its

spin-singlet ground state to the first excited state corresponding to the reversal of the spin orientation on one spin carrier. This energy gap is called spin gap. These situations are illustrated in Figure 1-7. [35, 36]

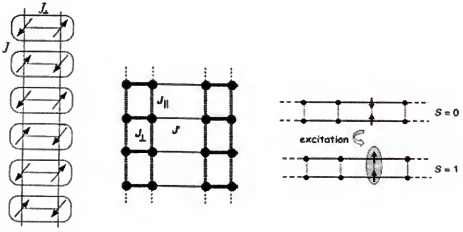


Figure 1-7. Ladder-like structure and spin gap. (Left) an illustration of a spin-ladder with an antiferromagnetic ground state. (Middle) the interactions between neighboring ladders should be negligible. (Right) spin gap in a spin-ladder system.

Although, synthetically, the only way to approach a spin-ladder system is to actually build a ladder-like structure; magnetically, a true spin-ladder system may not possess a ladder-like structure at all. An example of this will be presented below. Actually, in a covalent coordination polymer system, individual ladders are frequently associated with one another through various types of intermolecular forces provided by closely related organic ligands or counter ions which also propagate exchange interactions between ladders so that ladders are no longer magnetically isolated from each other although they are physically isolated in the crystal structure.

The interest in spin-ladders originated from the discovery of high-temperature superconductivity in some highly doped cuprates in 1986 by Bednorz and Müller.[1] Cuprates are compounds that have been known for many decades before such an exciting

property was observed among them. The structure of a doped superconducting cuprate is shown in Figure 1-8.[2, 3] The parent cuprate is an insulator having an antiferromagnetic spin-liquid ground state. Upon doping, the antiferromagnetic coupling disappears and the ground state becomes superconducting. Although the mechanism of such behavior is still under active investigation, it has been related to the antiferromagnetic coupling between the Cu(II) ions in the two-dimensional copper oxide network containing ladder-like structures. The magnetic couplings in a spin-ladder are only between the nearest neighbors so that the ground state is a spin-liquid state rather than an ordered state. So, to fully identify a spin ladder system, in addition to the characterization of macroscopic magnetic properties, the microscopic characterizations, such as neutron scattering and NMR experiments, are crucial to confirm that the ground state is not an ordered state and does fit into a ladder model.

The observed superconductivity in the doped cuprates very much resembles the theoretical predictions made for doped ladder-like structures.[3, 4] Therefore, many cuprates have been revisited in order to characterize their ground states and study their behavior upon doping.[37-43] However, to date, only one example has been identified as a potential spin ladder since its microscopic behavior is yet to be characterized.[44] The compound is bis(piperidinium)tetrabromocuprate(II),[45] also referred to as BPCB. Its structure is shown in Figure 1-9.

The structure of BPCB is not apparently ladder-like. Instead, the basic structural units are monomeric complexes, copper(II) tetrabromide, $[CuBr_4]^{2-}$. In the solid state, the through-space interactions between the bromide ions provide the exchange pathways that couple the Cu(II) ions, so that a ladder-like structure can be imagined to be running along

the crystal *a* axis. The ladders are both physically and magnetically isolated from each other. The magnetic properties of BPCB are reproduced in Figure 1-10.[44] The $\chi$ *vs T* plot shows antiferromagnetic coupling in the ground state and the plot has been fitted to a $S = 1/2$ spin ladder model. The results of the fitting of the $\chi$ *vs T* plot indicate that the coupling constant for the exchange along the rungs, $J_{\perp}$, is 13.3 K; the coupling constant for the exchange along the legs, $J_{//}$, is 3.8 K. So the ratio of these two coupling constants is well within the range for a spin ladder system. At 0.7 K, the magnetization remains zero up to 5 tesla before it starts increasing with the field indicating the existence of a spin gap. The fitting of the *M vs H* data reveals the spin gap is 9.5 K. The microscopic characterization of BPCB is ongoing.

Several other cuprates and metal oxides possessing ladder-like structures have been investigated but were eventually disproved as spin ladders on the ground of microscopic characterizations data.

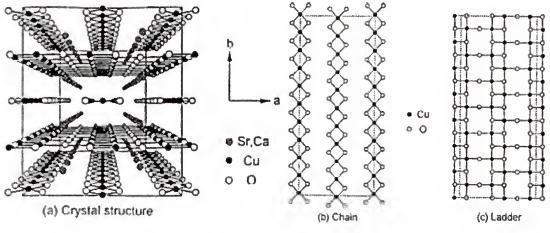


Figure 1-8. Structure of a superconducting cuprate, $(Sr, Ca)_{14}Cu_{24}O_{41}$. (a) is the crystal structure of the cuprate. (b) and (c) show the $CuO_2$ chain and $Cu_2O_3$ ladder subunits, respectively.

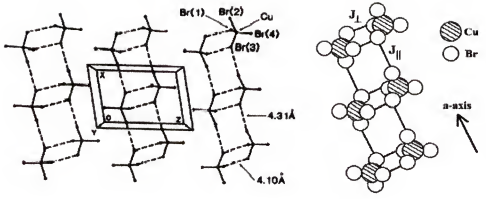


Figure 1-9. Crystal structure and the exchange pathways in BPCB.

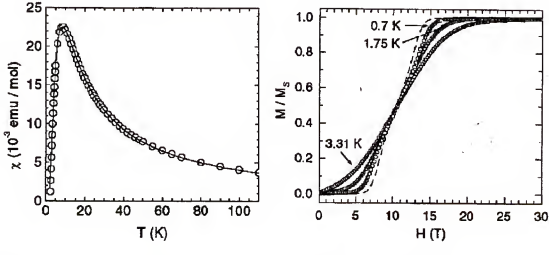


Figure 1-10. Plots of $\chi$ *vs* $T$ and $M$ *vs* $H$ for a powder sample of BPCB.

One example is $Cu_2$(1,4-diazacycloheptane)$_2Cl_4$, also known as CuHpCl, which has a ladder-like structure based on stacking Cu(II) dimers. Microscopic evidences show that its ground state is a dimerized state not a spin-ladder state.[41-43] Another example of a cuprate possessing a ladder-like structure is $LaCuO_{2.5}$. Its ground state has been characterized by $^{63}$Cu NMR and $\mu$SR experiments to be a magnetically ordered state instead of a spin-liquid state.[38] $(VO)_2P_2O_7$ also has a ladder-like structure comprised of $V^{4+}$ ions covalently bridged through $O^{2-}$ ions. It had been regarded as a true spin-ladder

system, but, after more than 10 years since its discovery, was finally identified to be an alternating chain system.[46-48]

In addition to cuprates, new examples of coordination polymers possessing ladder-like structures are also being reported. However, to date, only two examples present isolated noninterpenetrating ladders,[49, 50] while all the other examples are consisted of ladder-like structures interwoven with one another to minimize the void space in the crystal structures. Both of these two examples of isolated noninterpenetrating ladders have been magnetically characterized and neither is a spin-ladder system. One of them has been reported by Kahn *et al.* to exhibit ferromagnetic long range ordering.[50] The other one,[49] a paramagnetic system, will be presented later in Chapter 5. The ladder-like structure that was reported by Kahn *et al.* is $Gd^{III}_2[Cu^{II}(opba)]_3 \cdot 6DMSO \cdot 4H_2O$, where opba stands for *ortho*-phenylenebis(oxamato). The structure of $[Cu^{II}(opba)]^{2-}$ is shown in Figure 1-11.

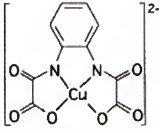


Figure 1-11. Structure of $[Cu^{II}(opba)]^{2-}$, a bisbidentate molecular building block.

This material was synthesized as single crystals by slow diffusion in a H-shaped tube at room temperature of equimolecular ($2.5\times10^{-4}$ mol) aqueous solutions of prefabricated $Na_2[Cu^{II}(opba)] \cdot 6H_2O$ and $GdCl_3 \cdot 6H_2O$ for 2 months. The crystal structure contains isolated noninterpenetrating ladders with Gd(III) as the nodes bridged through bisbidentate $[Cu^{II}(opba)]^{2-}$ ions both along the two legs and along the rungs.

Each Gd(III) is thus coordinated to six oxygen atoms belonging to three opba molecules. The ladder structure is shown in Figure 1-12.[50]

The average distance between two Gd(III) ions across a copper ion within a ladder is 11.1 Å. The shortest distance between two Gd(III) ions (9.8 Å) involves two isolated Gd(III) ions belonging to two neighboring ladders.

Magnetically, this material does not exhibit spin-ladder behavior. Instead, magnetic susceptibility measurement has shown that the exchange interaction between Gd(III) and Cu(II) is ferromagnetic, and a phase transition to a ferromagnetically ordered state is evidenced by a peak observed just below 2 K in the specific heat measurement. Given the fact that there is not any direct contact between neighboring ladders to provide interladder exchange pathway, the authors have attributed the onset of long range ordering to the dipolar interactions between Gd(III) ions belonging to neighboring ladders.

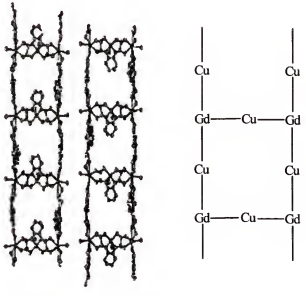


Figure 1-12. Ladder-like structure of $Gd^{III}_2$ $[Cu^{II}(opba)]_3 \cdot 6DMSO \cdot 4H_2O$.

CHAPTER 2
SYNTHESIS, STRUCTURE AND MAGNETIC PROPERTIES OF A CHARGE TRANSFER SALT, FERRICENYL(III)TRIS(FERROCENYL(II))BORATE, REVISITING AN OLD CASE

Ferricenyl(III)tris(ferrocenyl(II))borate ($Fc_4B$), **1**, was first discovered in 1979 as the by-product obtained from the synthesis of tris(ferrocenyl(II))borane.[51] The already available but unpublished data indicate that this material may have some very unusual magnetic properties as evidenced by the fluctuations of the $\chi T$ and $\chi^{-1}$ values as temperature decreases.[52] However, these observations have neither been confirmed nor further investigated. In this chapter, new evidences are presented and disprove the previous observations and explanations are given to account for the paramagnetic nature of $Fc_4B$.

**Introduction to Molecular Magnets Based on Ferrocene and Its Derivatives**

In the rapidly growing field of molecule-based magnetic materials, a breakthrough was made in 1986 when Miller *et al.* reported the preparation and characterization of the first ferromagnetically ordered molecular material, $[Fe(Me_5C_5)_2][TCNE]\cdot MeCN$.[53] This charge transfer salt was obtained at – 30 $^0$C as dark green needles by a simple reaction in acetonitrile between decamethylferrocene(II) and tetracyanoethylene that plays the role of electron donor (D) and acceptor (A), respectively. The solid structure of $[Fe(Me_5C_5)_2][TCNE]\cdot MeCN$ consists of alternating radical cation $[Fe(Me_5C_5)_2]^{\bullet +}$ with *S=1/2* and radical anion $[TCNE]^{\bullet -}$ with *S=1/2* units forming one-dimensional chains with . . . $D^{\bullet +}A^{\bullet -}$ $D^{\bullet +}A^{\bullet -}$ $D^{\bullet +}A^{\bullet -}$. . . arrangement. There are two pairs of chains in one unit cell. In one pair of chains, the two chains are out of registry, that is the cation of

one of the two chains has the anion of the other chain as the nearest neighbor. While in the other pair, the two chains are in registry. This situation is shown in Figure 2-1.[54] The intrachain distance between two neighboring Fe(III) ions is 10.415 Å. The $[TCNE]^{\bullet -}$ is planar and lies in between two essentially parallel $Me_5C_5$ rings, and the separation between a $Me_5C_5$ ring and neighboring TCNE plane is 3.51 Å. The adjacent TCNE and $Me_5C_5$ planes are not rigorously parallel, making a dihedral angle of 2.8°. $[Fe(Me_5C_5)_2]^{\bullet +}$ with $e_{2g}^3$ ($d_{x2-y2}$, $d_{xy}$) valence orbitals has three electrons in doubly degenerate partially occupied molecular orbitals (POMO) *i.e.*, $d^3$, while $[TCNE]^{\bullet -}$ has one electron in a nondegenerate $\pi^*$ POMO *i.e.*, $s^1$.

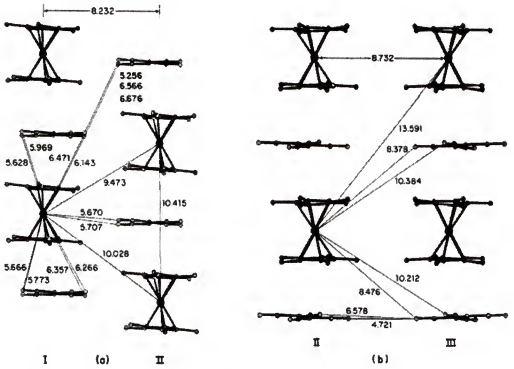


Figure 2-1. Chains of $[Fe(Me_5C_5)_2][TCNE]\cdot MeCN$. The out-of-registry chains I-II (a) and the in-registry chains II-III (b) with the intrachain and interchain Fe-N, N-N, and Fe-Fe distances.[54]

It should be noted that the acetonitrile-solvate is not the compound whose physical properties were investigated. This solvate easily loses its acetonitrile molecules with a transformation of the lattice from monoclinic to orthorhombic. The structure of the orthorhombic phase is strongly distorted and it has not been possible to refine it properly. All magnetic studies, however, were performed with this desolvated orthorhombic phase. The main properties of $[Fe(Me_5C_5)_2][TCNE]$ are displayed in Figures 2-2 and 2-3 for polycrystalline sample.[54]

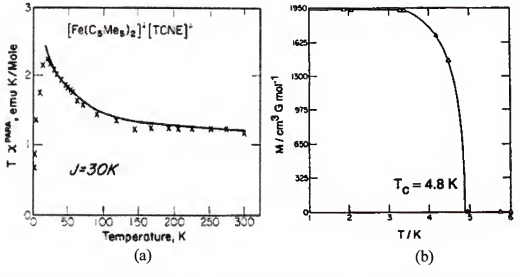


Figure 2-2. Magnetic properties of $[Fe(Me_5C_5)_2][TCNE]$. (a). The $\chi T$ *vs* $T$ plot fitted for a $S = 1/2$ 1-D Heisenberg model; (b). $M$ vs $H$ at 4.2 K.[54]

The magnetic susceptibility was measured on a polycrystalline sample using the Faraday technique between 1.7 K and 300 K and field between 300 and 80 kG. Above 60 K, the sample obeys the Curie-Weiss law with $\theta = 30$ K indicating dominant ferromagnetic interactions. This is also evidenced by the increase of the $\chi T$ value as temperature is lowered. Below 60 K, a substantial departure from the Curie-Weiss law is evident, and below 16 K the magnetization is no longer linearly proportional to the magnetic field. The temperature dependence of the magnetization of a polycrystalline

sample with only the magnetic field of the earth shows a break at $T_c = 4.8$ K, then saturates at a value close to $2 \times 10^3$ cm$^3$ G mol$^{-1}$ when cooling below $T_c$.

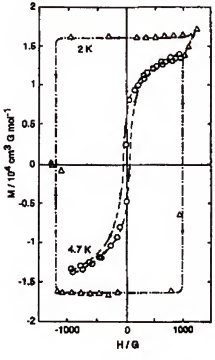


Figure 2-3. Magnetization hysteresis of [Fe(Me$_5$C$_5$)$_2$][TCNE] at 2 K.[54]

The magnetization of a single crystal at 4.2 K saturates at a value of $1.6 \times 10^4$ cm$^3$ G mol$^{-1}$ for a magnetic field parallel to the chain axis of a few tens of gauss. This value $M_S$ of the saturation magnetization is 36% greater than for iron metal on a per iron atom basis and agrees with the calculated saturation moment for ferromagnetic alignment of the donor ($S = 1/2$ , $g_{//} = 4$) and the acceptor ($S = 1/2$, $g = 2$). The magnetization versus field loop at 2 K shows a pronounced hysteresis with a coersive field of the order of $10^3$ G. All these experimental data are consistent with the following description of [Fe(Me$_5$C$_5$)$_2$][TCNE]. The $S = 1/2$ spins associated with both the donor and acceptor units are strongly coupled along the chains in a ferromagnetic fashion; the ferromagnetic chains are weakly coupled on the scale of the crystal lattice, again in a

ferromagnetic fashion. It results that the compound exhibits bulk ferromagnetic properties with a spontaneous magnetization below 4.8 K. The discovery of a ferromagnetic transition in $[Fe(Me_5C_5)_2][TCNE]$ provoked a great impulse among chemists working in the field of molecular magnetism, and soon after this discovery at least three novel decamethylmetallocenium charge-transfer salts ordering ferromagnetically were characterized. These are two decamethylmanganocenium derivatives, namely $[Mn(Me_5C_5)_2][TCNQ]$ (TCNQ = tetracyanoquinodimethane),[55] and $[Mn(Me_5C_5)_2][TCNE]$, [56] with $T_c$ = 6.2 and 8.8 K, respectively, and the chromocenium derivative $[Cr(Me_5C_5)_2][TCNE]$ with $T_c$ = 3.1 K.[57, 58] In addition, other decamethylmetallocenium derivatives were found to exhibit metamagnetic behavior, *i.e.,* stabilization of a ferromagnetic-like state when applying a magnetic field. This is the case for $[Fe(Me_5C_5)_2][TCNQ]$ and $[Mn(Me_5C_5)_2][M(tfd)_2]$,[59, 60] where M is Ni, Pd, or Pt, and tfd is bis(trifluoromethyl)ethylenedithiolato.

To understand the observed magnetic properties of $[Fe(Me_5C_5)_2][TCNE]$, there have been mainly two different points of views. McConnell proposed the configuration mixing mechanism for the stabilization of ferromagnetic coupling.[61, 62] This mechanism considers stacks of alternating donor cations and acceptor anions where either the donor or the acceptor, but not both, has a symmetry high enough to allow orbital degeneracy. The two situations to which McConnell explicitly referred are (1). $D^0$ is a triplet with two unpaired electrons occupying two degenerate orbitals, and $A^0$ is a closed-shell singlet; (2). $D^0$ is a closed-shell singlet, and $A^0$ is a triplet with two unpaired electrons occupying two degenerate orbitals. In both cases $D^+$ and $A^-$ are doublets and, if a $D^+A^-$ pair is singled out from the stack, the interaction within $D^+A^-$ gives rise to a low-lying

singlet and a low-lying triplet. Then, the coupling between the ground configuration $D^+A^-$ and the backward charge-transfer configuration $D^0A^0$ stabilizes the low-lying triplet, and therefore favors ferromagnetic coupling. Breslow reformulated McConnell's idea by assuming that $D^0$ and $A^0$ are such efficient donor and acceptor, respectively, that $D^{2+}A^{2-}$ is lower in energy than $D^0A^0$.[63] In other words, the forward charge transfer is favored with respect to the backward charge transfer. He then considered the following two situations: (1) $D^0$ is highly symmetrical, and has two orbitally degenerate HOMO's, and $A^0$, which has a lower symmetry, has a nondegenerate LUMO. The ground states of $D^+$ and $D^{2+}$ are then orbitally degenerate spin doublet and an orbitally nondegenerate spin triplet, respectively. Those of $A^-$ and $A^{2-}$ are an orbitally nondegenerate spin doublet and a closed-shell spin singlet, respectively, as

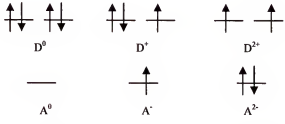


(2) $A^0$ is highly symmetric, and has two degenerate LUMO's, and $D^0$, which has a lower symmetry, has a nondegenerate HOMO, as

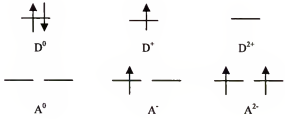


Due to the Hund's rule, in both cases the lowest state arising from $D^{2+}A^{2-}$ is a triplet and coupling between $D^{2+}A^{2-}$ and $D^+A^-$ stabilizes the triplet of lower energy. In an

infinitely long stack of donors and acceptors this would lead to one-dimensional ferromagnetic behavior. Extensive synthetic efforts were carried out by Breslow *et al.* to test this theory. However, no ferromagnetic interaction has ever been observed.[64-67] Based on the McConnell-Breslow mechanism, Miller *et al.* explained the ferromagnetic interaction in $[Fe(Me_5C_5)_2][TCNE]$ as following. The monocation $[Fe(Me_5C_5)_2]^+$ has $(a_1)^2(e_2)^3$ as the ground configuration with a local spin-doublet state, and the $[TCNE]^-$ has a singly-occupied antibonding $\pi^*$ orbital so that the local ground state is also a spin doublet. The interaction between the unpaired electrons of $D^+$ and $A^-$ leads to singlet and triplet states. It was also assumed that $D^{2+}A^{2-}$ was low enough in energy to interact with $D^+A^-$. The configuration of lower energy is $(a_1)^2(e_2)^2$ for $D^{2+}$ and $(\pi^*)^2$ for $A^{2-}$, which leads to a triplet state for a $D^{2+}A^{2-}$ pair singled out from the stack. The interaction between the two triplets, arising from $D^{2+}A^{2-}$ and $D^+A^-$, stabilizes the latter, which corresponds to a ferromagnetic interaction. However, this interpretation has been challenged by Kahn *et al.* [68, 69] who showed situations where the McConnell-Breslow mechanism does not operate. Actually, nothing proves that the $D^{2+}A^{2-}$ is lower in energy than $D^0A^0$. Two alternative mechanisms are provided by Kahn *et al.* to account for the ferromagnetic interactions in $[Fe(Me_5C_5)_2][TCNE]$. One possible mechanism involves the coupling between $D^+A^-$ and an excited configuration $D^0A^0$ corresponding to the electron transfer from $\pi^*$ of $A^-$ to $e_1^*$ of $D^+$. Such a transfer from a singly-occupied orbital of one unit to an empty orbital of the other unit favors ferromagnetic interactions. Another mechanism proposed by Kahn *et al.* is based on a spin-polarization effect. The unpaired electron of $[Fe(Me_5C_5)_2]^{+*}$ in a molecular orbital description is basically localized on the Fe(III), and significant negative charge is localized on the rings

according to configuration-interaction calculations. These predictions have been supported by NMR experiments. The ferromagnetic interactions along the stack of alternating donors and acceptors are then attributed to the coupling between the negative spin density on the pentamethylcyclopentadienyl rings and the positive spin density on the nearest-neighbor $[TCNE]^-$ units.

**Background Information on Ferricenyl(III)tris(ferrocenyl(II))borate**

Ferricenyl(III)tris(ferrocenyl(II))borate ($Fc_4B$) was first discovered in 1979 as the by-product obtained from the synthesis of tris(ferrocenyl(II))borane.[51] Research has shown that $Fc_4B$ is a zwitterion consisting of three ferrocenyl(II) and one ferricenyl(III) moieties covalently attached to a tetravalent boron atom as shown below in Figure 2-4.

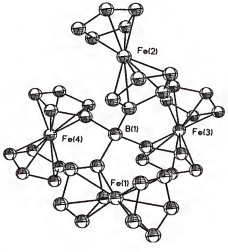


Figure 2-4. Molecular structure of $Fc_4B$.[51]

The low-spin iron(III) has one unpaired electron located in the $d_{xy}$ orbital which is degenerate with the doubly-occupied $d_{x2-y2}$ orbital and lies in the plane parallel to the two cyclopentadienyl rings. The magnetic moment lies parallel to the $C_5$ symmetry axis of ferrocene molecule. The bond length for the four boron-carbon bonds are found to

be 1.643, 1.650, 1.634, and 1.657 Å with the longest being that for ferricenyl(III) moiety. The material crystallizes out as black rectangular blocks and the crystal unit cell parameters are: $a = 17.224$ Å, $b = 11.444$ Å, $c = 15.547$ Å, $\beta = 94.50^{0}$, $Z = 4$, space group $P2_1/n$ (monoclinic).[1]

The already available data from magnetic studies on this material are given in Figure 2-5.[52] In weak magnetic fields of 20G, 100G, 400G, and 1000G, $\chi T$ value starts decreasing with temperature from 0.8 K $cm^3$ $mol^{-1}$ at 350 K to 0.73 K $cm^3$ $mol^{-1}$ at about 180 K. At 180 K, a sudden increase in $\chi T$ is observed and the $\chi T$ value reaches its maximum of 2.05 K $cm^3$ $mol^{-1}$ at about 130 K. As temperature is further lowered from 130 K, $\chi T$ quickly decreases to 0.6 K $cm^3$ $mol^{-1}$ as temperature approaches zero. The observed behavior is the same for all magnitudes of applied fields except that as the strength of the applied field goes up, the maximum value of $\chi T$ at 130 K decreases. The observed fluctuations of $\chi T$ values , seen as a decrease followed by a sharp increase and then another sharp decrease upon applied fields as temperature is lowered, is quite unusual. However, no further study on this behavior was pursued and the nature of these changes of $\chi T$ value remains unknown. Our goal is to carry out a series of experimental strategies to characterize the observed behavior and the function of the applied magnetic fields.

Several systems that display field-dependent magnetism behave similarly as $Fc_4B$. One example is a spin-flop system in its antiferromagnetic state. When the magnetic field applied parallel to the preferred axis increases, the moments opposite to the field start reversing their orientations until becoming aligned with the field and a ferromagnetically ordered state is achieved.

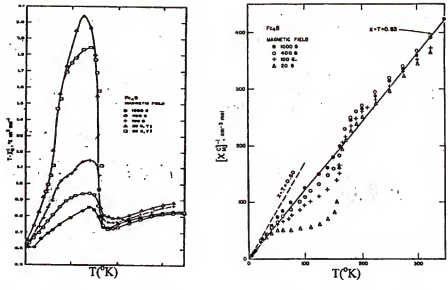


Figure 2-5. Plots of $\chi T$ *vs* $T$ and $\chi^{-1}$ *vs* $T$ for $Fc_4B$ under various magnetic fields (adapted from unpublished results).[52]

The spin-flop transition is observed at relatively low field. Another example is a metamagnetic system in which transition-metal ions are strongly coupled ferromagnetically to form a series of two-dimensional sheets which are weakly coupled antiferromagnetically. As temperature is lowered, the system exhibits ferromagnetic behavior due to the exchange coupling within individual sheets. At an even lower temperature, the net moments resulting from the ferromagnetic coupling in each sheets start coupling antiferromagnetically. Examples of a metamagnetic system include compounds such as $FeCl_2$, $(C_6H_{11}NH_3)CuCl_3$, $DyPO_4$, $CsCoCl_3 \cdot H_2O$, and $[Fe(\eta^5\text{–}C_5Me_5)_2]^{+\cdot}$ $(TCNQ)^{-\cdot}$.[54, 70-75] Systems with canted spins may also display transition from an antiferromagnetic state to a ferromagnetic state. As shown in Figure 1-5, in spin canting systems, the spins are coupled antiferromagnetically but with a small angle between the moments so that the moments cannot cancel completely. The result is a net moment is obtained. One example is $[Mn(4,4^{'}\text{–bipy})(N_3)_2]_n$.[76]

## Experimental Section

### Materials

Ferrocene, lithium chloride, mercury acetate, N-bromosuccinimide, *n*-butyllithium, diphenyl acetic acid, and tri-*n*-butylborate are purchased from Aldrich (Milwaukee, WI). Tri-*n*-butylborate is distilled, and diphenyl acetic acid is recrystallized from benzene before use. All other materials are used as received without further purifications. Dimethyl formamide, ethyl ether, and THF are freshly distilled before use.

### Synthesis of Chloromercuriferrocene

The synthetic procedure is adopted from that of Fish and Rosenblum.[77] At room temperature and under nitrogen atmosphere, 10.00 g (31.38 m mol) mercury acetate is dissolved in 96 ml absolute methanol and is then added dropwise to a three-neck round- bottom flask containing 11.82 g (63.53 m mol) of ferrocene dissolved in 64 ml of dried benzene. The mixture is then kept under stirring for 10 hours. Then, 2.794 g (0.066 mol) of lithium chloride dissolved in 13.72 ml of 1:1 ethanol/water mixed solvent is added dropwise to the flask at room temperature under stirring. The resulting yellow suspension is stirred for 2 hours at room temperature and then heated to reflux for 1 hour. The suspension is then collected by filtration, placed in a Soxhlet and extracted with methylene chloride. The methylene chloride extract is washed thoroughly with water and dried over magnesium sulfate for 20 minutes. Methylene chloride is then removed by using a rotatory evaporator. The solid residue is sublimed in vacuum using an oil bath at 110 $^0$C to remove unreacted ferrocene. 7.0 g of chloromercuriferrocnene is isolated as final product. $^1$H NMR: 4.108 (2H), 4.235 (5H), 4.473 (2H). Melting point: 196 $^0$C (literature value [77]: 196-198 $^0$C)

**Synthesis of 1-Bromoferrocene**

The synthetic procedure is adopted from that Fish and Rosenblum.[77] A solution of 0.6 g N-bromosuccinimide in 50 ml of dry and nitrogen-flushed dimethylformamide is added dropwise to a cold , stirred solution of 1 g of chloromercuriferrocene dissolved in 25 ml of the same solvent. Reaction is continued at 0 $^0$C under stirring and in a nitrogen atmosphere for 3 hours during which period the mixture turns into dark green solution. A 100 ml 10% sodium thiosulfate solution is then added to the solution dropwise and the resulting dark grey solution is stirred for 1 hour and poured onto 1 L of ice. The aqueous solution is extracted four times with 100 ml portions of low boiling point petroleum ether, and the combined organic extract is washed with water and dried over magnesium sulfate overnight. The petroleum ether is then removed using a rotatory evaporator and the product is recrystallized from cold ethanol. 400 mg 1-bromoferrocene is collected as the final product. $^1$H NMR: 4.101 (2H), 4.232 (5H), 4.417 (2H). Melting point: 32 $^0$C (literature value: [77] 31-32 $^0$C).

**Synthesis of Ferricenyl(III)tris(ferrocenyl(II))borate ($Fc_4B$), 1**

Under argon atmosphere, 2.36 ml (3.77 m mol) of *n*-butyllithium is added dropwise at −78 $^0$C to a three-neck round-bottom flask containing 1.00 g (3.77 m mol) of 1-bromoferrocene dissolved in 20 ml of dry ethyl ether. The reaction mixture is stirred at −78 $^0$C for 1 hour. Then, 0.255 ml (0.9434 m mol) of tri-*n*-butylborate is added dropwise at −78 $^0$C into the mixture which is then kept under stirring at −78 $^0$C for 1 hour. The yellow/brown mixture is then warmed to room temperature and kept under stirring for overnight, during which period the mixture turns to red/orange solution. Upon exposing to air, precipitation of black solid occurs. The mixture is stirred for an additional 20 minutes and is then filtered. The black solid thus collected is washed with

ethyl ether, yielding 150 mg of isolated product. This black material is then dissolved in minimum amount of methylene chloride and slow diffusion of ethyl ether into this methylene chloride solution affords black rectangular crystals which are collected as the final product, ferricenyl(III)tris(ferrocenyl(II))borate ($Fc_4B$). Single-crystal X-ray diffraction experiment shows the black crystalline material has the same unit cell parameters as published:[1] $a = 17.224(3)$ Å, $b = 11.444(2)$ Å , $c = 15.547(3)$ Å, $\beta = 94.50(1)^0$, $V = 3055.0$ Å$^3$, $Z = 4$; space group $P2_1/n$. Elemental analysis: calculated C: 63.98%, H: 4.83%, found C: 63.59%, H: 4.83%.

**EPR Measurements**

The EPR spectrum was recorded for a polycrystalline sample at room temperature with a Bruker ER 200D X-band (9 GHz) spectrometer modified with a digital signal channel and digital field controller.

**Magnetic Measurements**

Static-magnetization measurements were performed with a Quantum Design MPMS SQUID magnetometer. The sample was 98.4 mg of polycrystalline material placed in a plastic can that was held in a straw. The sample was zero-field cooled to 5 K before a measuring field was applied, and data were subsequently acquired up to 300 K. This procedure was repeated while cooling the sample in the presence of the measuring magnetic field. Two sets of data were acquired with the measuring field of 20 G and 100 G, respectively. Magnetization versus field measurements were performed at 5 K from 0 to 50 kG. The small background signals arising from the can and straw and the diamagnetic contribution were subtracted from the results.

## Results and Discussion

### Synthesis of $Fc_4B$

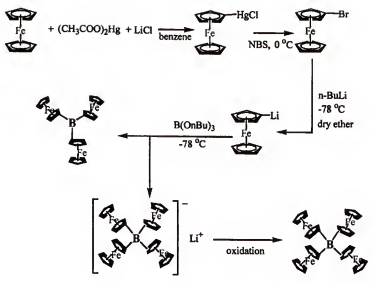


Figure 2-6. Synthetic route for $Fc_4B$.

The synthesis of $Fc_4B$ can be summarized in Figure 2-6. The conversion of 1-bromoferrocene to lithioferrocene is the key step in the synthesis of $Fc_4B$. *n*-butyllithium must be titrated by diphenyl acetic acid in dried THF every time before use to accurately determine its concentration. The *n*-butyllithium/tri-*n*-butylborate ratio is 4:1. However, since lithioferrocene is not stable and has to be used *in situ*, the determination of when tri-*n*-butylborate should be added is a problem. To solve this problem, the reaction is monitored by $^1H$ NMR to track the yield of lithioferrocene. To do this, a small sample of the reaction mixture containing 1-bromoferrocene, *n*-butyllithium, lithioferrocene, ethyl ether, and possibly other by-products is drawn out from the reaction vessel using a syringe several times as the reaction proceeds. The mixture is quickly blown to dryness by nitrogen and then treated with several drops of ethanol. Lithioferrocene reacts with ethanol and turns into ferrocene as $Li^+$ is such a strong

electrophile. 1-bromoferrocene remains unreacted with ethanol. Then a $^1$H NMR experiment is carried out for the resulting mixture. By monitoring the intensity of the ferrocene peak (4.170 (10H)) and those of 1-bromoferrocene (4.101 (2H), 4.232 (5H), 4.417 (2H)) as the reaction proceeds, the yield of lithioferrocene, and subsequently the timing for the addition of tri-*n*-butylborate, can be determined. Specifically, as the intensity of the 1-bromoferrocene peaks diminishes, we can assume *n*-butyllithium has completely converted to lithioferrocene and the yield of lithioferrocene is 100%. After the collecting of $Fc_4B$ by filtration, the red filtrate (ethyl ether solution) is concentrated to a small volume and added to cold methanol. The resulting red precipitation is collected by filtration and is characterized to be triferrocenyl(II)borate, a diamagnetic substance.

**Description of the Structure of $Fc_4B$**

$Fc_4B$ is a zwitterion with positively charged boron cation, three ferrocenyl(II) moieties, and one ferricenyl(III) moiety. In the solid state, $Fc_4B$ molecules are all isolated from each other with no apparently recognizable stacking pattern as shown in Figure 2-7. Seemingly one dimensional chains may be visualized running along both the crystal *b*-axis and *c*-axis. The Fe(III)-Fe(III) distances are shown in Figure 2-8.

**Magnetic Properties of $Fc_4B$**

The room-temperature X-band EPR spectrum is shown in Figure 2-9. Two resonance signals are observed, one at 3330 G ($g_{\perp} = 1.99$), and the other at 1580 G ($g_{//} = 4.19$) in good agreement with reported values for ferrocene. The $\chi T$ *vs* $T$ plot and the $\chi^{-1}$ *vs* $T$ plot are shown in Figures 2-10 and 2-11, respectively.

Based on the Curie law, the average $g$ value obtained from the measured $\chi T$ value at 300K, 0.47 emu K/mol and 0.535 emu K/mol for measuring field of 100G and 20G, respectively, is in the range of 2.24 ~ 2.39.

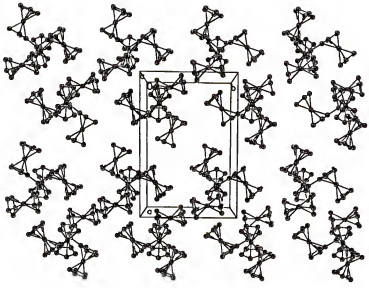

Figure 2-7. Packing diagram of $Fc_4B$.[51]

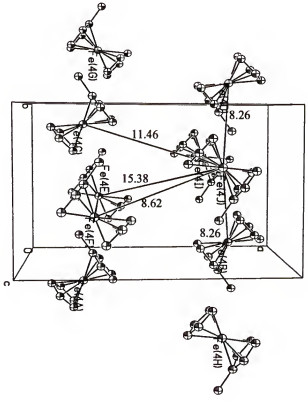


Figure 2-8. Selected distances between iron(III) ions in $Fc_4B$. ( only the ferricenyl(III) moieties are shown).[51]

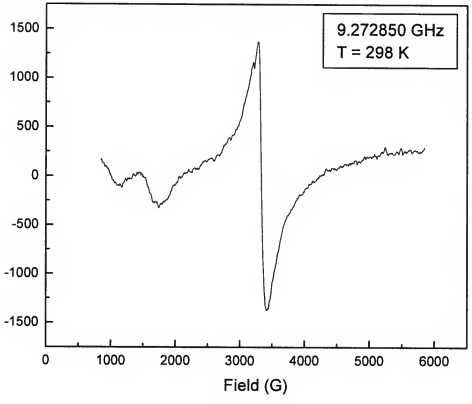


Figure 2-9. Room-temperature EPR spectrum of $Fc_4B$.

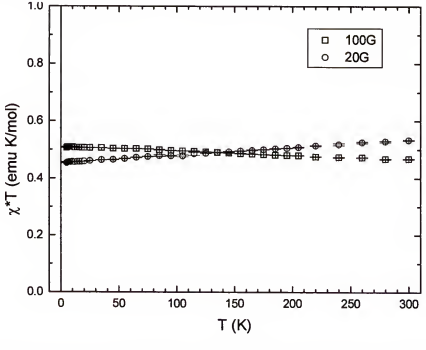


Figure 2-10. Plot of $\chi T$ *vs* $T$ for $Fc_4B$ obtained with 20 G and 100 G measuring field.

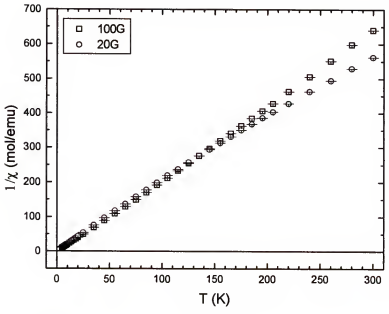


Figure 2-11. Plot of $\chi^{-1}$ *vs T* for $Fc_4B$ obtained with 20 G and 100 G measuring field.

Evidently, the unpublished result of magnetic behavior depicted in Figure 2-5 is not observed. The $\chi T$ *vs T* plot is basically a horizontal line. The change of the $\chi T$ value is very small as the temperature is lowered. When the measuring field is 20G, the $\chi T$ value changes from 0.535 emu K/mol at 300 K

to 0.455 emu K/mol at 5K. When the measuring field is 100G, the $\chi T$ value only changes from 0.47 emu K/mol at 300 K to 0.51 emu K/mol at 5K. The $\chi^{-1}$ *vs T* plot reveals no apparent ferromagnetic or antiferromagnetic behavior. The following factors may contribute to the lack of exchange interactions between Fe(III) ions. First, in the ferricenyl moiety, the magnetic orbitals are $d_{x2-y2}$, and $d_{xy}$ having negligible overlap with the $E_{2g}$ molecular orbital of the two $C_5H_5$ moieties due to the orientation of the two d orbitals. The two ferricenyl moieties belonging to two neighboring $Fc_4B$ molecules have their $C_5H_5$ rings perpendicular to each other as shown in Figure 2-8, thus making the overlap of their localized electron density on the rings also negligible. So the exchange pathways are significantly weakened. Second, in the solid state, all the Fe(III) ions are

isolated from each other without any bridging ligand directly connecting them and the shortest distance between any two Fe(III) ions is 8.26 Å, too long for any appreciable coupling to take place through space.[78] Finally, the original observed magnetic behavior may not be due to any intrinsic property of the sample, rather, it could be caused by magnetic impurity in the sample, or thermal and electronic fluctuations during the measurements, considering the measurements were made a few decades ago with a much less reliable instrument compared with today's standards. Unfortunately, no detailed information on the sample used and the procedure of the previous measurements is available.

## Conclusion

Ferricenyl(III)tris(ferrocenyl(II))borate has been synthesized based on an unpublished procedure with significant modifications. The identity of the product is confirmed by single crystal X-ray diffraction experiment and the result is consistent with the published unit cell parameters. The purity of the sample is checked by elemental analysis to be satisfactory. As the magnetic property has been measured repeatedly, no previously unpublished magnetic behavior could be observed. The sample behaves like a typical paramagnetic system as evidenced by the $\chi T$ *vs* $T$ plot and the $\chi^{-1}$ *vs* $T$ plot. The lack of exchange pathway and the large separations between Fe(III) ions have been considered to contribute to the absence of magnetic coupling between Fe(III) ions. The reliability of the previous unpublished measurements is also questionable.

# CHAPTER 3
# STRUCTURE AND MAGNETIC PROPERTIES OF $Cu_2Cl_4(CH_3CN)_2$

$Cu_2Cl_4(CH_3CN)_2$, **2**, has been synthesized and magnetically investigated due to the ladder-like structure it possesses. Although no spin-ladder behavior is observed for this material, a ferromagnetic ground state has been discovered for it. The unusual ferromagnetic ground state is unexpected based on knowledge accumulated in the past four decades on how the bridging angles in a copper(II) dimer affect the exchange interaction between the two Cu(II) ions in the dimer. The discovery of ferromagnetism in $Cu_2Cl_4(CH_3CN)_2$ has been rationalized in terms of the electronic effect of the terminal nonbridging ligands on the magnetic exchange interactions.

## Magnetism in Dimeric Systems

In the field of molecular magnetism, the magnetic properties of mononuclear transition metal complexes have been thoroughly studied. Their magnetism can be described by the Curie law with deviations in some systems caused by zero-field splitting. Today's research in molecular magnetism is almost entirely devoted to polynuclear systems composed of magnetically coupled paramagnetic metal ions, and this is the case for the materials discussed in the rest of this thesis. When the metal ions are interacting with one another, these systems can acquire new physical properties or a new reactivity. The magnetic properties of a coupled polynuclear complex are, in general, completely different from the sum of the magnetic properties of the individual ions. The study on magnetic polynuclear complexes started in 1952, when Bleaney and Bowers demonstrated that magnetic properties of copper(II) acetate was due to the dimeric nature

of the complex.[79] Dimers are the structurally simplest polynuclear complexes. In the following space, the basic electronic structure and magnetic properties of dimeric systems will be presented. The discussion will be based on the simplest scenario where two identical metal ions, each having one unpaired electron, form a dimer *i.e.*, two interacting spin doublets.

When the spin on the two spin *1/2* ions interact with one another, the individual spin quantum numbers for each metal center, $S_A = S_B = 1/2$, are no longer valid. The spin states of the dimer are now described by the total spin angular momentum quantum numbers $S = 0$ and $S = 1$, denoting a spin-singlet and a spin-triplet state, respectively. In general, the energies of these spin states are not equal, but separated by an energy gap, $J$, defined as [80]

$$J = E(S = 0) - E(S = 1). \tag{3-1}$$

The Hamiltonian for the isotropic exchange for a magnetic dimer is

$$\boldsymbol{H} = -2J\boldsymbol{S_A}\cdot\boldsymbol{S_B} + \mu_B B(g_A\cdot\boldsymbol{S_A} + g_B\cdot\boldsymbol{S_B}) \tag{3-2}$$

where $\boldsymbol{S}_A$ and $\boldsymbol{S}_B$ are the spin angular momentum operators representing the unpaired electrons on each metal center and $J$ is the isotropic exchange parameter that quantitatively accounts for the energy of the exchange interaction. The second term is the Zeeman perturbation. Figure 3-1 schematically illustrates the relation between the energy levels of the magnetic spin states as a function of applied field. At zero field, the spin-Hamiltonian splits the two degenerate $S = 1/2$ spin states into the $S = 0$ and $S = 1$ states. In the presence of a magnetic field, the Zeeman effect splits the triplet state but does not affect the singlet state. When $J < 0$, the $S = 0$ singlet state is the magnetic ground state and the exchange is antiferromagnetic. In this case, the spins are coupled in

an antiparallel fashion resulting in no net magnetic moment. When $J > 0$, the $S = 1$ triplet state is the ground state and the exchange is ferromagnetic. In this case, the spins are coupled in a parallel fashion resulting in a net magnetic moment. The magnitude of the coupling constant is related to the difference in energy, or energy gap, between the ground and first excited state. From both the spin and Zeeman Hamiltonians, the resulting four energy levels for an $S = 1/2$ dimer as a function of external field are $E_1 = 0$, $E_2 = J$, $E_3 = J + \mu_B g B$, and $E_4 = J - \mu_B g B$. The temperature dependence of the magnetic susceptibility, describing the changes in population of these magnetic energy levels, is given by

$$\chi_{dimer} = (2Ng^2\mu_B^2 / kT) / [3+exp(-2J/kT)] \qquad (3\text{-}3)$$

This equation is known as the Bleaney-Bowers equation.[81] It is applicable for dimeric systems where there is no magnetic interaction between dimers.

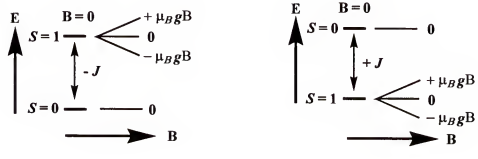


Figure 3-1. Splitting of the magnetic energy levels in an $S = 1/2$ dimer. The zero-field spin states of the dimer correspond to the $S = 0$ and $S = 1$ states. In an antiferromagnetically coupled dimer (left) the ground state is singlet while in a ferromagnetically coupled system (right) the ground state is triplet. The coupling constant, $J$, is the energy gap between the ground state and the nearest excited state.

**Magneto-structural Correlations in Cu(II) Dimers**

The most thoroughly investigated dinuclear compounds by far are Cu(II) dimers. In Cu(II) ions, the unpaired electron is located in the $d_{x2-y2}$ orbitals regardless of the coordination geometry of the Cu(II) ions. A general structure of such Cu(II) dimers is depicted in Figure 3-2 in which X represents diamagnetic bridging ligands and L the blocking ligands. The blocking ligands can also be bidentate chelating ligands.

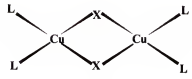


Figure 3-2. General structure of planar Cu(II) dimer complex. X is diamagnetic bridging ligand, and L is blocking ligands.

In real compounds, different kinds of coordination environments may exist around the Cu(II) ions, such as distorted tetrahedral (also referred to as 4), square pyramidal (4+1, or 5), elongated octahedral (4+2).[82] The structure of the dimer can also have several types of distortions as depicted in Figure 3-3. However, we will restrict our discussion to the simplest scenario as shown in Figure 3-2 where the dimer is planar.

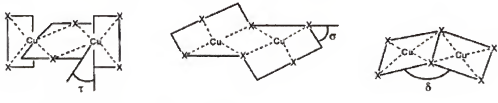


Figure 3-3. Distortions in copper(II) dimers.

In the past five decades, the study of Cu(II) dimers has been focused on the relationship between their structural features and their magnetic behavior, specifically, on how the bond angles and bond lengths at the bridging sites affect the sign and the strength of the exchange interaction propagated by the bridging ligands.[82] Due to the large number

of Cu(II) dimers that have been synthesized and the possibility to fine tune their structural features through synthesis, systematic studies have been carried out and several trends have been summarized regarding the magneto-structural correlations for Cu(II) dimers containing organic bridging ligands such as acetate, halides, hydroxyl group, azide, oxalate, and dicyanamide, etc.[82-88] Hatfield and Hodgson established a correlation that shows the magnitude of the interaction in planar dihydroxo-bridged Cu(II) dimers (X = $OH^-$ in Figure 3-2) depends on the Cu-O-Cu bridging angle.[89] Twelve compounds of this kind have been structurally characterized and magnetically investigated. These compounds differ by the nature of the terminal (blocking) ligands and/or of the counter ions. The Cu-O bond lengths across the series are almost identical, so are the Cu-L bond lengths. Hatfield and Hodgson have shown as the Cu-O-Cu bond angles change from $95.6^0$ to $104.1^0$, the singlet/triplet energy gap, *J*, varies in parallel from + 172 $cm^{-1}$ to -509 $cm^{-1}$ ( + 248 K to – 728 K). Hatfield and Hodgson subsequently derived a linear correlation between *J* and the Cu-O-Cu angle, $\varphi$:

$$2J\,(cm^{-1}) = -74.53\,\varphi + 7270 \qquad (3\text{-}4)$$

where *J* is the exchange parameter, $\varphi$ is the Cu-O-Cu bridging angle. According to this relationship, *J* is predicted to be zero for $\varphi = 97.5^0$. For $\varphi > 97.5^0$, the ground state is a singlet and for $\varphi < 97.5^0$ the ground state is a triplet. From Equation (3-4), it appears that a change of one degree in the bridging angle results in a change of about *74* $cm^{-1}$ in the singlet/triplet energy separation. A semiquantitative interpretation may be provided as follows.[80] As shown by the EPR experiments, the unpaired electrons are delocalized into the ligand orbitals which have both *s* and *p* contributions. Hay, Thibeault, and Hoffmann

have shown that the exchange energy, $J$, of two interacting $S = 1/2$ ions can be expressed as: [84]

$$E(S=0) - E(S=1) = J = K_{ab} - (e_1 - e_2)^2 / (J_{aa} - J_{ab}) = J_F - J_{AF} \quad (3\text{-}5)$$

where $K_{ab}$ is the two-electron exchange integral which is always positive and contributes to the stabilization of the ferromagnetic ground state. The self-repulsion integral $J_{aa}$ represents the electrostatic repulsion of two electrons on the same orbital. The Coulomb integral $J_{bb}$ is the repulsion energy between two electrons occupying different orbitals. However, the value of $(J_{aa} - J_{ab})$ does not change significantly with the varying bridging angle. $e_1$ and $e_2$ are the energies of the two singly-occupied molecular orbitals (SOMO) in the triplet state formed by the magnetic orbital on the two metal ions and the $p$ orbitals of the bridging ligands. These two molecular orbitals are shown in Figure 3-4.[80] The value of $(e_1 - e_2)$ determines the magnitude of the contribution to the antiferromagnetic ground state. From equation (3-5), a triplet state can be easily visualized when $e_1$ and $e_2$ are equal for two degenerate molecular orbitals and $J = K_{ab}$.

$b_{2u}$ $b_{1g}$

Figure 3-4. Molecular orbitals for di-$\mu$-hydroxo bridged copper(II) dimers. $b_{2u}$ is the combination of $d_{xy}$ and $p_y$, $b_{1g}$ is the combination of $d_{xy}$ and $p_x$.

The energy variation of these two molecular orbitals as the bridging angle changes is basically governed by the $3d_{xy}$(copper)-$2p$(oxygen) antibonding overlap. When the bridging angle is close to $90^0$ the overlaps $\langle d_{xy} | p_x \rangle$ in $b_{1g}$ and $\langle d_{xy} | p_y \rangle$ in $b_{2u}$ are

equal and both negative, the two SOMOs have the same energy. As the bridging angle increases, $<d_{xy}|p_x>$ becomes more negative and $<d_{xy}|p_y>$ less negative. Therefore, the energy difference between the two molecular orbitals, $(e_1-e_2)$ increases and the singlet state is stabilized. For an angle of a certain value, $97.5^0$ for the series of compounds Hatfield and Hodgson studied, ferromagnetic and antiferromagnetic contributions compensate each other and the singlet and triplet states are accidentally degenerate. The energy gap between the singlet and the triplet states is then zero. However, this does not mean that there is no interaction between the two local doublets. As the bridging angle decreases from this peculiar value, ferromagnetic contribution becomes dominant and the triplet state is stabilized.

However, the magneto-structural correlation for halide-bridged copper(II) dimers is not as straight forward as for di-$\mu$-hydroxo bridged copper(II) dimers.[82] First, the wide variety of geometries and bridging arrangements has made the simple one-parameter correlation impossible. Second, the value of $J$ is almost an order of magnitude smaller. The most noticeable work regarding the magneto-structural correlations in halide-bridged copper(II) dimers as well as those involve other types of bridges has been those published continuously by Willett *et al.* in the past four decades. Willett *et al.* studied a large number of copper(II) dimers and investigated the variation of their magnetic properties as a function of several structural parameters, such as bond lengths, bond angles, and coordination geometries.[90-98] Particularly, Willett *et al.* studied the effect of the Cu-X-Cu bridging angle on the magnetic behavior while other structural parameters were kept constant.[82] For the series of compoundes investigated, Willett *et al.* found that as the bridging angle decreases from $95.1^0$ to $94.3^0$ to $85.4^0$, the exchange coupling becomes

increasingly ferromagnetic as $J$ increases from – 55 K to – 43 K to +70 K. Willett *et al.* have also summarized their results in the form of a graph to show how the exchange interaction is affected by the bridging angle in a series of copper(II) chloride salts. The graph is reproduced in Figure 3-5 below.[82]

Finally, the nature of the substituents coordinated to the metal ions such as the terminal ligands can also influence the exchange interaction as they may change the electron density distribution in the dimeric structure.[84]

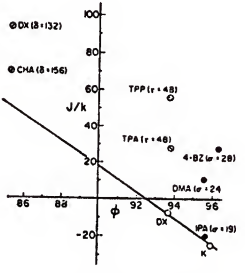


Figure 3-5. Exchange energy, $J/k$, as a function of bridging angle, φ, for a series of copper(II) chloride salts.[84]

## Experimental Section

### Materials

Anhydrous copper(II) chloride (99.99%) was purchased from Aldrich (Milwaukee, WI) and used as received. Acetonitrile was degassed and dried over calcium hydride before use.

**Synthesis of $Cu_2Cl_4(CH_3CN)_2$, 2**

Single crystals of $Cu_2Cl_4(CH_3CN)_2$ were produced by slow evaporation of an saturated acetonitrile solution of anhydrous $CuCl_2$ under an inert atmosphere according to the procedure of Willett and Rundle.[99] After about a week, dark yellow needle-like crystals were obtained and stored under an inert atmosphere due to the hygroscopic nature of the material. Single-crystal X-ray diffraction experiment confirmed that the unit cell parameters of the obtained material are the same as the reported values: $a = 3.84 \pm 0.01$ Å, $b = 7.91 \pm 0.01$ Å, $c = 18.35 \pm 0.02$ Å, $\beta = 91.1 \pm 0.1^0$, $Z = 2$, space group is $P2_1/c$. Elemental analysis: calculated C: 13.69%, H: 1.72%, N: 7.98%; found C: 13.65%, H: 1.67%, N: 7.91%.

**EPR Measurements**

The EPR spectra were recorded with a Bruker ER 200D X-band (9 GHz) spectrometer modified with a digital signal channel and digital field controller. Temperature control down to 4 K was achieved with an Oxford EPR 900 Flow Cryostat. Spectra were acquired for a polycrystalline sample as temperature was varied from 5 K to 300 K with increasing increments.

**Magnetic Measurements**

Static-magnetization measurements were performed with a Quantum Design MPMS SQUID magnetometer. The sample was 122.0 mg of polycrystalline material placed in a plastic can that was held in a straw. The sample was zero-field cooled to 2 K before the measuring field of 100 G was applied, and data were subsequently acquired up to 300 K. This procedure was repeated while cooling the sample in the presence of the measuring magnetic field. Isothermal magnetization studies were performed at 2 K while ramping the field between –50 kG to 50 kG. The small background signals arising from

the can and straw were subtracted from the results. Using Pascal's constants, the core diamagnetic signal of the sample was estimated to be $-171.18 \times 10^{-6}$ emu/mol of dimer, and this contribution was subtracted from the data.

## Results and Discussion

### Description of the Structure

The molecular structure of $Cu_2Cl_4(CH_3CN)_2$ is shown in Figure 3-6. Each planar dimer unit consists of two Cu(II) ions doubly bridged by two chloride ions with the Cu-Cl-Cu bridging angle being 94°. Each Cu(II) ion is further bonded to an additional non-bridging chloride ion and a nonbridging acetonitrile molecule through its nitrogen atom. The dimer units stack along the crystallographic *a* axis to form a ladder structure, where the Cu(II) ions are located along the two legs and the chloride double bridges form the rungs. Each Cu(II) ion is thus weakly bonded to a nonbridging chloride and a bridging chloride from its two neighboring dimer units to complete an axially elongated octahedral geometry (4+2).

### EPR Measurements

The X-band EPR spectra obtained for the polycrystalline sample show no apparent difference as temperature changes. The spectra all contain one featureless isotropic resonance signal centered at 3173 Gauss, corresponding to a $g$ value of $2.09 \pm 0.05$. The spectra obtained at a series of temperatures shown in Figure 3-7. All spectra are quite isotropic and the center field remains constant as temperature changes.

### Magnetic Properties of $Cu_2Cl_4(CH_3CN)_2$

The product of magnetic susceptibility times temperature ($\chi T$), normalized by the moles of dimer, is shown as a function of temperature in Figure 3-8. The increase in $\chi T$ at low temperatures is consistent with ferromagnetic interactions.

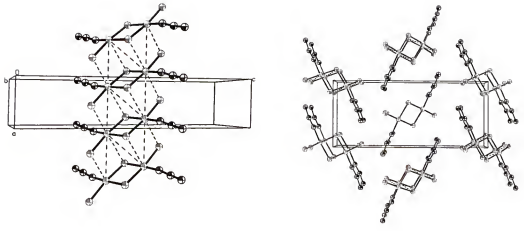

(a) (b)

Figure 3-6. Structure of $Cu_2Cl_4(CH_3CN)_2$. (a) one ladder consisted of stacking dimers. (b) top view of seven ladders.[99]

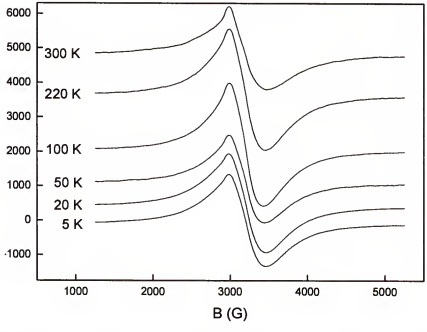


Figure 3-7. The X-band EPR spectra of a polycrsyatlline sample of $Cu_2Cl_4(CH_3CN)_2$ at various temperatures The data at 100 K and 220 K were obtained with receiver gain (RG) value set at 1000, while all other data were obtained with RG set at 200.

The data are well fit by Equation 3-6 (interacting-dimer model in Figure 3-8) [80] for the susceptibility that includes the *g* value, the intradimer coupling constant *J*, and the interdimer coupling constant *J'*.

$$\chi = 2Ng^2\beta^2[kT - \frac{2zJ'}{3 + exp(-J/kT)}]^{-1}[3 + exp(-J/kT)]^{-1} \quad (3\text{-}6)$$

where *N* is the Avogadro's number. The Hamiltonian [80] used for this model is

$$\boldsymbol{H} = -J\boldsymbol{S}_A \cdot \boldsymbol{S}_B + g\beta\boldsymbol{S}zH - zJ'\langle\boldsymbol{S}z\rangle\boldsymbol{S}z \quad (3\text{-}7)$$

The best fit of the $\chi T$ *vs* *T* data yielded $J/k_B = 40 \pm 2$ K, $J'/k_B = 0.9 \pm 0.1$ K, and $g = 2.14 \pm 0.01$. The *g* value from the fit is reasonable as EPR measurements show a broad signal with *g* value of $2.09 \pm 0.05$ between 300 K and 5 K. Further evidence of the ferromagnetic interactions is provided by the temperature dependence of the inverse susceptibility, Figure 3-8 inset, where a Weiss temperature, $\theta$, of $7.5 \pm 0.25$ K is obtained. The isothermal magnetization at 2 K is shown as a function of field in Figure 3-9, and no evidence of hysteresis was observed. Nevertheless, the magnetization does approach saturation faster than predicted for an isolated-dimer system (noninteracting-dimer model in Figure 3-9) by the Bleaney-Bowers equation, indicating a weak ferromagnetic coupling between dimers. In addition, it is noteworthy that the zero-field cooled and field cooled susceptibility data were the same down to 2 K and did not exhibit any subtle differences that may suggest long-range ordering.[100]

The research result presented above is the first time that the magnetic properties of $Cu_2Cl_4(CH_3CN)_2$ have been reported since the report of its structure in 1964 by Willett and Rundle.

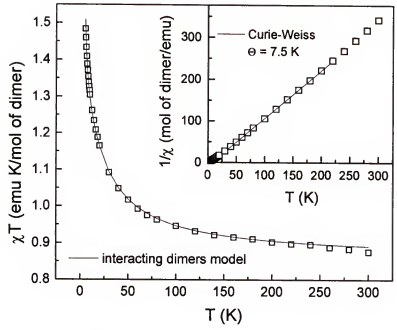


Figure 3-8. Plot of $\chi T$ *vs* $T$ for $Cu_2Cl_4(CH_3CN)_2$. The line is the fitting result using an interacting-dimer model (Equation 3-6). The inset is the inverse susceptibility *vs* temperature plot fitted with the Curie-Weiss law.

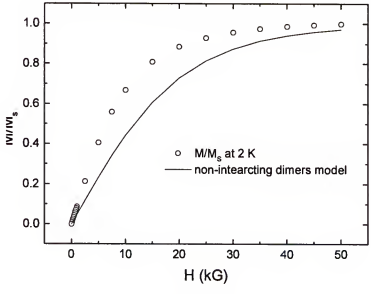


Figure 3-9. Magnetization as a function of field obtained at 2 K for $Cu_2Cl_4(CH_3CN)_2$. The solid line is a simulation of the Bleaney-Bowers equation.

The ferromagnetism observed in this material is rare, given the fact that only less than 5% of all the Cu(II) dimers studied to date show ferromagnetic behavior.[80] Moreover, the bridging angle Cu-Cl-Cu is $94^0$ in $Cu_2Cl_4(CH_3CN)_2$, which is expected, according to Willett's study, to propagate antiferromagnetic coupling between the Cu(II) ions as shown in Figure 3-5. However, quite strong ferromagnetic coupling is observed. We noticed that although the bond angle at the bridging sites is often cited as the factor that determines the sign of exchange, it is not the only variable that affects the exchange interaction. To explain the ferromagnetic intradimer interaction in $Cu_2Cl_4(CH_3CN)_2$, we can compare the behavior with related compounds possessing the same dihalogen bridged Cu(II) dimer core with four coplanar non-bridging terminal ligands, having similar bond lengths and bond angles. One example is $KCuCl_3$ and all the terminal ligands are chloride ions. In this case, the intradimer coupling is antiferromagnetic as ($J/k_B$) = – 49.8 K.[101] If two terminal chloride ions are replaced by nitrogen donors then the antiferromagnetic coupling decreases, as observed in the examples $Cu_2Br_4(C_5H_5N)_2$ ($J/k_B = -16$ K),[102] and $Cu_2Cl_4(C_{13}H_9N_3)_2$ ($J/k_B = -14.4$ K).[103] The explanation is that bonding to the nonbridging nitrogen donors is stronger, weakening the Cu-Cl (bridging) bonds *trans* to the Cu-N bonds, making the antiferromagnetic exchange pathway less effective.[104] If all four terminal chloride ions are replaced by nitrogen-donating ligands, model calculations have shown that intradimer exchange coupling is expected to become ferromagnetic,[105] and this has been observed experimentally in $Cu_2Cl_2[HB(1\text{-}pz)_3]_2$ ($J/k_B = 48.6$ K) with $HB(1\text{-}pz)_3$ being hydrotris(1-pyrazolyl)borate anion.[106]

In $Cu_2Cl_4(CH_3CN)_2$ only two of the terminal ligands are nitrogen donors. However, unlike the amine and pyridine ligands in previous examples, the nitrile group in

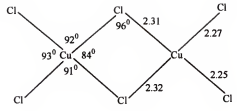


$KCuCl_3$ , $J/k_B = -49.8$ K

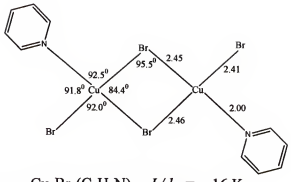


$Cu_2Br_4(C_5H_5N)_2$, $J/k_B = -16$ K

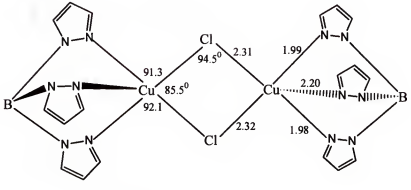


$Cu_2Cl_2[HB(1\text{-}pz)_3]_2$, $J/k_B = 48.6$ K
( $HB(1\text{-}pz)_3$ : hydrotris(1-pyrazolyl)borate anion )

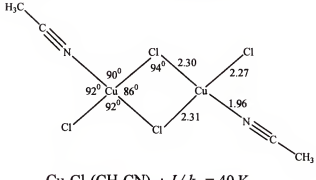


$Cu_2Cl_4(CH_3CN)_2$ : $J/k_B = 40$ K

Figure 3-10. Comparison of the exchange parameter of $Cu_2Cl_4(CH_3CN)_2$ with other isostructural Cu(II) dimers containing different types of terminal ligands.

$Cu_2Cl_4(CH_3CN)_2$ can also function as a $\pi$-acid ligand to further weaken the *trans* Cu-Cl bond, and lessen the antiferromagnetic contribution to exchange. As a result,

ferromagnetic coupling is observed even though only two nitrogen-donating terminal ligands are present. The foregoing discussion is summarized in Figure 3-10.

**Conclusion**

$Cu_2Cl_4(CH_3CN)_2$ was reproduced and its magnetic properties have been investigated. Despite of the ladder-like structure $Cu_2Cl_4(CH_3CN)_2$ possesses, no spin-ladder behavior was observed. Instead, unusual ferromagnetic coupling is discovered both within the dimeric structures and between dimers. The exchange parameters are $J/k_B = 40 \pm 2$ K for intradimer interaction and $J'/k_B = 0.9 \pm 0.1$ K for interdimer interaction. According to the previously published studies, the ferromagnetic interactions are not expected for the bridging angle, of $94^0$ in $Cu_2Cl_4(CH_3CN)_2$. This disagreement has been rationalized based on the *trans* influence due to the electron-withdrawing terminal ligands, $CH_3CN$, that significantly reduce the electron density located on the Cu(II) ions and subsequently weaken the antiferromagnetic exchange interactions.

CHAPTER 4

SYNTHESIS, STRUCTURE AND MAGNETISM OF LADDER-LIKE STRUCTURES $[Co(NO_3)_2(4,4'\text{-BIPYRIDINE})_{1.5}(MeCN)]_n$ AND $Ni_2$(2,6-PYRIDINEDICARBOXYLIC ACID)$_2(H_2O)_4$(PYRAZINE)

**Coordination Polymers with Ladder-like Structures**

Quite a few coordination polymers possessing ladder-like structures have been reported in the past several years. These materials were in general synthesized under hydrothermal conditions or *via* a self-assembling process. One example is Ni(4,4'-bipyridine)$_{2.5}(H_2O)_2(ClO_4)_2$•1.5(4,4'-bipyridine)•$2H_2O$ reported from Yaghi *et al.*[107] The structure is presented in Figure 4-1.

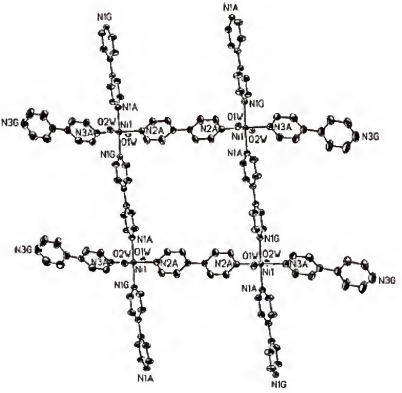


Figure 4-1. Structure of Ni(4,4'-bipyridine)$_{2.5}(H_2O)_2(ClO_4)_2$•1.5(4,4'-bipyridine)•$2H_2O$.[107]

This compound was synthesized as single crystals by mixing 1 equivalent of $Ni(ClO_4)_2)$•$6H_2O$ with 3 equivalents of 4,4'-bipyridine in water under hydrothermal conditions for 10 hours. Each Ni(II) is in an octahedral geometry and are linked by 4,4'-bipyridine along the legs and the rungs forming square cavities surrounded by four 4,4'-bipyridine molecules. The terminal nonbridging 4,4'-bipyridine molecules stack along the legs. Neighboring ladders are interdigitated with each other because of the terminal 4,4'-bipyridine molecules. 4,4'-bipyridine, perchlorate, and water molecules reside inside the cavities. Magnetically, the interactions between the Ni(II) ions are so weak that no assuring conclusion can be made. Close inspection of the structure has shown that the two pyridine rings in the 4,4'-bipyridine molecules are twisted with each other, magnetically isolating the Ni(II) ions.

Another example is $[Cd(L)_{1.5}][NO_3]_2$, where L = 1,4-bis(4-pyrodylmethyl)benzene. The structure of L, and the ladder structure of the material are shown in Figure 4-2.[108]

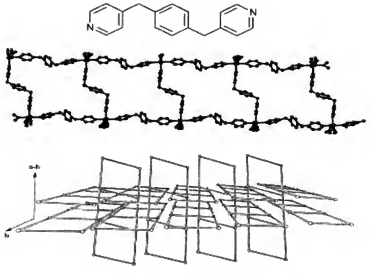


Figure 4-2. Structure of 1,4-bis(4-pyrodylmethyl)benzene and of [Cd(1,4-bis(4-pyrodylmethyl)benzene)$_{1.5}$][$NO_3$]$_2$ ladders.[108]

This ladder structure was obtained as single crystals by reacting $Cd(NO_3)_2$ with 1.5 equivalent of the ligand, L, in ethanol. Each Cd(II) is coordinated to three ligands and two nitrate ions to form a hepta-coordination geometry. In the solid state, as shown in Figure 4-2, the ladders interpenetrate each other to minimize the empty space and remain interpenetrated even after guest molecules, *p*-dibromobenzene, are introduced into the square cavities of the ladders.

A different kind of ladder structure has also been reported. $[Cu_2(bpm)(dca)_4]_n$,[109] where bpm is 2,2'-bipyrimidine and dca is dicyanamide, has a ladder-like structure that can be viewed as the result of stacking pre-fabricated dimers. Its structure is shown in Figure 4-3.

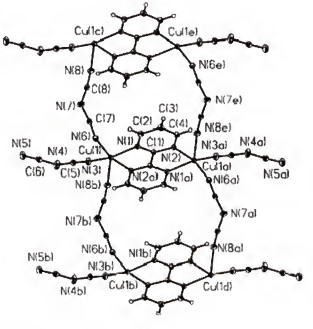


Figure 4-3. Ladder-like structure of $[Cu_2(bpm)(dca)_4]_n$.[109]

This compound was synthesized as single crystals by slow evaporation of aqueous solutions containing 0.5 mmol of (2,2'-bipyrimidine)copper(II) nitrate and 1.0 mmol

of $NaN(CN)_2$. In the solid state, the terminal nonbridging dca molecules protrude into the cavities of neighboring ladders. Magnetically, the bpm molecules propagate very efficiently antiferromagnetic exchange interactions between the two Cu(II) coordinated to it. The exchange mediated by the dca bridges is negligibly small so that the compound behaves like a noninteracting-dimer system.

**A Strategy for Synthesizing Ladder-like Structures**

Currently, only two examples of isolated noninterpenetrating ladder-like structures are known. The acquisition of the structures already discussed in this chapter and the example presented in Chapter 1, $Gd^{III}_2$ $[Cu^{II}(opba)]_3 \cdot 6DMSO \cdot 4H_2O$, was largely due to serendipity. To produce more examples of ladder-like structures, it is important to do the syntheses in a more rationalized and controlled fashion. Based on some of the structural features observed in real ladder-like examples, a synthetic strategy has been proposed to build coordination polymers with ladder structures. This is shown in Figure 4-4.

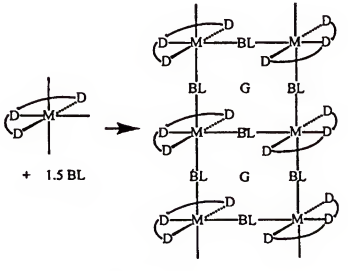


Figure 4-4. Proposed methodology for the synthesis of coordination polymers with a ladder-like structure. D-D-D is a planar tridentate blocking ligand, BL is bridging ligand, G is guest molecule.

In this strategy, a transition-metal ion that prefers octahedral coordination geometry is first reacted with a planar tridentate ligand so that three meridional coordination sites would be blocked by the ligand and the other three, also in a meridional arrangement, are left open. The resulting complex is a T-shaped molecular building block. Such molecular building blocks which serve as the nodes in the ladder-like structures are further reacted with linear bidentate ligands in a solution phase with the molar ration between the nodes and the bridging ligands being 2:3 because a ladder-like structure has the following repeating unit shown in Figure 4-5.

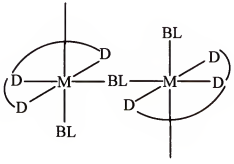


Figure 4-5. Repeating unit of a ladder-like structure.

The planar tridentate can be terpyridine, 2,6-pyridinedicarboxylic acid (dpa), or 2,6-pyridinedimethanol, etc. shown in Figure 4-6. Several factors are designed to promote the synthesis toward a ladder-like structure. The stoichiometry of 2:3 for M:BL favors the formation of a ladder. The tridentate ligands coordinate in meridional fashion and, as shown in Figure 4-4, the stacking of the pyridine rings can also encourage the structure to extend along one direction. The formation of square cavities inside the ladders provides opportunity for the segregation of dissimilar interactions. For example, a charged bridging ligand can be used to form polar cavities, while a neutral blocking ligand such as terpy is used to form non-polar environment between ladders through $\pi$-$\pi$

stacking. Conversely, a neutral bridging ligand such as 4,4'-bipyridine or pyrazine may be used to form nonpolar cavities which can be matched with charged blocking ligands that form polar or hydrogen-bonding environment between ladders. If needed, counter ions of the right charge and size can be used to occupy any void space such as the square cavities in the structure.

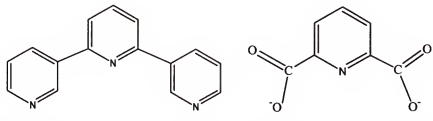

Figure 4-6. Structure of 2,2':6',2"–terpyridine (terpy) and 2,6-pyridinedicarboxylic acid (dpa) dianion.

In the following space, we will report the synthesis and magnetic properties of a new and a previously known example of ladder-like structures.

## Experimental Section

### Materials

$[Co(NO_3)_2]\cdot 6H_2O$, 4,4'-bipyridine, 2,6-pyridinedicarboxylic acid (dpa), and pyrazine (pyz) were purchased from Aldrich (Milwaukee, WI), $NiCO_3$ was purchased from Alfa Aesar. All materials were used as received.

### Synthesis of $[Co(NO_3)_2(4,4'\text{-bipyridine})_{1.5}(MeCN)]_n$, 3

$[Co(NO_3)_2(4,4'\text{-bipyridine})_{1.5}(MeCN)]_n$ was synthesized by modifying the procedure of Zaworotko *et al.*[110] A U-shaped tube with opening at both end is first filled with a 1:1 mixture of MeOH/MeCN to about 80% of the total volume. Red single crystals were obtained by slow diffusion of a solution of $[Co(NO_3)_2]\cdot 6H_2O$ (0.29 g, 1.0 mmol) in MeOH and a solution of 4,4'-bipyridine (0.23 g, 1.5 mmol) in MeCN. A large amount of

rectangular crystals appeared on the inner wall of the U-tube at the interface of the two solutions within 1 hour of the two solutions meeting. The crystals were collected by filtration and washed with a small amount of a cold solvent mixture of MeOH and MeCN. The crystals are stable for a few hours in the open air before turning opaque due to the loss of the solvent molecules, acetonitrile. The material was characterized by single-crystal X-ray diffraction which shows that the crystals obtained have the same unit cell dimensions as reported.[110]

**Synthesis of $Ni_2(dpa)_2(pyz)(H_2O)_4$, 4**

An aqueous mixture (20 ml) of $NiCO_3$ (2 mmol, 237.44 mg), 2,6-pyridinedicarboxylic acid (2 mmol, 334.24 mg), and pyrazine (3 mmol, 240.27 mg) was placed in a stainless steel vessel and heated to 150 $^0$C for 24 hours, then the system was cooled down to room temperature at a cooling rate of 1 $^0$C per minute. The resulting small blue crystals were collected, washed with water and air dried. The structure of the material was characterized by single-crystal X-ray diffraction and elemental analysis. Calculated: C: 36.05; H: 3.02; N: 9.34. Found: C: 35.68; H: 2.94; N: 9.14.

**X-ray Diffraction experiment on $Ni_2(dpa)_2(pyz)(H_2O)_4$**

Data were collected at 173 K on a Siemens SMART PLATFORM equipped with a CCD area detector and a graphite monochromator utilizing $MoK_\alpha$ radiation with wavelength of 0.71073 Å. Cell parameters were refined using up to 8192 reflections. A full sphere of data (1381 frames) was collected using the ω-scan method (0.3° frame width). The first 50 frames were remeasured at the end of data collection to monitor instrument and crystal stability (maximum correction on I

was < 1 %). Absorption corrections by integration were applied based on measured indexed crystal faces.

The structure was solved by the Direct Methods in *SHELXTL5,* and refined using full-matrix least squares. The nonhydrogen atoms were treated anisotropically, whereas the hydrogen atoms were calculated in ideal positions and were riding on their respective carbon atoms. The dimer is located on a center of inversion thus the asymmetric unit consists of a half dimer. A total of 179 parameters were refined in the final cycle of refinement using 2009 reflections with $I > 2\sigma(I)$ to yield $R_1$ and $wR_2$ of 2.85% and 6.57%, respectively. Refinement was done using $F^2$.

**Magnetic Measurements on $[Co(NO_3)_2(4,4'\text{-bipyridine})_{1.5}(MeCN)]_n$**

Static-magnetization measurements were performed with a Quantum Design MPMS SQUID magnetometer. The sample was 81.0 mg of polycrystalline material placed in a plastic can containing 186.0 mg of vacuum grease. The crystals were embedded into the grease to avoid contact with air. The entire assembly is then held inside a straw. The sample was zero-field cooled to 2 K before the measuring field of 100 G was applied, and data were subsequently acquired up to 300 K. This procedure was repeated while cooling the sample in the presence of the measuring magnetic field. Magnetization versus field measurements were performed at 2 K from 0 to 70 kG. The same procedure was also performed for the can and the grease and the data obtained has been subtracted from the measurement for can, grease, and sample. The diamagnetic contribution, estimated using Pascal's constants, is $-430.6\times10^{-6}$ emu per mole of structural repeating unit, $[Co(NO_3)_2]_2(4,4'\text{-bipyridine})_3(MeCN)$, and has also been subtracted.

**Magnetic Measurements on $Ni_2(dpa)_2(pyz)(H_2O)_4$**

Static-magnetization measurements were performed with a Quantum Design MPMS SQUID magnetometer. The sample was 155.53 mg of polycrystalline material placed in a plastic gelcap that was held in a straw. The sample was zero-field cooled to 2 K before the measuring field was applied, and data were subsequently acquired up to 300 K. Measurements were made with measuring fields of 100G and 1000G. The procedure was repeated while cooling the sample in the presence of the measuring magnetic field. Magnetization versus field measurements were performed at 2 K from 0 to 70 kG. The small background signals arising from the gelcap and straw were subtracted from the results. The diamagnetic contribution from the sample is calculated according to Pascal's constants to be $-246.2\times10^{-6}$ emu per mole of Ni(II) dimer, and has also been subtracted.

## Results and Discussion

**Structure Description of $[Co(NO_3)_2(4,4'\text{-bipyridine})_{1.5}(MeCN)]_n$**

The synthetic scheme of $[Co(NO_3)_2(4,4'\text{-bipyridine})_{1.5}(MeCN)]_n$ is shown in Figure 4-7.[110] Another ladder-like structure was also synthesized and the resulting material has the same covalent network as $[Co(NO_3)_2(4,4'\text{-bipyridine})_{1.5}(MeCN)]_n$ except the guest molecules are chloroform. In $[Co(NO_3)_2(4,4'\text{-bipyridine})_{1.5}(MeCN)]_n$, Co(II) ions function as the nodes and are linked together by 4,4'-bipyridine. Each Co(II) ion is also coordinated to two nitrate ions to form a hepta-coordination geometry. Solvent molecules are found to reside in the large hydrophobic square cavities surrounded by 4,4'-bipyridine molecules in the structure, and the exterior of the ladders is hydrophilic due to the nitrate ions. The ladders are depicted in Figure 4-8.[110] In the solid state, all ladders run parallel to the *a* axis with no contact between ladders.

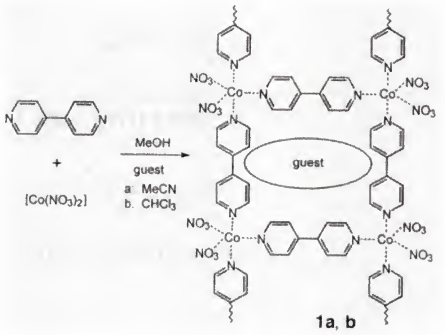


Figure 4-7. Synthetic scheme for $[Co(NO_3)_2(4,4'\text{-bipyridine})_{1.5}(solv)]_n$. (1a) solv = MeCN. (1b) solv = $CH_3Cl$.[110]

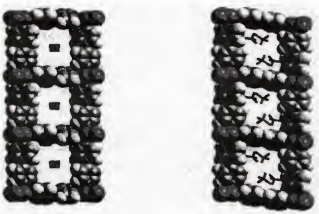

Figure 4-8. Ladder-like structure of $[Co(NO_3)_2(4,4'\text{-bipyridine})_{1.5}(solv)]_n$. (left) solv is MeCN (right) solv is $CH_3Cl$.[110]

**Structure Description of $Ni_2(dpa)_2(pyz)(H_2O)_4$**

Figure 4-9 shows the structural repeating unit of $Ni_2(dpa)_2(pyz)(H_2O)_4$. Each planar tridentate 2,6-pyridinedicarboxylic acid molecules coordinates to one Ni(II) ion in a meridional fashion blocking three coordination sites of an octahedron and leaving the

other three sites to form a T-shaped geometry. The octahedral geometry around Ni(II) ion is distorted as Ni(II) is coordinated to the planar tridentate ligand. The two Ni(II)-carboxylate bonds are stretched longer than the other four bonds while the Ni(II)-N(pyridine) bond is the shortest. So the equatorial plane may be viewed to contain the two Ni(II)-N bonds and the two Ni(II)-$H_2O$ bonds, and the elongated axis lies along the two Ni(II)-carboxylate bonds. Two Ni(II) complexes are bridged by a pyrazine molecule to form a dimer as the building unit of the ladder-like structure. For each Ni(II) ion, the two coordination sites left in the "T" at the axial position of the octahedron are occupied by two water molecules so that each dimer has four water molecules. The two 2,6-pyridinedicarboxylic acid molecules are coplanar, and form an angle of approximately 30° with the planar pyrazine molecule.

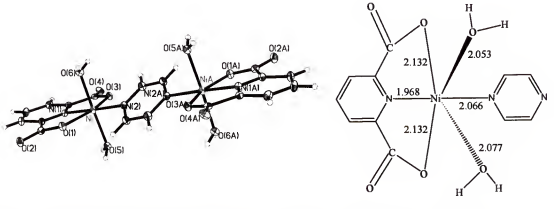


Figure 4-9. The repeating unit and seleted bond lengths of $Ni_2(dpa)_2(pyz)(H_2O)_4$

In the solid state, dimers stack on top of each other to form a ladder structure along the *a* axis with the pyrazine function as the rungs as shown in Figure 4-10. Although the synthesis was carried out with Ni(II):pyrazine ratio of 2:3, only one equivalent of pyrazine is incorporated in the final structure with no pyrazine occupying the axial position of the Ni(II) octahedron. The legs of the ladder are then provided by hydrogen

bonding due to the water molecules at the axial coordination sites. There are two types of hydrogen bonding within a ladder. One is O(water)-H(pyridine)-C(pyridine) and it provides the legs of the ladders. The other hydrogen bonding is O(water)-H(water)-O(carboxylate) and they occupy the cavities sandwiched by two pyrazine molecules. Along the *a* axis, the separation between two neighboring parallel pyridine rings is 3.3 Å, ideal for $\pi$-$\pi$ stacking. However, the two pyridine rings are completely offset along the molecular axis of the dimer (the Ni-pyrazine-Ni axis) so that the $\pi$-$\pi$ interaction is actually between a pyridine and a pyrazine. In the solid state, a hydrogen-bonding network exists in all three dimensions to connect individual ladders.

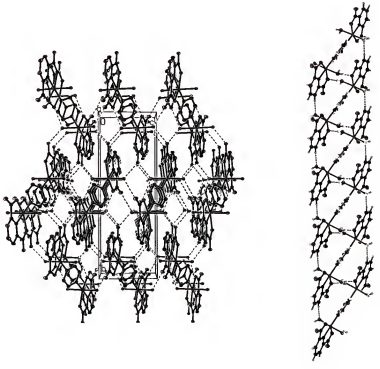

Figure 4-10. Ladder-like structure in $Ni_2(dpa)_2(pyz)(H_2O)_4$. On the left is the top view of ten ladders running along the *a* axis (perpendicular to the paper). On the right is the side view of the structure of one ladder.

One final remark on the synthesis of $Ni_2(dpa)_2(pyz)(H_2O)_4$ is that the same synthetic procedure has been repeated with excess amount of pyrazine, the resulting structures are the same as $Ni_2(dpa)_2(pyz)(H_2O)_4$. It has been proposed that nonhydrogen bonding solvents be used to incorporate covalent linkages along the two legs in the structure of $Ni_2(dpa)_2(pyz)(H_2O)_4$. However, no such solvent was found to be able to dissolve the starting material, $NiCO_3$ and 2,6-pyridinedicarboxylic acid.

**Magnetic Properties of $[Co(NO_3)_2(4,4'\text{-bipyridine})_{1.5}(MeCN)]_n$**

The magnetic properties of $[Co(NO_3)_2(4,4'\text{-bipyridine})_{1.5}(MeCN)]_n$ are presented in Figure 4-11. In the inset, the product of susceptibility and temperature, $\chi T$, is plotted as a function of temperature. As temperature is lowered, the value of $\chi T$ decreases. However, as evidenced by the *M vs H* plot that behaves very much like a paramagnetic system, the decrease of the $\chi T$ value is not due to antiferromagnetic coupling between the Co(II) ions but because of the depopulation of the excited state as temperature is lowered. This can be further explained as following.

A divalent Co(II) has $3d^7$ and a $^4T_1$ ground state in an octahedral environment. However, spin-orbital coupling of Co(II) is large ($\lambda$ is about – 180 $cm^{-1}$ for the free ion), and the true situation is better described by the energy-level diagram in Figure 4-12. Due to spin-orbital coupling, the $^4T_1$ ground state in an octahedral environment is split into three levels with *J* value of 5/2, 3/2, and 1/2, respectively. At high temperatures, the excited states are occupied with large orbital contribution. At low temperatures, only the doubly degenerate ground state with $J = 1/2$ is occupied. [111] The paramagnetic behavior of $[Co(NO_3)_2(4,4'\text{-bipyridine})_{1.5}(MeCN)]_n$ can be explained based on its structural features. As shown in Figure 4-13, the two pyridine rings in the 4,4'-bipyridine molecules are twisted to each other, magnetically isolating the Co(II) ions.

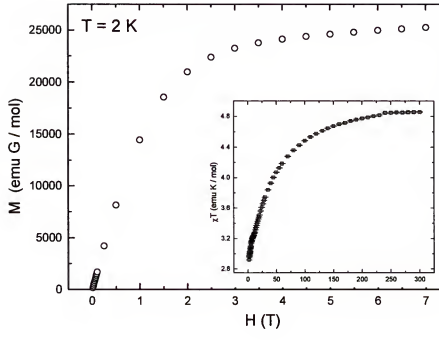


Figure 4-11. Plots of $M$ *vs* $H$ and $\chi T$ *vs* $T$ (inset) for $[Co(NO_3)_2(4,4'\text{-bipyridine})_{1.5}(MeCN)]_n$ at 2 K.

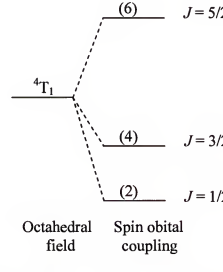


Figure 4-12. Fine-structure splitting of the lowest levels of Co(II) under the combined action of an octahedral field and spin-orbital coupling. The levels are labeled with the $J$ values and the degeneracies in the parentheses.

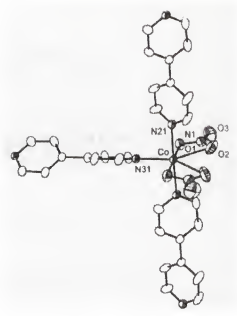


Figure 4-13. Coordination modes around Co(II) in $[Co(NO_3)_2(4,4'\text{-bipyridine})_{1.5}(MeCN)]_n$.[110]

**Magnetic Properties of $Ni_2(dpa)_2(pyz)(H_2O)_4$**

The magnetization measured as a function of field is shown in Figure 4-14. The plot shows no sign of zero magnetization at low field. So, $Ni_2(dpa)_2(pyz)(H_2O)_4$ is only a structural ladder, but not a spin-ladder. Also shown in Figure 4-14 is the simulation plot of the Brillouin function for 2 moles of $S = 1$ ions at 2 K. The $g$ value used for this simulation is 2.01 obtained from the fitting of the susceptibility plot as a function of temperature for $Ni_2(dpa)_2(pyz)(H_2O)_4$. The increase of the molar magnetization for 1 mole of $Ni_2(dpa)_2(pyz)(H_2O)_4$ is much slower than that predicated by the Brillouin function. This indicates the presence of antiferromagnetic exchange interactions in this material. However, even at 2 K, the molar magnetization of $Ni_2(dpa)_2(pyz)(H_2O)_4$ acquired when the field is 7 Tesla is only just above 15000 emu G, far from the saturation value of 22443 emu G calculated based on the Brillouin function. Such behavior may be caused by spin orientations that are strongly constrained by local magnetic anisotropy to

become aligned along certain directions and require a much higher field to be overcome. The fitting of the susceptibility data will provide more evidences on this issue.

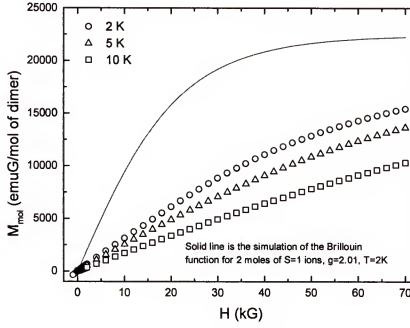


Figure 4-14. Magnetization measured as a function of field at 2 K, 5 K, and 10 K, respectively, for $Ni_2(dpa)_2(pyz)(H_2O)_4$. The solid line is the simulation of the Brillouin function for 2 moles of $S = 1$ ions at 2 K with $g = 2.01$.

The susceptibility of $Ni_2(dpa)_2(pyz)(H_2O)_4$ has been plotted as a function of temperature in Figure 4-15. Two measurements are plotted with measuring field of 100G, and 1 kG, respectively. The field-cooled and zero-field-cooled data obtained at 100 G show a difference indicating a possible long-range ordering. However, such difference is not observed when the measuring field is 1 kG. This could be due to a small canting angle between the spins that results in a small but nonzero net magnetization which retains when the measuring field is as weak as 100 G. With 1 kG measuring field, the canting is easily removed by the field so that the field-cooled and zero-field-cooled data are no longer distinguishable.

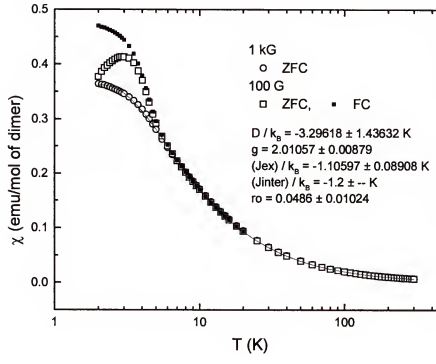


Figure 4-15. Susceptibility plotted as a function of temperature for $Ni_2(dpa)_2(pyz)(H_2O)_4$. The solid line is a fit using a dimer model including, axial-field zero-field splitting term, D, interdimer interaction, and intrinsic impurity.

The 1 kG data has been fitted to a dimer model that includes considerations of axial-field zero-field splitting effect, interdimer interaction, and paramagnetic impurity. The fitting results are summarized in Table 4-1. The model was reported in 1972 by Ginsberg *et al.* [112] The model was derived based on the Hamiltonian:

$$\boldsymbol{H} = -2J\boldsymbol{s}_1 \cdot \boldsymbol{s}_2 - \boldsymbol{g}\beta H S_z - 2Z'J'S_z\langle S_z\rangle - \boldsymbol{D}\cdot(s_{1z}^2 + s_{2z}^2) \qquad (4\text{-}1)$$

where $\boldsymbol{s}_1$ and $\boldsymbol{s}_2$ are the spin operators for the two Ni(II) ions, respectively. $\boldsymbol{S}_z$ is the $z$ component of the total dimer spin. $J$ and $J'$ are, respectively, the intradimer and interdimer exchange integral expressed in the unit of $k$. $Z'$ is the dimer lattice coordination number. $\boldsymbol{D}$ is the zero-field splitting parameter. $\boldsymbol{s}_{1z}$ and $\boldsymbol{s}_{2z}$ are the $z$ components of the spin operator for the Ni(II) ions. The first term is the isotropic-exchange Hamiltonian for

intradimer interactions. The second term is the Zeeman term. The third term is the Hamiltonian for interdimer interactions. The last term is the zero-field splitting term.

The fitting results indicate that the exchange interaction within the dimers, propagated by pyrazine, is antiferromagnetic with a magnitude of about 1.1 K which is in good agreement with other dimeric structures also bridged by pyrazine.[113, 114] The exchange interaction between the dimeric units is also antiferromagnetic of very similar magnitude. These results are consistent with the observation of magnetization as a function of field. Since the dimers are not covalently linked to each other, the interdimer interactions are most likely propagated through the extensive hydrogen bonding network both within individual ladders and between different ladders.

Table 4-1. Fitting results for the molar susceptibility *vs* temperature plot of $Ni_2(dpa)_2(pyz)(H_2O)_4$ fitted to Equation 4-1.

| Fitting Parameters | Value |
|---|---|
| $D / k_B$ (axial-field zero-field splitting term) | $-3.30 \pm 1.44$ K |
| $g$ | $2.01 \pm 0.01$ |
| $J / k_B$ (intradimer interaction) | $-1.10 \pm 0.09$ K |
| $J' / k_B$ (interdimer interaction) | $-1.20 \pm$ - - K |
| $ro$ (paramagnetic impurity) | $0.05 \pm 0.01$ |

The fitting results also indicate the $g$ value is 2.01. This is smaller than the average value of 2.25 observed for some other Ni(II) dimers,[111] but not uncommon.[115, 116, 117] The smaller $g$ value can be due to the quite strong zero-field splitting effect as evidenced by the $D/k_B$ value of $-3.3$ K.[9] The negative sign indicates that there may be a magnetization easy axis in the structure that could give rise to a local magnetic anisotropy.[118] However, the value of the zero-field splitting term strongly depends on the initial value assigned during the fitting process. As pointed out by Ginsberg,[112] the zero-field splitting and the

interdimer exchange parameters strongly affect each other in the fitting process and can not be determined with reasonable accuracy simultaneously.

## Conclusion

Two coordination polymers with ladder-like structures have been synthesized and magnetically investigated.

In $[Co(NO_3)_2(4,4'\text{-bipyridine})_{1.5}(MeCN)]_n$, the ladders are neutral covalent networks and are isolated from each other with no interpenetration between ladders. Magnetically, due to the twisting between the two pyridine rings in the 4,4'-bipyridine molecules that magnetically isolates the Co(II) ions, the system behaves basically as a paramagnetic system.

In $Ni_2(dpa)_2(pyz)(H_2O)_4$, the ladder consist of dimers stacking on top of each other through hydrogen bonding to form a ladder-like structure. The noninterpenetrating ladders are parallel to each other, but interconnected through an extensive hydrogen bonding network. Magnetically, no spin-ladder behavior is observed. Instead, weak antiferromagnetic exchange interactions of comparable magnitudes of about 1 K have been observed to propagate through pyrazine and the hydrogen-bonding network that exists both within individual ladders and between ladders. Due to the strong axial-field zero-field splitting of −3.3 K, spins are constrained along certain easy-magnetization axis and the molar magnetization remains much smaller than that predicted by the Brillouin function at 2 K with an external magnetic field of 7 Tesla.

# CHAPTER 5
# STRATEGIES FOR THE SYNTHESIS OF PRUSSIAN BLUE ANALOGUES WITH LADDER-LIKE STRUCTURES

In Chapter 4, we have seen it is possible to build a ladder-like structure using the self-assembling principle. But, many of the organic bridging ligands used in the construction of such structures are incapable of mediating magnetic exchange, or only propagate very weak interactions between paramagnetic ions. This does not become a problem so long as the magnetism of only one individual ladder is concerned. However, in the solid state where many ladders pack to form crystal structure, individual ladders are frequently associated with one another through various types of intermolecular forces provided by closely related organic ligands or counter ions which also propagate exchange interactions between ladders so that ladders are no longer magnetically isolated from each other although they are physically isolated in the crystal structure. In this case, the interladder exchange may be of comparable or even greater magnitude compared to the intraladder exchange, and such interference makes it impossible to obtain spin ladders.

All the examples discussed so far in this dissertation are monometallic systems in which all the metal ions are of the same element and have the same oxidation state and linked together through purely organic molecules. A distinctively different system that may also render ladder-like structures are low-dimensional analogues of Prussian Blue (PB). PB and its analogues can be described as cyanide-bridged bimetallic systems. Cyanide anion exemplifies the early use of linear bridging ligands. PB structure has been

known for many decades in which all the metal ions are bridged through cyanide anion and the structure extends in all three dimensions. Cyanide anion is known to propagate both ferromagnetic and antiferromagnetic exchange interactions depending on the orbitals involved in the exchange process. Some of the three dimensional (3-D) PB analogues exhibit ferromagnetic and ferrimagnetic long range ordering at temperatures as high as room temperature.[119-121] Such a strong exchange mediated by cyanide anions would offer an opportunity to build cyanide-bridged bimetallic ladder-like structures with the intraladder exchange strong enough so that the interladder exchange is negligible. In light of the many examples of low-dimensional PB analogues published in recent years, a similar attempt on the synthesis of ladder-like structure is reasonable.

In the following space, a survey on the synthesis and structural features of low dimensional PB analogues reported in recent years will be given. Then, strategies on building cyanide-bridged bimetallic ladder-like structures are discussed. Finally, synthetic results based on the proposed strategies are presented.

**Synthesis and Structures of Low-Dimensional Prussian Blue Analogues**

Prussian Blue (PB), $Fe^{III}_4[Fe^{II}(CN)_6]_3 \cdot xH_2O$, is obtained from the reaction between $[Fe(H_2O)_6]^{3+}$ and $[Fe^{II}(CN)_6]^{4-}$ in water as an insoluble blue precipitate.[122] Although single crystals of this compound have not been produced due to rapid coordination of cyanide anion with metal ions that produces precipitation rather than single crystals, its structure is commonly accepted based on data from X-ray powder diffraction and X-ray photoelectron spectroscopy as the one shown in Figure 5-1.[122] PB is the prototype of coordination polymers with extended structures. PB and its analogues usually contain two metal ions in their structures, one divalent and the other trivalent. The two metal ions which can be of different elements or different oxidation states of the same element are

bridged by cyanide anions. Each metal ion is surrounded by six cyanide anions to form an octahedral geometry.

In the past ten years, the research based on PB and its analogues has been focused on two frontiers: (1) synthesis of 3-D PB analogues as molecular magnets having high ordering temperatures, work in this area have been extensively published by Girolami and Verdagure,[121, 123] and (2) synthesis and characterization of PB analogues with reduced dimensionalities. To reduce the dimensionality, coordinatively unsaturated metal complexes have been used to substitute the divalent metal ions (simple ions) in the 3-D PB-like structures. Among the people working in the second area, Ohba and Okawa,[124] Long,[125, 126] Dunbar,[127, 128] and Kou,[129-131] among others,[132] have been the most noticeable. The following discussion will be presented according to the dimensionality of the structures.

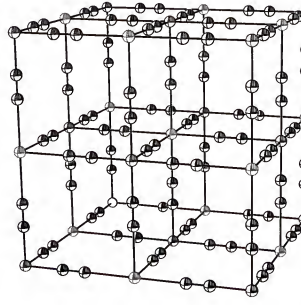

Figure 5-1. Idealized structure of Prussian Blue, $Fe^{III}_4[Fe^{II}(CN)_6]_3 \cdot xH_2O$ ($Fe^{II}$ red, $Fe^{III}$ green, C black, N blue).[122]

**Zero-Dimensional Systems**

Zero-dimensional (0-D) systems do not have extended structures. Examples include those reported from Long *et al.*[125] Long *et al.* used a neutral tridentate ligand, N,N',N''-trimethyl-1,4,7-triazacyclononane ($Me_3TACN$) to react with an octahedral transition metal ion so that three of the six coordination sites on the metal ion are blocked in a facial fashion and the other three site are left open for subsequent bridging reaction. As already discussed in Chapter 4, the bridging reaction is basically a ligand replacement reaction. Long *et al.* then reacted $[Cr^{III}(Me_3TACN)(CN)_3]^{3+}$ with $[Ni^{II}(H_2O)_3]^{2+}$ to form molecular cages shown in Figure 5-2.[125]

$$8\,[Cr^{III}(Me_3TACN)(CN)_3]^{3+} + 6\,[Ni(H_2O)_6]^{2+} \longrightarrow [(Me_3TACN)_8Cr_8Ni_6(CN)_{24}]^{12+}$$

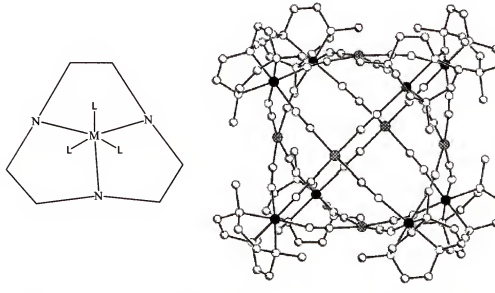


Figure 5-2. Structures of the $M(Me_3TACN)L_3$ (L = $CN^-$ or $H_2O$) molecular building block and $[(Me_3TACN)_8Cr_8Ni_6(CN)_{24}]^{12+}$ cluster. (black, crosshatched, shaded, and white spheres are Cr, Ni, C, and N atoms, respectively).[125]

The fact that the molecular building blocks have facial coordination geometry determines that the final product is going to be zero dimensional because the only possible bonding mode for all the components is *cis*. In order for the structure to extend

along certain directions, *trans* bonding mode would be needed. Clusters such as $[(Me_3TACN)_8Cr_8Ni_6(CN)_{24}]^{12+}$ frequently require large number of counter anions to balance the charge. In this particular case, the molecular cage is cocrystalized with as many as twelve counter ions including nitrate, perchlorate, chloride, and bromide, respectively, to afford different crystals. What is interesting is that the molecular cages are empty, all the counter ions are located outside the cages surrounding the zero dimensional clusters. Another example of cyanide-bridged bimetallic cluster is $[Ni(tetren)]_6[Cr(CN)_6](ClO_4)_9$ was reported by Mallah *et al.* [133] Again, as many as nine counter ions are needed in this structure.

**One-Dimensional Systems**

One-dimensional (1-D) bimetallic assemblies with general formula of $PPh_4[Ni^{II}(pn)_2][M^{III}(CN)_6]\bullet H_2O$ (PPh = tetraphenylphosphonium; pn = *rac*-1,2-propanediamine; M = Fe, Cr, Co) have been reported by Ohba and Okawa.[134, 135] These materials were prepared from the reaction of $[Ni(pn)_3]Cl_2$, $K_3[M(CN)_6]$ and $PPh_4Cl$ in the 1:1:1 stoichiometry in an aqueous solution. In the synthesis, the slow dissociation of $[Ni(pn)_3]^{2+}$ into $[Ni(pn)_2]^{2+}$ slows down the kinetics of the bridging reactions so that large single crystals are obtained in the self-assembling process. The pn molecules coordinated to the same Ni(II) ion are *trans* to each other such that an extended structure is possible. The crystal structure of $PPh_4[Ni(pn)_2][Fe(CN)_6]\bullet H_2O$ is shown in Figure 5-3. The counter ions $PPh_4^+$ are located between the chains to expand the interchain separation. The number of counter ions has also reduced dramatically compared to zero-dimensional systems. But, still, $PPh_4^+$ is quite bulky compared to many other commonly used counter ions.

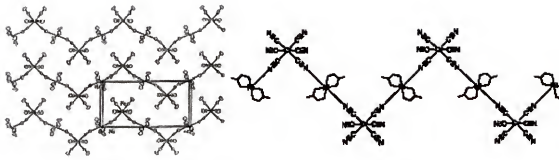

Figure 5-3. Three $PPh_4[Ni(pn)_2][Fe(CN)_6]\cdot H_2O$ 1-D chains (left), and a schematic illustration of the chain (right). ($PPh_4^+$ and $H_2O$ are omitted).[134, 135]

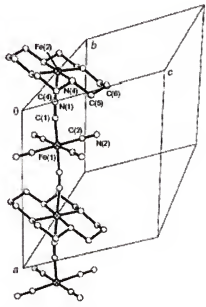


Figure 5-4. Chain structure of $[Fe^{III}(cyclam)][Fe^{III}(CN)_6]\cdot 6H_2O$.[136]

Another example of one-dimensional structure is $Fe^{III}(cyclam)][Fe^{III}(CN)_6]\cdot 6H_2O$, where cyclam is 1,4,8,11-tetraazacyclotetradecane.[136] It was synthesized when $[Ni(cyclam)](ClO_4)_2$ was reacted with excess $K_3[M(CN)_6]$. The structure, shown in Figure 5-4, is neutral and requires no counter ions. However, the synthesis of this material is quite serendipitous, and bimetallic cyanide-bridged structure containing two metal ions of the same oxidation state is very rare.

**Ladder-like Systems**

To date, the only known bimetallic cyanide-bridged ladder-like structures, also known as rope ladders, $[Ni^{II}(en)_2]_3[M^{III}(CN)_6]_2 \cdot 2H_2O$ (en = ethylenediamine, M = Fe, Cr, Co, Mn) were first reported by Ohba and Okawa in 1994.[137, 138] Good quality single crystals were obtained by the reaction of $[Ni(en)_3]Cl_2$ and $K_3[M(CN)_6]$ in 3:2 stoichiometry in water. Again, slow dissociation of $[Ni(en)_3]^{2+}$ to $[Ni(en)_2]^{2+}$ afforded large single crystals in a self-assembling fashion. The structure of one of the ladders is shown in Figure 5-5. All the four ladder-like structures for M = Fe, Mn, Cr, Co are isomorphous. Each $[Co^{III}(CN)_6]^{3-}$ bridges in a meridional fashion. The $[Ni^{II}(en)_2]^{2+}$ moieties on the two legs bridge in *cis* fashion, while those on the rungs bridge in *trans* fashion. Besides the stoichiometry of 3:2 for $[Ni(en)_3]Cl_2 : K_3[M(CN)_6]$, no other factors were exploited to encourage the formation of a ladder-like structure. So the bridging modes of $[Co^{III}(CN)_6]^{3-}$ and $[Ni^{II}(en)_2]^{2+}$ were unexpected. However, the structural features are quite informative for synthesizing ladder-like structures in a more predictable way. These ladders are all neutral structures without counter ions. The ladders form two dimensional layers in the *bc* planes *via* inter-ladder interactions and the water molecules reside in between the two-dimensional (2-D) layers rather than in the square cavity consisted of eight metal ions and eight cyanide anions.

The magnetic behavior of these ladders are worth mentioning. For the cases where $M^{III}$ = Fe, Mn, Cr, all three ladders show ferromagnetic interactions between $M^{III}$ and $Ni^{II}$ in the 2-D sheets. A 3-D antiferromagnetic ordering occurs at low temperatures as the 2-D layers are coupled antiferromagnetically.

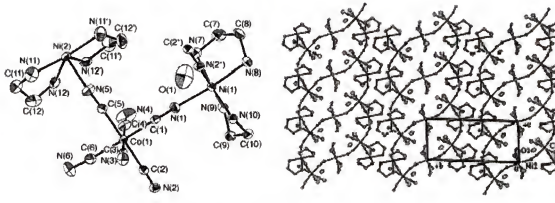


Figure 5-5. Structural repeating unit (left) and ladder structure in $[Ni^{II}(en)_2]_3[Co^{III}(CN)_6]_2 \cdot 2H_2O$ (right).[137, 138]

**Two-Dimensional Systems**

Examples in this category include $[Ni^{II}(N\text{-men})_2]_3[M^{III}(CN)_6]_2 \cdot nH_2O$, where N-men is N-methylethylenediamine and $M^{III}$ is Fe, Co. [124] They were synthesized by the reaction of $[Ni^{II}(N\text{-men})_3]Cl_2$ and $K_3[M(CN)_6]$ in 3:2 molar ratio in water. The extended network has a 2-D honeycomb structure. Three cyano nitrogen atoms of $[M(CN)_6]^{3-}$ coordinate to $Ni^{II}$ in facial fashion and the $[Ni^{II}(N\text{-men})_2]^{2+}$ moieties coordinate in *trans* fashion so that a hexagonal unit forms with $M^{III}$ at each corner and $Ni^{II}$ at the center of each edge. The structure of $[Ni^{II}(N\text{-men})_2]_3[Fe^{III}(CN)_6]_2 \cdot nH_2O$ is shown in Figure 5-6. Again, this 2-D honeycomb structure is neutral with no counter ions needed. As many as 15 water molecules per repeating unit were found residing inside the 2-D sheets. Comparing the rope ladder and this 2-D honeycomb structures, it can be seen that the introduction of a methyl group onto the nitrogen in ethylenediamine changes the structure of the resulting network from ladder to 2-D honeycomb although both structures have the same stoichiometry of 3:2 for [bridge]:[node]. The same neutral 2-D honeycomb networks were also obtained by replacing the two N-men molecules on $Ni^{II}$ by one tetradentate 1,4,8,11-tetraazacyclotetradecane (cyclam) molecule.[139, 140]

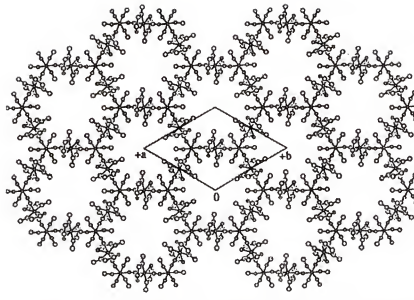


Figure 5-6. Top view of one layer of the 2-D $[Ni^{II}(N\text{-men})_2]_3[Fe^{III}(CN)_6]_2 \cdot nH_2O$ network.[124]

Other 2-D networks reported include 2-D square grid networks with general formula of $[Ni(L)_2]_2[Fe(CN)_6]X \cdot nH_2O$, where L is en, pn, 1,1-dmen; 1,1-dmen is 1,1-dimethylethylenediamine, and X is counter anion.[141] A structure of the 2-D grid network is shown in Figure 5-7.

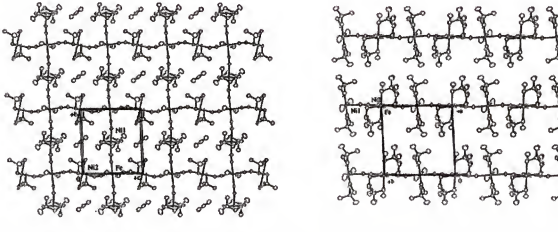

Figure 5-7. Structure of the 2-D $[Ni^{II}(1,1\text{-dmen})_2]_2[Fe^{III}(CN)_6]N_3 \cdot 4H_2O$ network. (left) top view. (right) side view of three layers of the same network.[124]

Since en, pn, and 1,1-dmen have different sizes, the resulting 2-D square grids have different thickness as the diamine molecules build up a fence perpendicular to the 2-D

grid plane. This in turn gives rise to different volume of the square cavities defined by eight metal ions and eight cyanide anions. As a consequence, counter ions of different sizes are accommodated within the cavities of different volumes. The water molecules reside in between the 2-D grids. Note only one counter ion is needed per repeating unit.

**Strategies for Synthesizing PB Analogues with Ladder-like Structures**

Let's first summarize the facts that have been learned by studying the structures of the examples of low-dimensional PB analogues discussed above. They are: (1) In all cases, cyanide are introduced into the final structures by using hexacyano-metal(III) complexes, except in the case of the clusters reported by Long *et al.* where tricyano-metal complexes were prefabricated and then used as building blocks. (2) Hexacyano-metal(III) complexes prefer *cis* and facial coordination modes, rather than *trans* and meridional modes. (3) All extended structures involve *trans*-coordination geometry. Zero-dimensional structures are obtained if only *cis* coordination geometry is present. (4) The use of divalent metal complexes with three bidentate diamine ligands which later slowly dissociate into *trans*- or *cis*-coordinating bridging ligands afforded single crystals. (5) As substituents are introduced onto the backbone of ethylenediamine, the $[M^{II}(diamine)_2]^{2+}$ complexes bridge exclusively in a *trans* fashion. (6) The linear segment of $M^{'}$-CN-M-CN-$M^{'}$ has a dimension of about 10.2 Å. (7) As the dimensionality increases, the number of counter ions drops significantly. Many structures were obtained as neutral networks that do not need counter ions. (8) The volume of the hexagonal or square cavities in the 2-D structures and the rope ladders depends on the size of the diamine molecules.

Among all the observations summarized above, we feel that charge balance is a crucial factor in the formation of low-dimensional PB analogues, and a neutral structure

and a structure with at most one counter ion are the most promosing. For PB-like systems, charge balance is manifested in the synthesis by the choice of transition metal ion oxidation states, the choice of neutral or charged blocking and bridging ligands, and also by the choice of the counter ions. Based on the proposed strategy of synthesizing ladders by using T-shaped building blocks, shown in Figure 4-4, we present the following analysis using the rope ladder as an example. In the structures, hexacyano-metal(III) complexes function as the nodes, while $[M^{II}(diamine)_2]^{2+}$ provide the bridges. Hexacyano-metal(III) complexes have charge of −3, and each bridge has charge of +2. The structural repeating unit, shown in Figure 5-5, in the rope ladder includes two hexacyano-metal(III) nodes and three bridges so that all opposite charges cancel and the final network is neutral. However, this is not the case according to our proposed strategy, discussed in Chapter 4, of synthesizing ladders using T-shaped building blocks. If a neutral planar tridentate blocking ligand is used to prepare the tricyano-metal(III) complex functioning as the nodes in the ladder, then six negative charges are lost for each repeating unit and must be compensated somewhere else in the final structure. Based on the known examples, it may be difficult to accommodate six monovalent counter ions or even two trivalent counter ions.

This is an appropriate place to recall the structure of the clusters reported by Long *et al.* since those structures are the only examples where part of the negative charges of the hexacyano-metal(III) complexes had to be compromised in order to incorporate a neutral tridentate blocking ligand, a situation very similar to the one we are facing. Indeed, as evidenced by the chemical formula of their clusters, Long *et al.* encountered the same problem that they had to introduce a large number of monovalent counter ions

into the structures to balance the charge, frequently as many as 12 per cluster. However, the structures Long *et al.* were trying to synthesize happened to be clusters which are zero dimensional systems, and there seems no problem for such systems to accommodate that many of counter ions. On the other hand, our systems are extended networks which, as shown by the examples of 1-D, 2-D structures and the rope ladders, have limited space in the crystal structure for counter ions to reside. So, the problem we are facing has to be solved indirectly.

Apparently, incorporating counter ions is not the only way to compensate negative charges. To minimize the number or even eliminate the use of counter ions while still maintain the necessary number of negative charges to build a neutral network, one can use a negatively charged planar tridentate blocking ligand, or to lower the oxidation state of the metal ions in the structure, or simultaneously both. In principle, the organic ligand on the bridging metal complex can also be charged. But, based on the fact that trisdiamine metal complexes have the unique ability to dissociate slowly and allow single crystals to form, diamine and similar compounds are our primary choice and they are all neutral compounds. In general, the repeating unit of a ladder structure can be represented as $[bridge]_3[node]_2$, neutral or charged, as shown in Figure 5-8.

Since the diamine molecules are neutral, to build a neutral ladder network, we need two $M_A^{n+}$, three $M_B^{m+}$, and two negatively charged blocking ligands to balance six cyanide anion. The variables here are the oxidation state of the five metal ions, and the negative charge of the blocking ligands. Our choices of metal ions include all oxidation states for each ion from vanadium to copper. However, all the known PB analogues contain only divalent and trivalent metal ions. No PB analogues containing metal

oxidation states of other kinds have been reported. 2,2':6',2"–terpyridine (terpy) and its known derivatives are all neutral blocking ligands. The only charged blocking ligand that is currently available in our laboratory is the dianion of 2,6-pyridinedicarbixylic acid (dpa) which has −2 charge.

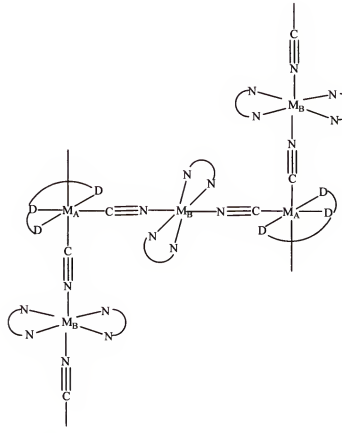

Figure 5-8. Structural repeating unit of a ladder-like PB analogue. D-D-D is the planar tridentate blocking ligand, N-N represents a neutral diamine molecule.

Based on the principle of charge balance discussed above, simple arithmetic calculations were carried out in search of neutral ladder structures. The results presented here are those in which counter ions are anions. The results are:

$[M_B^{II}(\text{diamine})_2]_3[M_A^{II}(\text{dpa})]_2(CN)_6$, $[M_B^{II}(\text{diamine})_2]_3[M_A^{III}(\text{dpa})]_2(CN)_6X_2$,

$[M_B^{II}(\text{diamine})_2]_3[M_A^{II}(\text{terpy})]_2(CN)_6X_4$, $[M_B^{II}(\text{diamine})_2]_3[M_A^{III}(\text{terpy})]_2(CN)_6X_6$.

$[M_B^{III}(diamine)_2]_3[M_A^{II}(dpa)]_2(CN)_6X_3$, $[M_B^{III}(diamine)_2]_3[M_A^{III}(dpa)]_2(CN)_6X_5$, $[M_B^{III}(diamine)_2]_3[M_A^{II}(terpy)]_2(CN)_6X_7$, $[M_B^{III}(diamine)_2]_3[M_A^{III}(terpy)]_2(CN)_6X_9$. X represents a negatively charged counterion. Among all the formula obtained from calculations, only $[M_B^{II}(diamine)_2]_3[M_A^{II}(dpa)]_2(CN)_6$ is a neutral structure. Another neutral structure, $[Ni^{II}(CN)_4]_3[M^{III}(terpy)]_2$, is also found as a unique example offered by the use of $[Ni(CN)_4]^{2-}$ as the bridging ligand. This case is actually also predicted by the calculations outlined above if we consider to reduce the positive charge on the bridges. However, $[Ni(CN)_4]^{2-}$ is the only complex available to achieve this purpose. Therefore, it was considered as a separate case.

Similar calculations were also performed for metal ions having oxidation state of I, IV, and V. It has been noticed that there seems to be a correlation between the oxidation state of the metal ion on the bridges and the number of counter anions needed. When the oxidation state is an odd number, the number of counter anions needed is also an odd number, which means the structure will contain at least one counter ion, cation or anion. When the oxidation state is an even number, the number of counter ions needed is also an even number, which means a neutral structural is possible.

There are different ways to synthesize $[M_B^{II}(diamine)_2]_3[M_A^{II}(dpa)]_2(CN)_6$. The cyanide anions can be introduced through the metal complexes at the nodes, which means that a T-shaped complex like $[M_A^{II}(dpa)(CN)_3]^-$ must be synthesized. However, such compound is unknown in synthetic literatures. So the cyanide anions must be provided by the bridging metal complexes. Again, *trans*-$M_B^{II}(diamine)_2(CN)_2$ is also an unknown compound in the literature. But, the synthesis of *trans*-$M_B^{II}(cyclam)(CN)_2$ has been reported for Fe(II). Cyclam is 1,4,8,11-tetraazacyclotetradecane, a tetradentate chelating

ligand which has, synthetically, the same effect as two diamine molecules. The structure of a metal complex with cyclam is shown in Figure 5-9. The $M_A^{II}(dpa)(L)_3$ is known for Ni(II) as $Ni^{II}(dpa)(H_2O)_3$.

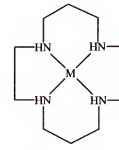


Figure 5-9. Structure of a metal ion coordinated to a cyclam molecule.

## Experimental Section

### Materials

2-acetyl pyridine, benzaldehyde, ammonium acetate, 2,6-pyridinedicarboxylic acid (dpa), electroanalytical grade iron powder, trifluoromethanesulfonic acid (98%), ammonium hexafluorophosphate (95%), 1,4,8,11-tetraazacyclotetradecane (cyclam), potassium nickel tetracyanide, 2,2':6',2"-terpyridine (terpy), and anhydrous iron(III) chloride were purchased from Aldrich (Milwaukee, WI). Anhydrous nickel carbonate was purchased from Alfa Aesar. Potassium cyanide and sodium hydroxide were purchased from Fisher. All chemicals were used as received. Acetonitrile is degassed and dried over calcium hydride prior to use. Water is purified using a NANOpure purification system.

### Synthesis of $Ni(dpa)(H_2O)_3$

$Ni(dpa)(H_2O)_3$ is synthesized using the procedure of Walton *et al.* [142] of reacting equimolecular $NiCO_3$ and 2,6-pyridinedicarboxylic acid in water at 60 $^0$C. According to

Walton *et al.*, the resulting aqueous solution of $Ni(dpa)(H_2O)_3$ is used *in situ* without characterization.

**Synthesis of 4'-Phenyl-2,2':6',2"-terpyridine (Ph-terpy)**

The synthesis of 4'-phenyl-2,2':6',2"-terpyridine is performed following the procedure of Constable *et al.*[143] 5.200 g of NaOH is dissolved in 200.0 ml of a mixture of water and ethanol (v/v=1:1) in a round-bottom flask. To this NaOH solution is added 2.745 g (0.02586 mol) of benzaldehyde and the solution turns to bright yellow. Then, 6.262 g (0.05172 mol) of 2-acetyl pyridine is added slowly through a dropping funnel to the flask. Precipitation starts to form and the mixture turns to pink-orange color. After 24 hours of stirring at room temperature, the mixture turns to a milk-coffee color, precipitation is then collected by filtration and washed thoroughly with ethanol until the filtrate is colorless and the solid on the filter paper is white. 8.6 g (quantitative yield) of white solid is obtained as intermediate product. This intermediate product is used without characterization.

This white powder (8.6 g) and 20 g (large excess) of ammonium acetate are put into a round-bottom flask (with a condenser) containing 300 ml of ethanol and heated up to boiling . If a solution can not be obtained, about 50 ml of THF is then added to help dissolve the reactants to form a solution. The solution is stirred for 7 hours at boiling during which period the color of the solution turns to dark green. Then the volume of the solution is reduced by heating until precipitation starts to form (by doing so, THF is all removed since the final product is very soluble in THF). After the solution is placed in freezer for a few hours, a green-white solid is collected by filtration and washed with ethanol until the filtrate is colorless. This solid is then recrystallized from boiling ethanol and small amount of THF. 3.6 g of pale yellow crystals (needles or blocks) is obtained as

the final product (50% yield). This final product is characterized by $^1$H NMR spectroscopy according to the published data.[143] 8.75 ppm (2H, 3' and 5'), 8.74 ppm (2H, 6 and 6"), 8.69 ppm (2H, 3 and 3"), 7.90 ppm (2H, 4 and 4"), 7.36 ppm (2H, 5 and 5"), 7.45 ~ 7.55 ppm (3H, para and meta to 4'), 7.86 ppm (2H, ortho to 4').

**Synthesis of $[Fe^{III}(Ph\text{-}terpy)]Cl_3$**

A sample of anhydrous $Fe^{III}Cl_3$ is dissolve in minimum amount of tetrahydrofuran (THF). A THF solution of equimolecular 4'-phenyl-2,2':6',2"-terpyridine is then added to the $Fe^{III}Cl_3$ solution. After the mixture is stirred for a while, it is poured into ice cold methanol. The yellow precipitate is then collected by filtration and washed with addition cold methanol to give the final product, $[Fe^{III}(Ph\text{-}terpy)]Cl_3$. The material is sensitive to light and should be kept in dark. The product is characterized by elemental analysis. Calculated: C 53.49%, H 3.20%, N 8.91%, found: C 53.29%, H 3.36%, N 9.10%.

**Synthesis of $[Fe^{III}(terpy)]Cl_3$**

$[Fe^{III}(terpy)]Cl_3$ is synthesized using the same procedure as that for $[Fe^{III}(Ph\text{-}terpy)]Cl_3$. The yellow powder product is characterized by IR which shows a series of bands below 1500 cm$^{-1}$ due to various CH stretching modes.

**Synthesis of $[Ni^{II}(CN)_4]_3[Fe^{III}(terpy)]_2$**

$[Ni^{II}(CN)_4]_3[Fe^{III}(terpy)]_2$ was synthesized by a slow diffusion experiment in a U-tube. 1 equivalent of $[Fe^{III}(terpy)]Cl_3$ and 1.5 equivalents of $K_2[Ni^{II}(CN)_4]$ were dissolved separately in a small amount (2 to 3 ml) of water. Each solution is then added into a U-tube that is already filled with water to about 90% of the volume in the U-tube. After 2 weeks, the $[Fe^{III}(terpy)]Cl_3$ solution and the $K_2[Ni^{II}(CN)_4]$ solution started diffusing into each other. However, no crystals formed, only dark brown powder precipitate was obtained.

**Synthesis of $[Fe(MeCN)_6](CF_3SO_3)_2$**

This is done following the procedure of Busch *et al.*[144] 366 mg of iron powder is charged into a three neck round bottom flask containing a magnetic stirring bar and equipped with a condenser. Then the system is evacuated and filled with argon as a continuing stream of argon is passed into the flask. 15 ml of acetonitrile is transferred into the flask *via* canula. 2 grams of trifluoromethanesulfonic acid is then added through syringe to the flask. The mixture is warmed for a few minutes until reflux begins and then kept under reflux for 24 hours. After 24 hours, no insoluble substance is visible in the flask. A 100% yield is assumed and the resulting pale-yellow acetonitrile solution of $[Fe(MeCN)_6](CF_3SO_3)_2$ is used *in situ*.

**Synthesis of $[Fe(cyclam)(MeCN)_2](PF_6)_2$**

This is carried out following the procedure reported by Busch *et al.* [145] 1.314 g ( 1 equivalent) of cyclam is then added into the flask containing the acetonitrile solution of $[Fe(MeCN)_6](CF_3SO_3)_2$. The mixture is refluxed for 30 minutes and a hot ethanolic solution of excess of ammonium hexafluorophosphate ($NH_4PF_6$) is added into the mixture. The condenser is then removed and the mixture is stirred while being gently heated. As the solvent evaporates, pink precipitation occurs and is collected by filtration and washed with ethanol and air dried. The powder product, $[Fe(cyclam)(MeCN)_2](PF_6)_2$, is characterized by elemental analysis and IR. Calculated: C 26.76%, H 4.81%, N 13.38%, found: C 27.02%, H 4.76%, N 13.35%. IR: 560(s) and 835 (vs, $\upsilon_{PF}{}^{6-}$), 2260 (vw, $\upsilon_{CN}$ $CH_3CN$), 3288 (m, $\upsilon_{NH}$), 2879 (m, $\upsilon_{CH2}$).

**Synthesis of $[Fe(cyclam)](CN)_2$**

This is done according to the procedure of Busch *et al.*[145] 1 equivalent of $[Fe(cyclam)(MeCN)_2](PF_6)_2$ is dissolved in boiling acetonitrile. Excess (3 equivalents) of

KCN in hot methanol is added to the acetonitrile solution. The mixture is then refluxed for 2.5 hours and then evaporated to dryness. The solid is extracted with several portions of chloroform. The chloroform solution is then reduced to small volume and poured into ice cold diethyl ether. The purple precipitate is collected by filtration and washed with additional diethyl ether and air dried. This solid is characterized as the final product by IR and elemental analysis. IR: 2034 (vs, $\upsilon_{CN}$), 2080 (w, free $CN^-$), 2867 (m, $\upsilon_{CH2}$), 3252 (w, $\upsilon_{NH}$), 3420 (m, $\upsilon_{OH}$ $CH_3OH$). Elemental nalysis: calculated C 46.76%, H 7.85%, N 27.27%, found C 43.57%, H 6.58%, N 25.69%.

**Results and Discussion**

Due to the difficulty of obtaining crystalline product, only the powder product of $[Ni^{II}(CN)_4]_3[Fe^{III}(terpy)]_2$ has been analyzed by IR and elemental analysis. The powder is collected and by filtration and washed with water and air dried. The IR spectrum for the cyanide region presents cyanide stretching frequencies at 2129 $cm^{-1}$ (medium) and 2155 $cm^{-1}$ (very weak). In $K_2[Ni^{II}(CN)_4]$, the cyanide stretching frequency is at 2122 $cm^{-1}$. It is known that the stretching frequency for bridging cyanide is higher than the non-bridging cyanide, so both frequencies at 2155 $cm^{-1}$ and 2129 $cm^{-1}$ indicate bridging cyanide in the powder product, and the frequencies are consistent with those reported for other PB analogues containing $Fe^{III}$-CN-$Ni^{II}$ structure.[137, 138] However, whatever the resulting network may be, it is not a ladder-like structure as shown by the result of elemental analysis. Calculated for $[Ni^{II}(CN)_4]_3[Fe^{III}(terpy)]_2$ : C 47.30%, H 2.08%, N 23.64%, found: C 44.98%, H 2.58%, N19.72%.

One potential problem in reactions involving metal-terpy complexes is that the mono-terpy complexes are very unstable in water and even so in methanol. The formation constant of bis-terpy complexes is reportedly 200 times that formation constant of mono-

terpy complexes.[146] So, $[Fe^{III}(terpy)]Cl_3$ could have converted into a bis-terpy complex even before it diffused into $K_2[Ni^{II}(CN)_4]$. This event is evidenced by the color change of the solution. The aqueous solution of the mono-terpy complex is brown, while the color of the bis-terpy complex is red. This is especially problematic in a slow diffusion experiment because, in order to form crystals, the mono-terpy complex has to be kept in the solution for a prolonged period before it reacts with the other reactant so that when they do react, their concentrations are low enough to prevent powdering from happening. However, this strategy does not work well for cyanide bridged bimetallic systems as exemplified by the difficulty of obtaining a crystalline sample for Prussian Blue itself.

**Conclusion**

The charge balancing mechanism in low-dimensional cyanide bridged bimetallic systems has been carefully researched according to the reported examples. Charge balancing in PB type of structures is exemplified by the choice of transition metal ion oxidation states, neutral or charged blocking and bridging ligands, and also by the choice of the counter ions. Subsequently, calculations have been designed and carried out in search of all possible chemical formulae for PB analogues having a ladder-like structure. Two model structures, $[Ni^{II}(CN)_4]_3[Fe^{III}(terpy)]_2$ and $[Fe^{II}(cyclam)_2]_3[Ni^{II}(dpa)]_2(CN)_6$, which consist of neutral ladder-like networks have been identified based on the calculations and experimentally approached under the synthetic conditions currently available in our laboratories. After repeated attempts, no crystalline sample could be obtained for $[Ni^{II}(CN)_4]_3[Fe^{III}(terpy)]_2$ and the analyses of the powder product were also inconsistent with the results anticipated for the proposed ladder-like structure of $[Ni^{II}(CN)_4]_3[Fe^{III}(terpy)]_2$. For $[Fe^{II}(cyclam)_2]_3[Ni^{II}(dpa)]_2(CN)_6$, the synthesis of the

starting material [Fe(cyclam)]$(CN)_2$ is problematic and has not been successfully accomplished at the time this thesis was written.

# CHAPTER 6
# SYNTHESES, STRUCTURES AND MAGNETISM OF $Cu_2(C_2O_4)(HISTAMINE)_2(N_3)_2$, $Cu_2(C_2O_4)(HISTAMINE)_2[N(CN)_2]_2$, $[Cu_4(4,4'\text{-}BIPYRIMIDINE)_2(N_3)_8]_n$, AND $[Cu(TEREPHTHALATO)(H_2O)_2{\cdot}H_2O]_n$

## Introduction

In Chapter 4, we have seen that ladder-like structures can be built using T-shaped molecular building blocks which are joined together through linear bidentate bridging ligands. These T-shaped building blocks are made by reacting an octahedral metal ion with a planar tridentate blocking ligand. In the subsequent bridging reactions, such T-shaped building blocks are assembled in a face-to-face fashion with the opening coordination sites facing each other to form the interior of the ladder while the planar blocking ligands facing the exterior of the ladder. A potential problem in this process is that the length of the bridges must be long enough so that the steric interactions between the planar tridentate blocking ligands will not repel each other. However, increasing length of the bridging ligands could compromise the rigidity of the molecules and their ability to bridge in a linear bidentate fashion. This may have contributed to our unsuccessful attempts to use terpyridine-based T-shaped building blocks to build ladder structures. The two side pyridine rings may be too bulky that bridging ligands such as cyanide anion is too short to keep the two terpy apart. Actually, to the best of our knowledge, in no known examples of dimers and chains constructed by assembling terpyridine-based monomers, have the terpy ligands been found to adopt a coplanar and face-to-face conformation.[147-157] The two terpy molecules are always found to be twisted with each other or noncoplanar. A variety of bridging ligands of different lengths were

used in these examples including cyanide anion, azide, and bridges involving as many as 7 atoms.

One alternative is to build ladder-like structures by stacking dimeric building blocks. A bis-bidentate ligand may be used to coordinate two metal ions at the same time to form a dimer. Such dimers function as the rungs of the ladders which can then be linked together up and down the two legs by linear bidentate ligands. This way, the problem of electrostatic interaction is alleviated since the bisbidentate ligand is planar. Actually, there are known examples of this alternative strategy and one of them has been introduced in Chapter 4, Figure 4-3.[158-160] In that example, two Cu(II) ions are coordinated to one 2,2'-bipyrimidine to form dimeric units which are subsequently bridged by two dicyanamide anions to stack on top of each other to form ladders. Thus each Cu(II) ion is in a trigonal bipyramidal geometry in which two equatorial coordination sites are blocked by the bisbidentate ligand and the third equatorial site is occupied by a nonbridging ligand while the two axial coordination sites form the legs *via* linear bidentate bridging ligands. However, in this particular example, the dicyanamide bridges span as many as six bonds and significantly weaken their ability to propagate magnetic exchange.

In our approach, we would like to follow along the same line but also explore bis-bidentate ligands other than 2,2'-bipyrimidine, such as oxalate and terephthalate, and bridging ligands shorter than dicyanamide to enhance magnetic exchange interaction along the legs. We will continue to use Cu(II) as the spin carrier .

## Experimental Section

### Materials

Potassium oxalate monohydrate, sodium terephthalate, copper(II) nitrate pentahydrate, copper(II) perchlorate pentahydrate, sodium hydroxide, sodium azide, sodium dicyanamide, histamine dihydrochloride, and 2,2'-bipyrimidine were purchased from Aldrich (Milwaukee, WI) and used as received.

### Synthesis of $Cu_2(C_2O_4)(histamine)_2[N(CN)_2]_2$, 5

The first step is to synthesize a dimeric material, $Cu_2(C_2O_4)(histamine)_2(ClO_4)_2$. This is done following the procedure of Suh *et al.*[159] To an aqueous solution of 1 equivalent of Cu(II) perchlorate pentahydrate, were slowly added an aqueous solution containing 1 equivalent of histamine dihydrochloride and 2 equivalents of sodium hydroxide, and an aqueous solution of 0.5 equivalent of sodium oxalate. The mixture was stirred for 1 hour at room temperature and left to stand to allow water to evaporate. Deep blue crystals were collected by filtration, washed with water and dried in air. The product was characterized by IR and the result was compared with the published data. IR: 1650 ($C_2O_4^{2-}$), 1090 ($ClO_4^-$).

$Cu_2(C_2O_4)(histamine)_2(ClO_4)_2$ was used as the starting material for the synthesis of $Cu_2(C_2O_4)(histamine)_2[N(CN)_2]_2$. 1 equivalent of $Cu_2(C_2O_4)(histamine)_2(ClO_4)_2$ was dissolved in water and, to this solution, was added an aqueous solution of 2 equivalents of sodium dicyanamide. The resulting solution was stirred for 10 minutes and let stand to allow water to evaporate. After a few days, deep blue blocks of crystals were collected by filtration, washed with water and dried in air. The material was characterized by X-ray diffraction, IR, and elemental analysis. IR: 1650 ($C_2O_4^{2-}$), 2254, 2204, 2146 (dicyanamide). Elemental analysis: calculated C 33.74%, H 3.18%, N 29.51%, found

C 33.59%, H 2.90%, N 29.79%.

**Synthesis of $Cu_2(C_2O_4)$(histamine)$_2(N_3)_2$, 6**

$Cu_2(C_2O_4)$(histamine)$_2(N_3)_2$ was synthesized in a similar manner as $Cu_2(C_2O_4)$(histamine)$_2[N(CN)_2]_2$. 1 equivalent of $Cu_2(C_2O_4)$(histamine)$_2(ClO_4)_2$ was dissolved in water and, to this solution, was added an aqueous solution of 2 equivalents of sodium azide. The resulting solution was stirred for 10 minutes and let stand to allow water to evaporate. After a few days, dark green diamond-shaped crystals were collected by filtration, washed with water and dried in air. The material was characterized by single-crystal X-ray diffraction, IR, and elemental analysis. IR: 1650 ($C_2O_4^{2-}$), 2040 ($N_3^-$). Elemental analysis: calculated C 27.64%, H 3.48%, N 32.24%, found C 27.53%, H 3.17%, N 32.42%.

**Synthesis of [$Cu_4$(2,2'-bipyrimidine)$_2(N_3)_8]_n$, 7**

To a U-tube filled with water to about 80% of its total volume, an aqueous solution (a few milliliters) of 38 mg (0.24 mmol) of 2,2'-bipyrimidine and 62.5 mg (0.96 mmol) of sodium azide, and another aqueous solution (a few milliliters) of 112 mg (0.48 mmol) of Cu(II) nitrate pentahydrate are separately added into the U-tubes. 1 month later, slow diffusion of the two solutions afforded two types of crystals. One is dark green needles and the other is brown plates. The dark green needles are too small to be characterized by single-crystal X-ray diffraction experiment. Only the brown plates were characterized by single-crystal X-ray diffraction experiment. Since only very few crystals were obtained for this compound, no magnetic investigation was performed on it.

**Synthesis of [Cu(terephthalato)$(H_2O)_2$•$H_2O]_n$, 8**

To a U-tube filled with water to about 80% of its total volume, a methanol solution (a few milliliters) of 2 equivalents of Cu(II) nitrate pentahydrate is carefully layered on

top of the water surface in the U-tube. Into the other arm of the U-tube, an aqueous solution (a few milliliters) of 1 equivalent of sodium terephthalate and 4 equivalents of sodium azide is very slowly added. 1 month later, slow diffusion of the two solutions afforded rectangular light blue crystals growing on the inner wall of the U-tube. The crystals were collected by filtration and washed with cold water and dried in air. The product is characterized by single crystal X-ray diffraction experiments.

**X-ray Diffraction Experiments**

Data were collected at 173 K on a Siemens SMART PLATFORM equipped with a CCD area detector and a graphite monochromator utilizing $MoK_\alpha$ radiation with wavelength of 0.71073 Å. Cell parameters were refined using up to 8192 reflections. A full sphere of data (1850 frames) was collected using the ω-scan method (0.3° frame width). The first 50 frames were remeasured at the end of data collection to monitor instrument and crystal stability (maximum correction on I was < 1 %). Absorption corrections by integration were applied based on measured indexed crystal faces.

The structure was solved by the Direct Methods in *SHELXTL6,* and refined using full-matrix least squares. The nonhydrogen atoms were treated anisotropically, whereas the hydrogen atoms were calculated in ideal positions and were riding on their respective carbon atoms. A total of 163 parameters were refined in the final cycle of refinement using 2205 reflections with $I > 2\sigma(I)$ to yield $R_1$ and $wR_2$ of 3.85% and 10.21%, respectively. Refinement was done using $F^2$.

**EPR Measurements**

The EPR spectra were recorded with a Bruker ER 200D X-band (9 GHz) spectrometer modified with a digital signal channel and digital field controller. Room temperature spectra for all compounds were acquired using polycrystalline samples.

**Magnetic Measurements**

Static-magnetization measurements were performed with a Quantum Design MPMS SQUID magnetometer.

For $Cu_2(C_2O_4)(histamine)_2[N(CN)_2]_2$, a polycrystalline sample of 117.47 mg was used. The sample was placed in a plastic gelcap which was held in a straw. The sample was zero-field cooled to 5 K before the measuring field of 1 kG was applied, and data were subsequently acquired up to 300 K. The procedure was repeated while cooling the sample in the presence of the measuring magnetic field. Magnetization versus field measurements were performed at 5 K from 0 to 70 kG. The small background signals arising from the gelcap and straw were subtracted from the results. The diamagnetic contribution from the sample is calculated according to the Pascal constants to be $-238.62\times10^{-6}$ emu for per mole of dimer for $Cu_2(C_2O_4)(histamine)_2[N(CN)_2]_2$. The diamagnetic contribution has also been subtracted from the data.

For $Cu_2(C_2O_4)(histamine)_2(N_3)_2$, the static magnetic measurements were performed using the same procedure with a polycrystalline sample of 98.96 mg. The sample was zero-field cooled to 2 K before the measuring field of 1 kG was applied. Magnetization *vs* field measurements were performed at 2 K from 0 to 70 kG. The diamagnetic contribution subtracted for $Cu_2(C_2O_4)(histamine)_2(N_3)_2$ was $-190.22\times10^{-6}$ emu for per mole of dimer.

For [Cu(terephthalato)$(H_2O)_2$•$H_2O$]$_n$, the static magnetic measurements were performed using the same procedure for a polycrystalline sample of 11.48 mg. The sample was zero-field cooled to 2 K before the measuring field of 100 G was applied. Magnetization vs. field measurements were performed at 2 K and 5 K from 0 to 70 kG. The diamagnetic contribution subtracted was $-130.00\times10^{-6}$ emu for per mole of Cu(terephthalato)$(H_2O)_2$•$H_2O$.

**Results and Discussion**

A common structural feature of $Cu_2(C_2O_4)$(histamine)$_2[N(CN)_2]_2$ and $Cu_2(C_2O_4)$(histamine)$_2(N_3)_2$ is that they both have the repeat unit of a ladder as shown in Figure 6-1 and Figure 6-4. However, neither possesses a ladder-like structure or a covalent network of other topologies. The final structures for both compounds are dimers held together through intermolecular forces. The Cu(II) ions are in square pyramidal coordination geometry rather than an octahedral geometry since the dicyanamide and the azide anions did not bridge Cu(II) ions as anticipated. The same synthetic procedure was repeated using slow diffusion method for Ni(II) and Co(II), but, no crystalline product could be obtained.

**Description of the Structure of $Cu_2(C_2O_4)$(histamine)$_2[N(CN)_2]_2$.**

$Cu_2(C_2O_4)$(histamine)$_2[N(CN)_2]_2$ does not have a covalently linked extended network. Its structural repeating unit is a dimeric unit as shown in Figure 6-1. Two Cu(II) ions are bridged by an oxalate anion to form a dimer. Each Cu(II) ion is further coordinated to a histamine molecule and a dicyanamide anion to complete a square pyramidal coordination environment including three nitrogen atoms and two oxygen atoms. The four bond lengths in the square basal plane are very similar to each other, 1.997 Å (Cu-O1), 2.016 Å (Cu-O2), 1.967 Å (Cu-N2), and 1.984 Å (Cu-N1). The bond

between the Cu(II) and the nitrogen of the dicyanamide is 2.427 Å, significantly longer than the four bonds in the basal plane. Each Cu(II) is also further associated with the nitrogen atom belonging to the dicyanamide molecule from a neighboring dimeric unit. The distance between the Cu(II) and this nitrogen is 2.602 Å, very close to the Cu-N(dicyanamide) bond length of 2.427 Å. Therefore, the Cu(II) ions can be viewed as having an elongated octahedral environment.

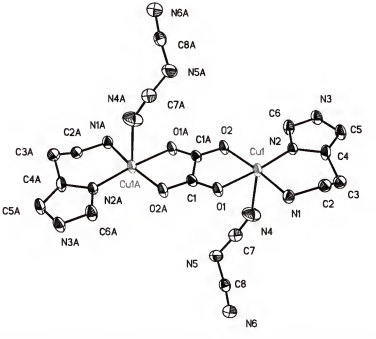


Figure 6-1. The dimeric structural repeating unit of $Cu_2(C_2O_4)(histamine)_2[N(CN)_2]_2$.

In the solid state, instead of forming ladders with dimeric units stacking on top of each other, each dimeric unit is connected to four separate dimeric units rather than two dimeric unit so that a 2-D structure is formed in the *bc* planes. The situation is shown in Figure 6-2 and Figure 6-3. The 2-D sheets stack along the *a* axis to form a 3-D structure. The planar histamine molecules from neighboring sheets interdigitate with each other to hold the sheets together and also provide hydrogen bonding between sheets.

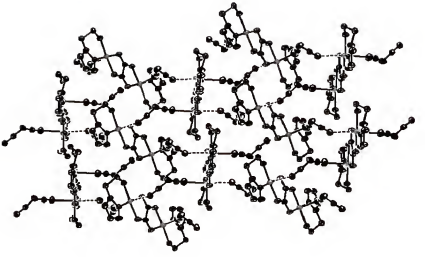

Figure 6-2. Top view of the 2-D sheet of $Cu_2(C_2O_4)(histamine)_2[N(CN)_2]_2$.

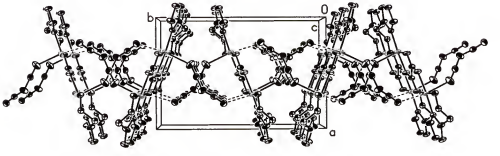


Figure 6-3. Side view of $Cu_2(C_2O_4)(histamine)_2[N(CN)_2]_2$.

**Description of the Structure of $Cu_2(C_2O_4)(histamine)_2(N_3)_2$.**

The structure of $Cu_2(C_2O_4)(histamine)_2(N_3)_2$ is very similar to that of $Cu_2(C_2O_4)(histamine)_2[N(CN)_2]_2$. It is also consisted of individual dimeric units. Its major difference with $Cu_2(C_2O_4)(histamine)_2[N(CN)_2]_2$ is that $[N(CN)_2]^-$ anions exhibit a tendency to bridge Cu(II) ions so that each Cu(II) ions is in an elongated octahedral geometry in $Cu_2(C_2O_4)(histamine)_2[N(CN)_2]_2$, while in $Cu_2(C_2O_4)(histamine)_2(N_3)_2$,

the azide anions show no tendency to bridge Cu(II) ions so that each Cu(II) ion is in a true square pyramidal geometry. Its structural repeating unit is shown in Figure 6-4.

In the solid state, the Cu(oxo)Cu planar units stack to form a 2-D sheet in the *bc* plane. The 2-D sheets then stack along the *a* axis to form a 3-D structure. This is shown in Figure 6-5 and Figure 6-6.

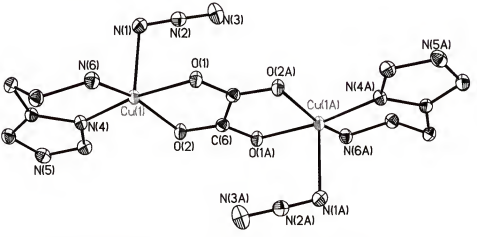


Figure 6-4. Structural repeating unit of $Cu_2(C_2O_4)(histamine)_2(N_3)_2$.

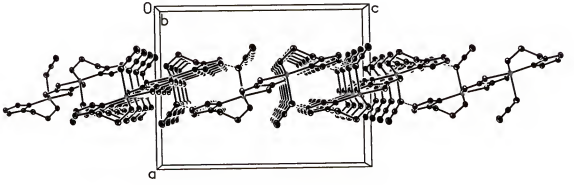


Figure 6-5. Side view of one 2-D sheet of $Cu_2(C_2O_4)(histamine)_2(N_3)_2$.

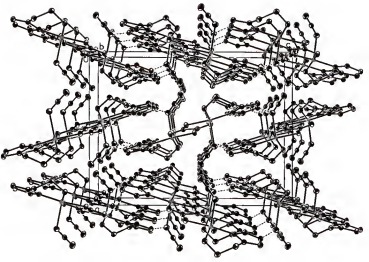

Figure 6-6. Side view of $Cu_2(C_2O_4)(histamine)_2(N_3)_2$ stacking along the *a* axis.

**Description of the Structure of $[Cu_4(2,2'\text{-bipyrimidine})_2(N_3)_8]_n$.**

$[Cu_4(2,2'\text{-bipyrimidine})_2(N_3)_8]_n$ has a true 2-D covalently linked network structure. The synthesis of this material was aimed at a ladder-like structure similar to the one depicted in Figure 4-3 in which the [Cu(bipyrimidine)Cu] units serve as the rungs that stack and are simultaneously linked by azide anions to form a ladder. Each Cu(II) ion will further coordinate to a nonbridging azide anion to form a trigonal bipyramidal geometry. The anticipated ladder-like structure is shown in Figure 6-7. Although the synthesis was design to react 2 equivalents of $Cu^{2+}$, 1 equivalent of 2,2'-bipyrimidine, and 4 equivalents of azide anions, the resulting structure is not a ladder, but, it did turn out to have the designed stoichiometry.

In the resulting 2-D structure of $[Cu_4(2,2'\text{-bipyrimidine})_2(N_3)_8]_n$, the [Cu(bipyrimidine)Cu] units did form and stack as predicted. However, these units are linked differently as anticipated for a ladder structure. Specifically, each Cu(II) ion is in a square pyramidal geometry instead of trigonal bipyramidal. The square pyramidal environment includes two Cu(II)-O bonds and three Cu(II)-N(azide) bonds. Each Cu(II)

ion is bridged to neighboring [Cu(bipyrimidine)Cu] units *via* two of the three azide anions in end-on modes, the third azide anion is in a nonbridging mode. Thus, the repeating unit is $[Cu_4(2,2'\text{-bipyrimidine})_2(N_3)_8]$ rather than $[Cu_2(2,2'\text{-bipyrimidine})(N_3)_4]$ for a ladder. The structure of $[Cu_4(2,2'\text{-bipyrimidine})_2(N_3)_8]_n$ is shown in Figure 6-8 and Figure 6-9.

Thus, the 2-D sheets can be viewed as being consisted of a series of ladders linked together through end-on azide bridges. The rungs of neighboring ladders are tilted with each other. In the solid state, 2-D sheets stack along the diagonal of the *ac* plane and are connected by hydrogen bonding *via* N(azide)-H(bipyrimidine)-C(bipyrimidine).

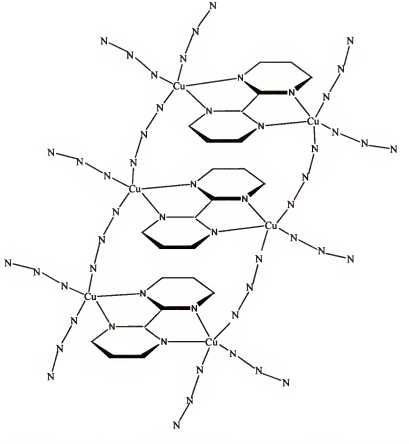


Figure 6-7. Anticipated ladder-like structure of $[Cu_4(2,2'\text{-bipyrimidine})_2(N_3)_8]_n$.

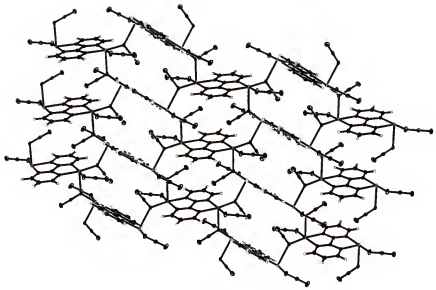

Figure 6-8. The 2-D network of $[Cu_4(2,2^{'}\text{-bipyrimidine})_2(N_3)_8]_n$.

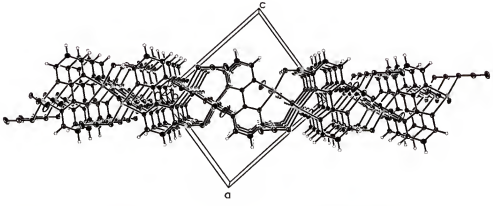


Figure 6-9. Side view of the 2-D sheet of $[Cu_4(2,2^{'}\text{-bipyrimidine})_2(N_3)_8]_n$.

**Description of the Structure of $[Cu(terephthalato)(H_2O)_2 \cdot H_2O]_n$**

Despite of the stoichiometry of the starting materials, the final structure of $[Cu(terephthalato)(H_2O)_2 \cdot H_2O]_n$ is not a ladder and does not even contain azide anions. The terephthalate dianion can coordinate in several different modes as depicted in Figure 6-10. In $[Cu(terephthalato)(H_2O)_2 \cdot H_2O]_n$, the third coordination mode (C) is adopted and a covalently linked one dimensional chain was obtained as shown in

Figure 6-11 and Figure 6-12. In the chain, Cu(II) ions are bridged through the carboxylate groups and each Cu(II) ion is further coordinated to two water molecules. The Cu-O(water) bonds (1.924 Å) are slightly longer than the Cu-O(carboxylate) bonds (1.981 Å). The chains extend along the *c* axis. Each carboxylate group also has a noncoordinating water molecule closely associated with it providing hydrogen bonding that connects chains together.

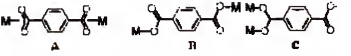

Figure 6-10. Coordination modes of terephthalate dianion: A. bisbidentate, B. bismonodentate, C. monodentate.

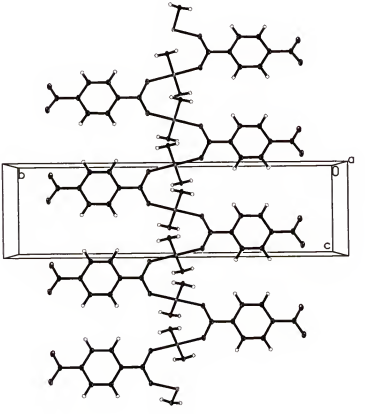

Figure 6-11. A top view of the chain structure of $[Cu(terephthalato)(H_2O)_2 \cdot H_2O]_n$.

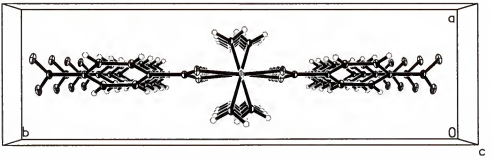


Figure 6-12. A view along the chain (*c* axis) of $[Cu(terephthalato)(H_2O)_2 \cdot H_2O]_n$.

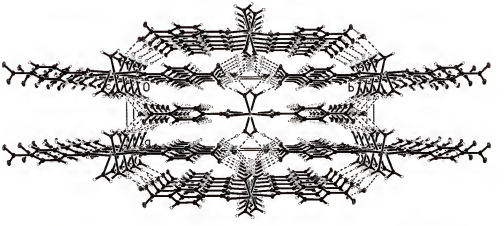


Figure 6-13. Packing diagram of seven chains of $[Cu(terephthalato)(H_2O)_2 \cdot H_2O]_n$.

In the solid state, chains are connected through hydrogen bonding *via* the noncoordinating water molecules. The packing diagram is shown in Figure 6-13. Thus, there are two different exchange pathways between the neighboring chains. One is along the *b* axis involving hydrogen bonding and a terephthalate anion, the other is along the *a* axis and is shorter involving only two coordinated water molecules and the noncoordinated water molecule in between.

**EPR Measurements**

The room-temperature EPR spectra for $Cu_2(C_2O_4)(histamine)_2[N(CN)_2]_2$ and $Cu_2(C_2O_4)(histamine)_2(N_3)_2$ are shown in Figure 6-14 and Figure 6-15, respectively. The *g* value for both compounds has been calculated from the EPR spectra. For

$Cu_2(C_2O_4)$(histamine)$_2[N(CN)_2]_2$, the spectrum shows a resonance signal at 3203 G corresponding to $g_\perp = 2.07$, and also a signal at about 3000 G. However, the signal at 3000 G is so weak that the g value is taken as $g_\perp$. The room-temperature EPR spectrum of $Cu_2(C_2O_4)$(histamine)$_2(N_3)_2$ shows a very symmetric and featureless signal centered at 3130 G and the $g$ value is 2.12. The room temperature EPR spectrum for [Cu(terephthalato)$(H_2O)_2$•$H_2O]_n$ is shown in Figure 6-16. The spectrum shows two resonance signals centered at 2991 G and 3162.5 G corresponding to $g_{//} = 2.21$ and $g_\perp = 2.10$, respectively. The average $g$ value is 2.14 according to [161]

$$\langle g \rangle = [(2\, g_\perp^2 + g_{//}^2)/3]^{1/2} \qquad (6\text{-}1)$$

As $g_{//} > g_\perp$, this suggests that the unpaired electron resides in the $d_{x2-y2}$ orbital, expected for Cu(II) ions in square planar geometry.

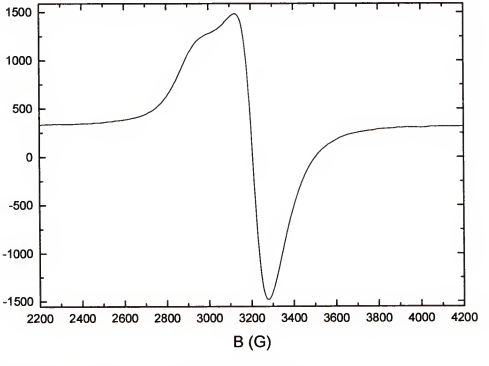


Figure 6-14. Room-temperature X-band EPR spectrum of $Cu_2(C_2O_4)$(histamine)$_2[N(CN)_2]_2$.

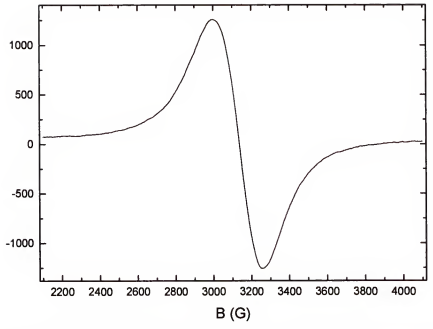


Figure 6-15. Room-temperature X-band EPR spectrum of $Cu_2(C_2O_4)(histamine)_2(N_3)_2$.

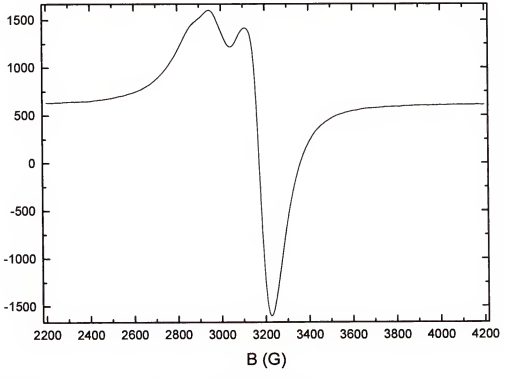


Figure 6-16. Room-temperature X-band EPR spectrum of $[Cu(terephthalato)(H_2O)_2 \cdot H_2O]_n$.

**Magnetic Properties of $Cu_2(C_2O_4)(histamine)_2[N(CN)_2]_2$**

The plot of susceptibility normalized for per mole of Cu(II) dimeric units as a function of temperature is shown in Figure 6-17. In the plot, the susceptibility reaches a maximum at 270 K and then decreases as temperature is lowered to 50 K. This behavior indicates a strong antiferromagnetic interaction. The increase of susceptibility below 50 K is due to paramagnetic impurities.[161] It is known that oxalate group, $C_2O_4^{2-}$, propagates antiferromagnetic coupling very efficiently.[161-168] So the initial interpretation of the magnetic data is that $Cu_2(C_2O_4)(histamine)_2[N(CN)_2]_2$ is basically a quasiisolated dimeric system with predominantly antiferromagnetic coupling propagated by the oxalate bridges within each dimer and very weak interdimer interactions propagated through the dicyanamide ($[N(CN)_2]^{1-}$) groups.

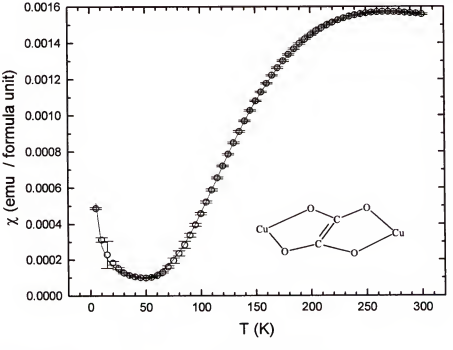


Figure 6-17. Magnetic susceptibility normalized of per mole of $Cu_2(C_2O_4)(histamine)_2[N(CN)_2]_2$. The solid line is a fit to a dimer model including an interdimer interaction.

The plot in Figure 6-17 has been fit to a dimer model including the interdimer interaction term.[161, 169] The Hamiltonian used for this model is given below in Equation 6-2. A good fit has been obtained and the fitting results are summarized in Table 6-1. The results indicate that the intradimer coupling is antiferromagnetic with $J/k_B = -435$ K and the interdimer interaction is negligibly small of about 2 K with 0.3% of paramagnetic impurities. Since the interdimer interaction is so much smaller compared to the intradimer interaction, the fitting procedure can not accurately determine its sign and value. The *g* value obtained from fitting result is 2.03 ± 0.04 and agrees well with the calculated value of 2.07 from the EPR measurement.

$$\boldsymbol{H} = -J\boldsymbol{S}_A \bullet \boldsymbol{S}_B + g\beta \boldsymbol{S}z H - zJ' \langle \boldsymbol{S}z \rangle \boldsymbol{S}z \qquad (6\text{-}2)$$

Table 6-1. Fitting results for the molar susceptibility *vs* temperature plot of $Cu_2(C_2O_4)$(histamine)$_2[N(CN)_2]_2$.

| Fitting Parameters | Value |
|---|---|
| *g* | 2.03 ± 0.04 |
| $J/k_B$ (intradimer interaction) | − 435 ± 3.08 K |
| $J'/k_B$ (interdimer interaction) | 2.21 ± - - K |
| *ro* (paramagnetic impurity) | $3.03\times10^{-3} \pm 0.13\times10^{-3}$ |

**Magnetic Properties of $Cu_2(C_2O_4)$(histamine)$_2(N_3)_2$**

The plot of susceptibility normalized for per mole of Cu(II) dimeric units as a function of temperature is shown in Figure 6-18. The susceptibility *vs* temperature plot has been fit to the same model used for $Cu_2(C_2O_4)$(histamine)$_2[N(CN)_2]_2$ as shown in Figure 6-18. The magnetic behavior of $Cu_2(C_2O_4)$(histamine)$_2(N_3)_2$ is essentially the same as that of $Cu_2(C_2O_4)$(histamine)$_2[N(CN)_2]_2$. The magnetic interactions are dominated by the strong antiferromagnetic coupling with $J/k_B = -438$ K propagated by the oxalate bridges with the interdimer interactions being even smaller, 1.7 K, than that in $Cu_2(C_2O_4)$(histamine)$_2[N(CN)_2]_2$. This weaker interdimer interaction may be explained

by structural difference in the two compounds. In $Cu_2(C_2O_4)(histamine)_2[N(CN)_2]_2$, there is a close contact of 2.602 Å between the nonbridging nitrogen of the dicyanamide anions and Cu(II) ions. This distance is comparable to the bond length, 2.427Å, of N(dicyanamide)-Cu(II). However, in $Cu_2(C_2O_4)(histamine)_2(N_3)_2$, the azide anions show no tendency to coordinate with adjacent Cu(II) ions. The *g* value obtained is 2.09 ± 0.10, and agrees well with the measured value of 2.12 based on the EPR experiment.

Table 6-2. Fitting results for the molar susceptibility *vs* temperature plot of $Cu_2(C_2O_4)(histamine)_2(N_3)_2$.

| Fitting Parameters | Value |
|---|---|
| *g* | 2.09 ± 0.10 |
| $J/k_B$ (intradimer interaction) | − 438 ± 8.02 K |
| $J'/k_B$ (interdimer interaction) | 1.72 ± - - K |
| *ro* (paramagnetic impurity) | $2.16\times10^{-2} \pm 0.22\times10^{-2}$ |

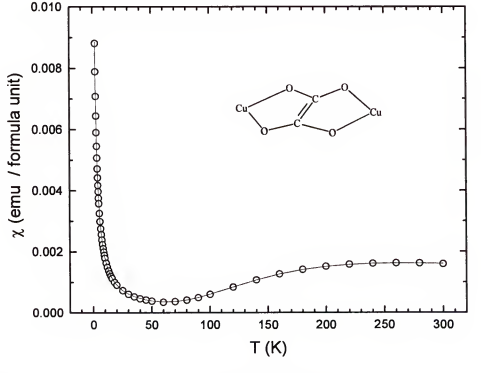


Figure 6-18. Magnetic susceptibility normalized of per mole of $Cu_2(C_2O_4)(histamine)_2(N_3)_2$. The solid line is a fit to a dimer model including an interdimer interaction.

**Magnetic Properties of $[Cu(terephthalato)(H_2O)_2 \cdot H_2O]_n$**

The product of magnetic susceptibility normalized to per mole of Cu(II) ions and temperature, $\chi T$, is plotted as a function of temperature in Figure 6-19. At 300 K, the $\chi T$ value is 0.43 emu K/mol, in good agreement with the calculated value of 0.44 emu K/mol according to the Curie law. As temperature is lowered, the value of $\chi T$ decreases to a minimum of 0.409 emu K/mol at 40 K indicating the onset of weak antiferromagnetic exchange interactions. Then the magnetization rapidly increases to a maximum of 1.017 emu K/mol at 13 K. This is attributed to the occurrence of spontaneous moments. As temperature is reduced below 13 K, $\chi T$ rapidly drops to approach zero due to another antiferromagnetic interaction in the system.

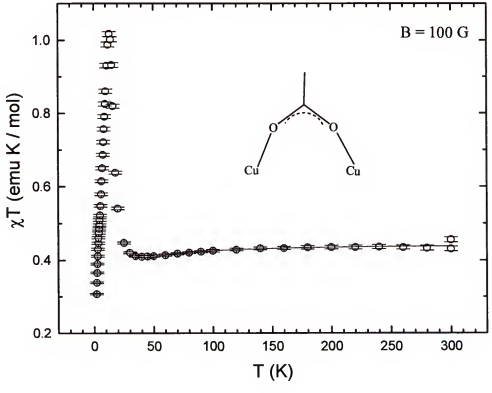


Figure 6-19. Plot of $\chi T$ *vs* $T$ for $[Cu(terephthalato)(H_2O)_2 \cdot H_2O]_n$ fitted to the Bonner Fisher expression for an $S=1/2$ chain.

Initially, the plot in Figure 6-19 was fit to the Bonner Fisher expression for a uniformly spaced $S = 1/2$ chain with $J < 0$. A good fit was obtained only for the $\chi T$ *vs* $T$ data above 50 K as shown in Figure 6-19. The Hamiltonian used for fitting is

$$\boldsymbol{H} = -2J\boldsymbol{S}_1 \cdot \boldsymbol{S}_2 \tag{6-3}$$

and the numerical expression is [170]

$$\chi = \frac{N g^2 \beta^2}{kT} \frac{0.25 + 0.074975x + 0.075235x^2}{1.0 + 0.9931x + 0.172135x^2 + 0.757825x^3} \tag{6-4}$$

where $x = |J| / kT$.

The fitting results show that the exchange coupling constant $J/k$ is $-6.59 \pm 1.03$ K indicating an antiferromagnetic coupling with magnitude of 13.2 K between Cu(II) ions within individual chains propagated by the carboxylate groups. The magnitude is expected based on other similar examples.[161, 171, 172] The average $g$ value obtained from the fitting is $2.177 \pm 0.006$, in good agreement with the average $g$ value of 2.14 calculated from the EPR measurements. The antiferromagnetic nature of the coupling is also confirmed by the fitting of the inverse susceptibility plotted as a function of temperature to the Curie-Weiss law shown in Figure 6-20. The fitting results show that the Weiss temperature is $-4.75 \pm 1.87$ K and the $g$ value of $2.18 \pm 0.01$.

The onset of spontaneous moments around 13 K is likely due to canting of the antiferromagnetically coupled spins within the individual chains. As mentioned earlier, the two Cu-O(carboxylate) bonds around a Cu(II) ion are shorter than the Cu-O(water) bonds, and the unpaired electron on Cu(II) ions is located in the $d_{x2-y2}$ orbital which extends along these four bonds. Therefore, it is reasonable to propose that the spin magnetic moments on the Cu(II) ions within an individual chain are oriented along

the O(carboxylate)-Cu-O(carboxylate) bonds and naturally form a small angle with each other, giving rise to spin canting. This type of behavior has been reported for Cu(II) compounds.[171, 173] The existence of spin canting within individual chains is also highly possible because in order for spin canting to exist, two neighboring Cu(II) ions must be related by an inversion center or joined together by a rotational axis, which is not the case in this compound. The spin canting situation is depicted in Figure 6-21.

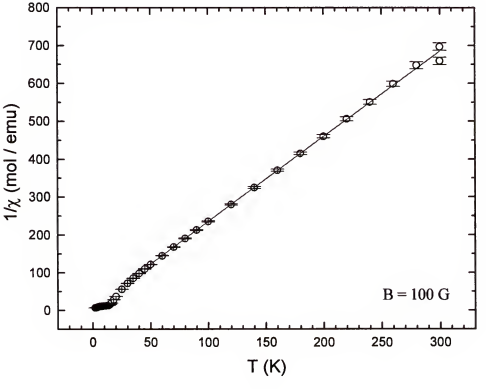


Figure 6-20. Plot of inverse susceptibility as a function of temperature for $[Cu(terephthalato)(H_2O)_2 \cdot H_2O]_n$. The solid line is a fit to the Curie Weiss law for data above 50 K.

The result of spin canting is that a net magnetic moment is achieved within each chain along the direction that the chains extend, the *c* axis. Subsequently, the chains are coupled ferromagnetically resulting in the maximum of the $\chi T$ value at 13 K. Based on the packing diagram of Figure 6-13, the most likely exchange pathway that

ferromagnetically couples the neighboring chains is the short hydrogen bonding along the *a* axis that involves two coordinated water and the noncoordinated water in between. This means that only the chains that are directly above and below each other in the *ac* planes are coupled, and the system can be described magnetically as being consisted of 2-D sheets parallel to the *ac* plane (perpendicular to the *b* axis) with each sheet possessing a net magnetic moment oriented along the *c* axis.

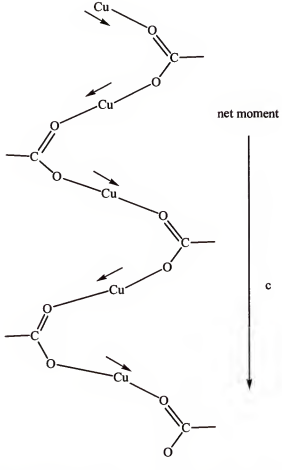


Figure 6-21. Spin canting along the chain (*c* axis) of $[Cu(terephthalato)(H_2O)_2 \cdot H_2O]_n$. The arrows represent the spin magnetic moments. Water molecules are omitted for clarity. Only one carboxylate group is shown for each terephthalate dianion.

In order to model the ferromagnetic coupling between chains, the Hamiltonian for the Bonner Fisher model must be modified by adding a mean field correction term to

account for the interchain exchange interactions. The basic equation has the following general form,[174-176]

$$\chi_{2\text{-}D} = \chi_{1\text{-}D} / [1-(2ZJ'/Ng^2\beta^2)\chi_{1\text{-}D}] \quad (6\text{-}5)$$

where $\chi_{1\text{-}D}$ is the susceptibility due to individual chains given by Equation 6-4 and $\chi_{2\text{-}D}$ is the susceptibility of the resulting 2-D sheets due to the coupling between chains. $Z$ is the number of the nearest-neighbor chains. $J'$ is the interchain exchange integral between nearest neighbor chains. A Curie term is often included to account for the paramagnetic impurities so that the Equation 6-5 is then written as

$$\chi_{2\text{-}D} = \{\chi_{1\text{-}D} / [1-(2ZJ'/Ng^2\beta^2)\chi_{1\text{-}D}]\}(1-\rho) + (Ng^2\beta^2/2k)\rho \quad (6\text{-}6)$$

where $\rho$ is the percentage of the impurities.

Using the average $g$ value of 2.14 measured from the EPR experiment and restricting $Z$ to 2, the $\chi T$ *vs* $T$ data has been fit to Equation 6-6. A fit cannot be obtained for the data of the entire temperature range. However, a best fit is obtained from 300 K down to 13 K as shown in Figure 6-22. The fitting results are summarized in Table 6-3. The fitting results indicate that the intrachain exchange is antiferromagnetic and the coupling constant $J/k_B$ is $-16.89 \pm 1.45$ K. The interchain interaction is ferromagnetic and the coupling constant $J'/k_B$ is $11.79 \pm 1.32$ K, [176] in good agreement with the experimental observation of the maximum $\chi T$ value at 13 K.

Table 6-3. Fitting results for the molar susceptibility *vs* temperature plot of $[Cu(terephthalato)(H_2O)_2 \cdot H_2O]_n$.

| Fitting Parameters | Value |
|---|---|
| $g$ | $2.14 \pm 0$ |
| $J/k_B$ (intrachain interaction) | $-16.9 \pm 1.45$ K |
| $J'/k_B$ (interchain interaction) | $11.8 \pm 1.32$ K |
| $Z$ (number of nearest neighbors) | $2.00 \pm 0$ |

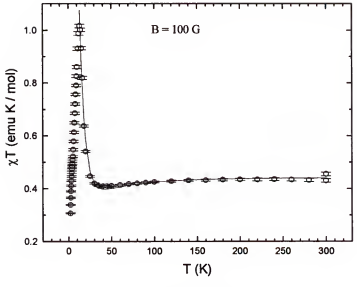


Figure 6-22. Plot of $\chi T$ *vs* $T$ for $[Cu(terephthalato)(H_2O)_2 \cdot H_2O]_n$ fitted to a modified Bonner Fisher expression. (see text).

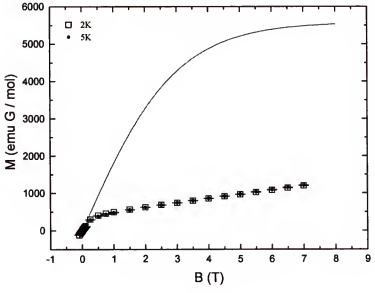


Figure 6-23. Plot of molar magnetization of $[Cu(terephthalato)(H_2O)_2 \cdot H_2O]_n$ as a function of field at 2 K and 5 K, respectively. The solid line is a simulation of the Brillouin function for an $S = 1/2$ system with average g value of 2.14.

As temperature is lowered below 13 K, the 2-D sheets are coupled antiferromagnetically along the *b* axis through the terephtalate dianions giving rise to the decrease in the $\chi T$ value below 13 K. Bridging terphthalate dianion is known to propagate

very weak antiferromagnetic exchange interaction in the range from a fraction of a Kelvin to 1~2 K.[177-180] The antiferromagnetic nature of the coupling between sheets below 13 K is also indicated by the magnetization measured as a function of field at 2 K and 5 K shown in Figure 6-23. At 2 K and 5 K, the magnetization increases much more slowly than predicted by the Brillouin function for an $S = 1/2$ system. As the antiferromagnetic interaction between sheets propagated by the terephthalate dianions is so weak, accurate determination of its sign and magnitude may be difficult. The change of magnetic coupling from ferromagnetically coupled chains to antiferromagnetically coupled sheets as temperature is lowered is summarized in Figure 6-24.

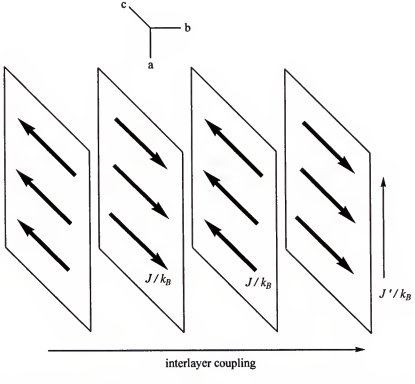


Figure 6-24. Magnetic couplings in $[Cu(terephthalato)(H_2O)_2 \cdot H_2O]_n$. The couplings include ferromagnetic coupling *via* hydrogen bonding between chains residing in the *ac* planes, and the antiferromagnetic coupling between the resulting 2-D sheets through terephthalate dianions along the *b* axis. Each arrow represents the net magnetic moment within an individual chain.

## Conclusion

Attempts to synthesize ladder-like structures have been carried out using oxalate, 2,2'-bipyrimidine, and terephthalate as the bisbidentate ligands to form dimeric units, while azide and dicyanamide are used as the linear bidentate bridging ligands to provide the legs of ladders. Four new materials have been synthesized and no ladder-like structure has been obtained. Three 2-D structures, $Cu_2(C_2O_4)(histamine)_2(N_3)_2$, $Cu_2(C_2O_4)(histamine)_2[N(CN)_2]_2$, and $[Cu_4(2,2'\text{-bipyrimidine})_2(N_3)_8]_n$, and a one dimensional chain, $[Cu(terephthalato)(H_2O)_2{\cdot}H_2O]_n$, have been isolated and investigated structurally and magnetically. $Cu_2(C_2O_4)(histamine)_2(N_3)_2$ and $Cu_2(C_2O_4)(histamine)_2[N(CN)_2]_2$ are both consisted of dimeric structural repeating units which are related to each other through Van der Waals interactions and hydrogen bonding to form 3-D structures. Magnetically, both compounds behave as a non-interacting dimer system with the strong intradimer antiferromagnetic exchange propagated by the oxalate groups being the predominant interaction in the system, while the interactions mediated through the azide and dicyanamide groups being negligibly small. On the other hand, $[Cu_4(2,2'\text{-bipyrimidine})_2(N_3)_8]_n$ has a covalently linked 2-D network structure in which 2-D sheets are linked to each other *via* hydrogen bonding to form a 3-D structure. Unfortunately, magnetic characterizations could not be carried out due to the extremely small quantity of the sample. $[Cu(terephthalato)(H_2O)_2{\cdot}H_2O]_n$ is consisted of one dimensional covalent chains that are held together in the solid state by hydrogen bonding. At high temperature, Cu(II) ions in individual chains are coupled antiferromagnetically *via* the carboxylate bridges. Spin canting has been proposed to give rise to a net magnetic moment within each chain and subsequently attributes to the onset of spontaneous moment as temperature is lowered to 13 K when chains located in the

individual *ac* planes begin to couple ferromagnetically resulting in magnetic 2-D sheets. Below 13 K, the 2-D sheets parallel to the *ac* plane are coupled weakly through terephthalate dianions.

Although ladder-like structures based on bisbidentate ligands have been reported, none of the known examples has displayed spin-ladder behavior. The primary problem is that the currently used bisbidentate ligands are either very efficient, such as oxalate and 2,2'-bipyrimidine, or very inefficient, such as terephthalate, of propagating magnetic exchange interaction between paramagnetic ions located along the legs. The result is that the final synthetic product is either a noninteracting dimer system or a noninteracting one-dimensional chain system.

# CHAPTER 7
# EPILOGUE

Since the known examples of noninterpenetrating ladder-like structures are very scarce in literatures, in addition to reproducing and investigating magnetic properties of known ladder-like cuprates as presented in Chapter 3, the primary focus of the research presented in this dissertation is to synthesize and magnetically characterize new examples of ladder-like coordination polymers in search of a true magnetic spin-ladder system, and the results are described in Chapter 4, 5, and 6.

The synthesis of ladder-like structures and, in that matter, any other tailored original structure, represents a real challenge in the field of crystal engineering. During the course of this research, the synthesis of ladder-like coordination polymers has been attempted from several different directions, and a new dimer-based ladder-like structure, $Ni_2$(2,6-pyridinedicarboxylic acid)$_2$($H_2O$)$_4$(pyrazine), discussed in Chapter 4, has been obtained in addition to several other materials including dimers, chains, and sheets. Although no spin-ladder magnetic behavior has been observed, new insights and analyses have been developed regarding the synthesis of ladder-like structures.

Ladder-like coordination polymers can be classified into two different categories, monometallic system and bimetallic system. A monometallic system is a material containing only one type of transition-metal ions located at the vertexes of a ladder serving as the nodes of the structure. These transition-metal ions can be linked together by linear bidentate organic bridging ligands to form ladders. On the other hand, a bimetallic system contains two different types of transition-metal ions, which either

belong to two different elements or to two different oxidation states of the same element. For bimetallic system, although there are examples of ladder-like structures that are consisted of a first-row transition metal ion and a lanthanide ion, our work has focused on low-dimensional Prussian Blue (PB) analogues due to the large number of such materials reported in the past ten years and the strong ability of cyanide to propagate magnetic exchange interactions.

For both monometallic systems and low-dimensional PB analogues, a ladder-like structure may be synthesized by connecting T-shaped building blocks through linear bidentate ligands as outlined in Chapter 4. For monometallic systems, a ladder-like structure may also be achieved by linking dimeric units prefabricated by reacting one equivalent of a bis-bidentate ligand with two equivalents of a transition-metal ion. Some results along this direction have been presented in Chapter 6.

The synthesis of a monometallic system possessing ladder-like structure is largely a trial and error process, although we have utilized some structure-directing factors to promote the structures toward a ladder, such as $\pi$-$\pi$ interaction due to the stacking of the planar tridentate blocking ligands, and the stoichiometry between the transition-metal ions and bridging ligands. We have noticed that 2,2':6',2"-terpyridine (terpy), as a planar tridentate ligand, cannot form a stable monoterpy complex with a transition-metal ion. The formation constant of a bisterpy-metal complex is reportedly 200 times greater than that of a monoterpy-metal complex. Once the bisterpy-metal complex is formed, the stoichiometry is lost and no ladder-like structure is possible. This is especially problematic since the syntheses are carried out using slow diffusion in U-tubes, and it is preferred to slow down the diffusion rate as much as possible to allow product to

crystallize as single crystals. This allows ample time for bisterpy-metal complex to form. We have been unsuccessful in all of our synthetic attempts involving the usage of terpy as the planar tridentate blocking ligand not only because of the issue of the formation of bisterpy-metal complex, but also because of the large size of terpy molecules that requires a relatively long linear bridging ligand to separate the transition-metal ions on the vertexes, which compromises the rigidity of the bridging ligands and its ability to propagate magnetic exchange interactions. We did, however, partially succeed in our syntheses when a smaller blocking ligand, 2,6-pyridinedicarboxylic acid dianion, was used to form the T-shaped molecular building block, as described in Chapter 4. We were then able to connect such T-shaped building blocks with pyrazine, a linear bidentate ligand. Unfortunately, the bridging effect only occurred in the equatorial plane defined by the plane of the 2,6-pyridinedicarboxylic acid dianion so that only dimers were obtained. Without covalent bridges along the axial positions of the octahedron, the dimers stack *via* hydrogen-bonding to form a ladder. Another adverse effect brought to us by the slow diffusion experiments is that, by the time the reactants diffuse into each other, they are so diluted that the initial stoichiometry intended for a ladder is no longer available. However, more structure-directing factors may be utilized to encourage the formation of a ladder, such as the separation of a polar (or nonpolar) environment inside a ladder from a nonpolar (or polar) environment between ladders. This is a possibility we have not explored.

Compared to monometallic system, the synthesis of a PB analogue can be engineered from the point of view of charge balance. In Chapter 5, we have reviewed a large number of literatures and summarized the structural features of PB analogues of

various dimensionalities in order to carry out educated attempts on the synthesis instead of trying randomly different combinations of starting materials. We have noticed the change in the number and type of counter ions is drastic as dimensionality increases from clusters to three dimensional structures. Based on the materials available in our laboratory, we have found all the possible chemical formulae for PB analogues having a ladder-like structure. Two neutral structures have been chosen for experimental attempts. However, it has been very difficult to obtained single crystals due to the rapid formation of powder product even when the slow diffusion experiments were slowed down such that it took three weeks for the reactants to start diffusing into each other. In order to take advantage of the well-known method of using a tris(diamine)-metal complex to slow down the kinetics of the reaction to afford single crystals as reported by Ohba *et al.* and practiced by many others, we will have to synthesize a T-shaped molecular building block containing three cyanide. To the best of our knowledge, such transition-metal complexes have not been reported in literatures. Although we have successfully synthesized a large quantity of $[N(C_2H_5)_4]Fe(II)(terpy)(CN)_3$ in the form of single crystals, we have not been able to use it for subsequent reactions to build ladders due to the instability of this compound compared to $[Fe(II)(terpy)_2]^{2+}$ in aqueous and organic solutions.

In summery, from the physics and also a personal point of view, the most promising area where more true spin-ladder systems may be discovered is still the cuprates, possibly with some modifications to the known structures through synthesis to enhance magnetic exchange coupling along the two legs of the ladder. Another attractive category is molecular solids in which a couple of materials have already been reported to

behave magnetically as a spin-ladder system. Coordination polymers offer unlimited possibilities for new materials, and, hopefully, more examples of ladders will be discovered.

APPENDIX A
CRYSTAL STRUCTURAL DATA FOR COMPOUND **4**

Table A-1. Atomic coordinates ( x $10^4$) and equivalent isotropic displacement parameters for **4** ($Å^2$x $10^3$). (U(eq) is defined as one third of the trace of the orthogonalized $U_{ij}$ tensor.)

| | x | y | z | U(eq) |
|---|---|---|---|---|
| Ni | 1683(1) | 4000(1) | 1701(1) | 16(1) |
| O1 | -160(2) | 4747(1) | 2488(2) | 20(1) |
| O2 | -2811(2) | 4828(1) | 3784(2) | 26(1) |
| O3 | 2658(2) | 3011(1) | 1294(2) | 20(1) |
| O4 | 1912(2) | 1936(1) | 1703(2) | 25(1) |
| O5 | 2937(2) | 4023(1) | 4339(2) | 19(1) |
| O6 | 518(2) | 4004(1) | -1019(2) | 21(1) |
| N1 | -287(2) | 3446(1) | 2545(2) | 16(1) |
| N2 | 3697(2) | 4592(1) | 738(3) | 18(1) |
| C1 | -1580(3) | 4504(1) | 3133(3) | 19(1) |
| C2 | -1756(3) | 3749(1) | 3073(3) | 17(1) |
| C3 | -3257(3) | 3386(1) | 3467(3) | 22(1) |
| C4 | -3178(3) | 2696(1) | 3307(3) | 25(1) |
| C5 | -1630(3) | 2385(1) | 2806(3) | 22(1) |
| C6 | -179(3) | 2781(1) | 2421(3) | 17(1) |
| C7 | 1614(3) | 2554(1) | 1757(3) | 17(1) |
| C8 | 3942(3) | 5226(1) | 1313(3) | 24(1) |
| C9 | 4759(3) | 4370(1) | -585(3) | 24(1) |

Table A-2. Bond lengths [Å] and angles [°] for **4**.

| | |
|---|---|
| Ni-N1 | 1.9683(16) |
| Ni-O5 | 2.0527(17) |
| Ni-N2 | 2.0661(17) |
| Ni-O6 | 2.0771(17) |
| Ni-O1 | 2.1320(14) |
| Ni-O3 | 2.1324(14) |
| O1-C1 | 1.279(3) |
| O2-C1 | 1.238(3) |
| O3-C7 | 1.259(2) |
| O4-C7 | 1.256(2) |
| O5-H5A | 0.76(2) |
| O5-H5B | 0.80(3) |
| O6-H6A | 0.80(3) |
| O6-H6B | 0.77(3) |
| N1-C2 | 1.332(3) |
| N1-C6 | 1.335(3) |
| N2-C9 | 1.337(3) |
| N2-C8 | 1.340(3) |
| C1-C2 | 1.516(3) |
| C2-C3 | 1.384(3) |
| C3-C4 | 1.385(3) |
| C3-H3A | 0.9500 |
| C4-C5 | 1.384(3) |
| C4-H4A | 0.9500 |
| C5-C6 | 1.388(3) |
| C5-H5C | 0.9500 |
| C6-C7 | 1.521(3) |
| C8-C9#1 | 1.387(3) |
| C8-H8A | 0.9500 |
| C9-C8#1 | 1.387(3) |
| C9-H9A | 0.9500 |
| N1-Ni-O5 | 93.36(7) |
| N1-Ni-N2 | 178.04(7) |
| O5-Ni-N2 | 88.45(7) |
| N1-Ni-O6 | 89.47(7) |
| O5-Ni-O6 | 177.16(6) |
| N2-Ni-O6 | 88.71(7) |
| N1-Ni-O1 | 78.71(6) |
| O5-Ni-O1 | 91.42(6) |
| N2-Ni-O1 | 100.54(6) |
| O6-Ni-O1 | 89.24(6) |
| N1-Ni-O3 | 77.84(6) |
| O5-Ni-O3 | 89.81(6) |
| N2-Ni-O3 | 102.91(6) |
| O6-Ni-O3 | 90.67(6) |

Table A-2. Continued

| | |
|---|---|
| O1-Ni-O3 | 156.54(6) |
| C1-O1-Ni | 113.24(13) |
| C7-O3-Ni | 114.45(13) |
| Ni-O5-H5A | 112.9(18) |
| Ni-O5-H5B | 120(2) |
| H5A-O5-H5B | 108(3) |
| Ni-O6-H6A | 118.2(18) |
| Ni-O6-H6B | 114(2) |
| H6A-O6-H6B | 107(3) |
| C2-N1-C6 | 121.74(17) |
| C2-N1-Ni | 118.58(14) |
| C6-N1-Ni | 119.42(13) |
| C9-N2-C8 | 116.60(18) |
| C9-N2-Ni | 120.98(14) |
| C8-N2-Ni | 122.31(15) |
| O2-C1-O1 | 126.11(19) |
| O2-C1-C2 | 117.69(19) |
| O1-C1-C2 | 116.20(17) |
| N1-C2-C3 | 121.11(19) |
| N1-C2-C1 | 112.86(17) |
| C3-C2-C1 | 126.01(18) |
| C2-C3-C4 | 117.8(2) |
| C2-C3-H3A | 121.1 |
| C4-C3-H3A | 121.1 |
| C5-C4-C3 | 120.6(2) |
| C5-C4-H4A | 119.7 |
| C3-C4-H4A | 119.7 |
| C4-C5-C6 | 118.44(19) |
| C4-C5-H5C | 120.8 |
| C6-C5-H5C | 120.8 |
| N1-C6-C5 | 120.24(19) |
| N1-C6-C7 | 112.00(17) |
| C5-C6-C7 | 127.70(19) |
| O4-C7-O3 | 126.22(19) |
| O4-C7-C6 | 117.71(18) |
| O3-C7-C6 | 116.07(18) |
| N2-C8-C9#1 | 121.8(2) |
| N2-C8-H8A | 119.1 |
| C9#1-C8-H8A | 119.1 |
| N2-C9-C8#1 | 121.6(2) |
| N2-C9-H9A | 119.2 |
| C8#1-C9-H9A | 119.2 |

Symmetry transformations used to generate equivalent atoms: #1 -x+1,-y+1,-z

Table A-3. Hydrogen coordinates($x10^4$) and isotropic displacement parameters for **4** ($Å^2 x 10^3$).

| | x | y | z | U(eq) |
|---|---|---|---|---|
| H5A | 2690(30) | 3727(12) | 4960(30) | 17(6) |
| H5B | 2900(40) | 4358(14) | 4960(40) | 39(9) |
| H6A | 420(30) | 4355(13) | -1560(40) | 24(7) |
| H6B | 940(40) | 3758(14) | -1700(40) | 33(8) |
| H3A | -4307 | 3603 | 3836 | 27 |
| H4A | -4196 | 2435 | 3544 | 30 |
| H5C | -1563 | 1911 | 2727 | 26 |
| H8A | 3207 | 5403 | 2245 | 29 |
| H9A | 4622 | 3925 | -1038 | 29 |

Table A-4. Hydrogen bond lengths and angles for **4** [Å and °].

| D-H...A | d(D-H) | d(H...A) | d(D...A) | <(DHA) |
|---|---|---|---|---|
| O5-H5A...O4#2 | 0.76(2) | 1.92(3) | 2.681(2) | 172(2) |
| O5-H5B...O2#3 | 0.80(3) | 1.86(3) | 2.656(2) | 175(3) |
| O6-H6A...O1#4 | 0.80(3) | 1.92(3) | 2.713(2) | 171(2) |
| O6-H6B...O4#5 | 0.77(3) | 1.95(3) | 2.719(2) | 174(3) |

Symmetry transformations used to generate equivalent atoms:
#1 -x+1,-y+1,-z #2 x,-y+1/2,z+1/2 #3 -x,-y+1,-z+1
#4 -x,-y+1,-z #5 x,-y+1/2,z-1/2

APPENDIX B
CRYSTAL STRUCTURAL DATA FOR COMPOUND **5**

Table B-1. Atomic coordinates ( x $10^4$) and equivalent isotropic displacement parameters for **5** ($Å^2$x $10^3$). U(eq) is defined as one third of the trace of the rthogonalized $U_{ij}$ tensor.

| | x | y | z | U(eq) |
|---|---|---|---|---|
| Cu1 | 3133(1) | 5643(1) | 2172(1) | 25(1) |
| O1 | 5067(2) | 5140(2) | 2320(2) | 28(1) |
| O2 | 3297(2) | 5324(2) | -420(2) | 28(1) |
| N1 | 3200(2) | 5898(2) | 4783(3) | 26(1) |
| N2 | 1212(2) | 6055(2) | 1893(3) | 22(1) |
| N3 | -839(2) | 6295(2) | 763(3) | 31(1) |
| N4 | 4222(3) | 7084(2) | 1464(4) | 50(1) |
| N5 | 6458(3) | 7760(2) | 675(4) | 40(1) |
| N6 | 7630(3) | 8965(2) | 2372(4) | 35(1) |
| C1 | 5513(2) | 4945(2) | 797(3) | 22(1) |
| C2 | 1903(6) | 5989(6) | 5792(7) | 26(2) |
| C3 | 983(8) | 6708(6) | 4971(8) | 29(2) |
| C2' | 2175(12) | 6552(8) | 5549(15) | 25(3) |
| C3' | 745(14) | 6440(20) | 5150(17) | 16(3) |
| C2" | 1771(13) | 5674(13) | 5674(17) | 17(4) |
| C3" | 745(14) | 6124(17) | 5251(19) | 22(4) |
| C4 | 364(3) | 6380(2) | 3221(4) | 32(1) |
| C5 | -923(3) | 6523(2) | 2523(4) | 32(1) |
| C6 | 450(3) | 6013(2) | 428(4) | 34(1) |
| C7 | 5280(3) | 7414(2) | 1176(4) | 31(1) |
| C8 | 7026(3) | 8406(2) | 1631(4) | 27(1) |

Table B-2. Bond lengths [Å] and angles for **5** [°].

| | |
|---|---|
| Cu1-N2 | 1.967(2) |
| Cu1-N1 | 1.984(2) |
| Cu1-O2 | 1.9969(19) |
| Cu1-O1 | 2.0163(18) |
| Cu1-N4 | 2.427(3) |
| O1-C1 | 1.249(3) |
| O2-C1#1 | 1.251(3) |
| N1-C2 | 1.472(6) |
| N1-C2' | 1.497(11) |
| N1-C2" | 1.571(14) |
| N2-C6 | 1.319(3) |
| N2-C4 | 1.374(3) |
| N3-C6 | 1.339(4) |
| N3-C5 | 1.357(4) |
| N4-C7 | 1.154(4) |
| N5-C7 | 1.304(4) |
| N5-C8 | 1.309(4) |
| N6-C8 | 1.151(4) |
| C1-O2#1 | 1.251(3) |
| C1-C1#1 | 1.556(5) |
| C2-C3 | 1.512(8) |
| C3-C4 | 1.515(6) |
| C2'-C3' | 1.426(18) |
| C3'-C4 | 1.487(12) |
| C2"-C3" | 1.24(2) |
| C3"-C4 | 1.603(16) |
| C4-C5 | 1.366(4) |
| N2-Cu1-N1 | 94.25(9) |
| N2-Cu1-O2 | 92.70(8) |
| N1-Cu1-O2 | 173.03(8) |
| N2-Cu1-O1 | 175.42(9) |
| N1-Cu1-O1 | 89.30(8) |
| O2-Cu1-O1 | 83.73(7) |
| N2-Cu1-N4 | 96.81(11) |
| N1-Cu1-N4 | 92.00(11) |
| O2-Cu1-N4 | 87.68(11) |
| O1-Cu1-N4 | 85.94(10) |
| C1-O1-Cu1 | 110.92(16) |
| C1#1-O2-Cu1 | 111.55(16) |
| C2-N1-C2' | 34.8(5) |
| C2-N1-C2" | 18.1(5) |
| C2'-N1-C2" | 52.3(7) |
| C2-N1-Cu1 | 119.6(3) |
| C2'-N1-Cu1 | 118.5(4) |
| C2"-N1-Cu1 | 110.4(6) |

Table B-2. Continued

| | |
|---|---|
| C6-N2-C4 | 106.2(2) |
| C6-N2-Cu1 | 126.90(19) |
| C4-N2-Cu1 | 126.71(18) |
| C6-N3-C5 | 108.4(2) |
| C7-N4-Cu1 | 142.6(3) |
| C7-N5-C8 | 119.6(3) |
| O1-C1-O2#1 | 126.7(2) |
| O1-C1-C1#1 | 116.8(3) |
| O2#1-C1-C1#1 | 116.6(3) |
| N1-C2-C3 | 111.0(5) |
| C2-C3-C4 | 110.9(5) |
| C3'-C2'-N1 | 119.2(12) |
| C2'-C3'-C4 | 116.6(12) |
| C3"-C2"-N1 | 119.2(13) |
| C2"-C3"-C4 | 123.4(12) |
| C5-C4-N2 | 109.0(2) |
| C5-C4-C3' | 125.8(5) |
| N2-C4-C3' | 124.7(5) |
| C5-C4-C3 | 129.7(3) |
| N2-C4-C3 | 119.7(3) |
| C3'-C4-C3 | 18.4(9) |
| C5-C4-C3" | 127.2(6) |
| N2-C4-C3" | 117.6(6) |
| C3'-C4-C3" | 16.8(8) |
| C3-C4-C3" | 34.0(8) |
| N3-C5-C4 | 105.9(2) |
| N2-C6-N3 | 110.5(2) |
| N4-C7-N5 | 173.9(4) |
| N6-C8-N5 | 173.6(3) |

Symmetry transformations used to generate equivalent atoms: #1 -x+1,-y+1,-z

Table B-3. Hydrogen coordinates($x10^4$) and isotropic displacement parameters for **5** ($Å^2x$ 10).

| | x | y | z | U(eq) |
|---|---|---|---|---|
| H1A | 3677 | 6418 | 4933 | 32 |
| H1B | 3697 | 5453 | 5300 | 32 |
| H3C | -1516 | 6327 | -23 | 37 |
| H2A | 2113 | 6153 | 7050 | 32 |
| H2B | 1411 | 5399 | 5795 | 32 |
| H3A | 1530 | 7265 | 4752 | 34 |
| H3B | 233 | 6861 | 5818 | 34 |
| H2'A | 2277 | 6538 | 6869 | 30 |
| H2'B | 2442 | 7169 | 5150 | 30 |
| H3'A | 232 | 6950 | 5688 | 19 |
| H3'B | 424 | 5874 | 5747 | 19 |
| H2"A | 1561 | 5029 | 5419 | 20 |
| H2"B | 1890 | 5729 | 6988 | 20 |
| H3"A | 813 | 6706 | 5913 | 27 |
| H3"B | -65 | 5800 | 5744 | 27 |
| H5A | -1715 | 6738 | 3142 | 39 |
| H6A | 771 | 5811 | -707 | 40 |

APPENDIX C
CRYSTAL STRUCTURAL DATA FOR COMPOUND **6**

Table C-1. Atomic coordinates ( x $10^4$) and equivalent isotropic displacement parameters for **6** ($E^2$x $10^3$). (U(eq) is defined as one third of the trace of the orthogonalized $U_{ij}$ tensor.)

| | x | y | z | U(eq) |
|---|---|---|---|---|
| Cu(1) | 4430(1) | 2420(1) | 5906(1) | 14(1) |
| O(1) | 4749(1) | 2752(2) | 4811(1) | 17(1) |
| O(2) | 4684(1) | 5081(2) | 5952(1) | 18(1) |
| N(1) | 6026(1) | 1548(2) | 6097(1) | 22(1) |
| N(2) | 6593(1) | 2515(2) | 5787(1) | 18(1) |
| N(3) | 7137(2) | 3492(3) | 5477(1) | 30(1) |
| N(4) | 3986(1) | 2384(2) | 6949(1) | 16(1) |
| N(5) | 3669(1) | 3189(2) | 8108(1) | 20(1) |
| N(6) | 3746(1) | 143(2) | 5633(1) | 18(1) |
| C(1) | 3434(2) | 1399(3) | 8056(1) | 20(1) |
| C(2) | 3634(1) | 894(2) | 7335(1) | 16(1) |
| C(3) | 3524(2) | -879(3) | 6952(1) | 18(1) |
| C(4) | 3057(2) | -729(3) | 6174(1) | 18(1) |
| C(5) | 3997(2) | 3740(3) | 7436(1) | 18(1) |
| C(6) | 4981(1) | 5671(2) | 5330(1) | 15(1) |

Table C-2. Bond lengths [E] and angles for **6** [°].

| | |
|---|---|
| Cu(1)-N(4) | 1.9452(16) |
| Cu(1)-N(6) | 1.9909(17) |
| Cu(1)-O(1) | 2.0087(14) |
| Cu(1)-O(2) | 2.0152(13) |
| Cu(1)-N(1) | 2.2680(17) |
| O(1)-C(6)#1 | 1.256(2) |
| O(2)-C(6) | 1.254(2) |
| N(1)-N(2) | 1.185(2) |
| N(2)-N(3) | 1.171(2) |
| N(4)-C(5) | 1.330(2) |
| N(4)-C(2) | 1.389(2) |
| N(5)-C(5) | 1.338(3) |
| N(5)-C(1) | 1.375(3) |
| N(5)-H(5A) | 0.8800 |
| N(6)-C(4) | 1.486(2) |
| N(6)-H(6A) | 0.86(3) |
| N(6)-H(6B) | 0.89(3) |
| C(1)-C(2) | 1.362(3) |
| C(1)-H(1A) | 0.93(2) |
| C(2)-C(3) | 1.495(3) |
| C(3)-C(4) | 1.521(3) |
| C(3)-H(3A) | 0.95(3) |
| C(3)-H(3B) | 0.90(3) |
| C(4)-H(4A) | 0.94(2) |
| C(4)-H(4B) | 0.94(3) |
| C(5)-H(5A) | 0.95(2) |
| C(6)-O(1)#1 | 1.256(2) |
| C(6)-C(6)#1 | 1.542(4) |
| N(4)-Cu(1)-N(6) | 94.58(7) |
| N(4)-Cu(1)-O(1) | 171.71(6) |
| N(6)-Cu(1)-O(1) | 88.12(6) |
| N(4)-Cu(1)-O(2) | 91.57(6) |
| N(6)-Cu(1)-O(2) | 158.10(7) |
| O(1)-Cu(1)-O(2) | 83.15(5) |
| N(4)-Cu(1)-N(1) | 98.25(7) |
| N(6)-Cu(1)-N(1) | 103.22(7) |
| O(1)-Cu(1)-N(1) | 88.73(6) |
| O(2)-Cu(1)-N(1) | 96.65(6) |
| C(6)#1-O(1)-Cu(1) | 111.75(12) |
| C(6)-O(2)-Cu(1) | 111.37(12) |
| N(2)-N(1)-Cu(1) | 111.37(13) |
| N(3)-N(2)-N(1) | 178.6(2) |
| C(5)-N(4)-C(2) | 106.89(16) |
| C(5)-N(4)-Cu(1) | 127.24(13) |
| C(2)-N(4)-Cu(1) | 125.83(12) |

Table C-2. Continued

| | |
|---|---|
| C(5)-N(5)-C(1) | 108.27(16) |
| C(5)-N(5)-H(5A) | 125.9 |
| C(1)-N(5)-H(5A) | 125.9 |
| C(4)-N(6)-Cu(1) | 120.18(12) |
| C(4)-N(6)-H(6A) | 108.1(16) |
| Cu(1)-N(6)-H(6A) | 107.1(16) |
| C(4)-N(6)-H(6B) | 108.7(17) |
| Cu(1)-N(6)-H(6B) | 109.0(17) |
| H(6A)-N(6)-H(6B) | 102(2) |
| C(2)-C(1)-N(5) | 106.63(17) |
| C(2)-C(1)-H(1A) | 131.5(15) |
| N(5)-C(1)-H(1A) | 121.9(15) |
| C(1)-C(2)-N(4) | 108.10(17) |
| C(1)-C(2)-C(3) | 130.77(18) |
| N(4)-C(2)-C(3) | 121.12(16) |
| C(2)-C(3)-C(4) | 112.91(16) |
| C(2)-C(3)-H(3A) | 108.9(15) |
| C(4)-C(3)-H(3A) | 110.3(14) |
| C(2)-C(3)-H(3B) | 112.9(15) |
| C(4)-C(3)-H(3B) | 105.2(15) |
| H(3A)-C(3)-H(3B) | 106(2) |
| N(6)-C(4)-C(3) | 111.28(16) |
| N(6)-C(4)-H(4A) | 109.1(14) |
| C(3)-C(4)-H(4A) | 106.1(15) |
| N(6)-C(4)-H(4B) | 111.6(15) |
| C(3)-C(4)-H(4B) | 107.3(14) |
| H(4A)-C(4)-H(4B) | 111(2) |
| N(4)-C(5)-N(5) | 110.11(17) |
| N(4)-C(5)-H(5A) | 125.0(15) |
| N(5)-C(5)-H(5A) | 124.9(15) |
| O(2)-C(6)-O(1)#1 | 126.58(17) |
| O(2)-C(6)-C(6)#1 | 116.9(2) |
| O(1)#1-C(6)-C(6)#1 | 116.5(2) |

Symmetry transformations used to generate equivalent atoms: #1 -x+1,-y+1,-z+1

Table C-3. Hydrogen coordinates($x10^4$) and isotropic displacement parameters for **6** ($E^2 x10^3$).

| | x | y | z | U(eq) |
|---|---|---|---|---|
| H(5A) | 3613 | 3858 | 8514 | 23 |
| H(6A) | 3425(19) | 340(30) | 5222(14) | 21(6) |
| H(6B) | 4200(20) | -660(40) | 5487(14) | 26(6) |
| H(1A) | 3200(18) | 750(30) | 8467(13) | 25(6) |
| H(3A) | 3137(18) | -1650(30) | 7263(14) | 26(6) |
| H(3B) | 4108(19) | -1440(30) | 6877(13) | 21(6) |
| H(4A) | 2486(18) | -10(30) | 6232(13) | 19(6) |
| H(4B) | 2886(19) | -1890(40) | 6021(13) | 24(6) |
| H(5A) | 4208(18) | 4930(30) | 7322(13) | 24(6) |

Table C-4. Hydrogen bond lengths and angles for **6** [Å and °].

| D-H...A | d(D-H) | d(H...A) | d(D...A) | <(DHA) |
|---|---|---|---|---|
| N(6)-H(6A)...N(3)#2 | 0.86(3) | 2.30(3) | 3.098(3) | 154(2) |
| N(6)-H(6B)...O(1)#3 | 0.89(3) | 2.17(3) | 3.061(2) | 176(2) |
| N(5)-H(5A)...N(3)#4 | 0.88 | 2.69 | 3.258(3) | 123.5 |
| N(5)-H(5A)...N(1)#5 | 0.88 | 2.18 | 2.904(2) | 139.8 |

Symmetry transformations used to generate equivalent atoms:
#1 -x+1,-y+1,-z+1 #2 x-1/2,-y+1/2,-z+1 #3 -x+1,-y,-z+1
#4 x-1/2,y,-z+3/2 #5 -x+1,y+1/2,-z+3/2

APPENDIX D
TITLE OF APPENDIX D

Table D-1. Atomic coordinates ( x $10^4$) and equivalent isotropic displacement parameters for **7** ($Å^2$x $10^3$). U(eq) is defined as one third of the trace of the orthogonalized $U_{ij}$ tensor.

| | x | y | z | U(eq) |
|---|---|---|---|---|
| Cu1 | 1271(1) | 863(1) | 2165(1) | 15(1) |
| N1 | -547(3) | -167(4) | 1422(2) | 13(1) |
| N2 | 1639(2) | 977(4) | 439(2) | 14(1) |
| N3 | 609(3) | 916(5) | 3700(2) | 24(1) |
| N4 | 1386(3) | 1288(4) | 4532(2) | 20(1) |
| N5 | 2110(3) | 1612(5) | 5342(2) | 35(1) |
| N6 | 1967(2) | -2843(4) | 2335(2) | 17(1) |
| N7 | 1097(3) | -4076(4) | 2017(2) | 21(1) |
| N8 | 236(3) | -5212(5) | 1720(3) | 44(1) |
| C1 | -1649(3) | -754(5) | 1920(3) | 17(1) |
| C2 | -2781(3) | -1435(5) | 1248(3) | 20(1) |
| C3 | 2741(3) | 1538(5) | -63(3) | 18(1) |
| C4 | 609(3) | 310(4) | -269(3) | 13(1) |

Table D-2. Bond lengths [Å] and angles for **7** [°].

| | |
|---|---|
| Cu1-N3 | 1.955(3) |
| Cu1-N6#1 | 1.986(2) |
| Cu1-N1 | 2.050(3) |
| Cu1-N2 | 2.066(2) |
| Cu1-N6 | 2.448(3) |
| N1-C4#2 | 1.334(4) |
| N1-C1 | 1.347(4) |
| N2-C4 | 1.327(4) |
| N2-C3 | 1.345(4) |
| N3-N4 | 1.204(4) |
| N4-N5 | 1.150(4) |
| N6-N7 | 1.203(4) |
| N6-Cu1#3 | 1.986(2) |
| N7-N8 | 1.152(4) |
| C1-C2 | 1.384(4) |
| C1-H1A | 0.9500 |
| C2-C3#2 | 1.378(4) |
| C2-H2A | 0.9500 |
| C3-C2#2 | 1.378(4) |
| C3-H3A | 0.9500 |
| C4-N1#2 | 1.334(4) |
| C4-C4#2 | 1.476(6) |
| N3-Cu1-N6#1 | 95.61(11) |
| N3-Cu1-N1 | 91.20(10) |
| N6#1-Cu1-N1 | 170.89(10) |
| N3-Cu1-N2 | 170.01(10) |
| N6#1-Cu1-N2 | 91.85(10) |
| N1-Cu1-N2 | 80.72(9) |
| N3-Cu1-N6 | 93.54(11) |
| N6#1-Cu1-N6 | 97.54(6) |
| N1-Cu1-N6 | 88.04(9) |
| N2-Cu1-N6 | 92.05(9) |
| C4#2-N1-C1 | 116.5(3) |
| C4#2-N1-Cu1 | 113.4(2) |
| C1-N1-Cu1 | 130.1(2) |
| C4-N2-C3 | 116.2(2) |
| C4-N2-Cu1 | 112.73(19) |
| C3-N2-Cu1 | 131.0(2) |
| N4-N3-Cu1 | 118.7(2) |
| N5-N4-N3 | 178.3(3) |
| N7-N6-Cu1#3 | 115.1(2) |
| N7-N6-Cu1 | 113.7(2) |

Table D-2. Continued

| | |
|---|---|
| Cu1#3-N6-Cu1 | 131.11(12) |
| N8-N7-N6 | 177.9(3) |
| N1-C1-C2 | 120.7(3) |
| N1-C1-H1A | 119.7 |
| C2-C1-H1A | 119.7 |
| C3#2-C2-C1 | 118.3(3) |
| C3#2-C2-H2A | 120.8 |
| C1-C2-H2A | 120.8 |
| N2-C3-C2#2 | 121.3(3) |
| N2-C3-H3A | 119.3 |
| C2#2-C3-H3A | 119.3 |
| N2-C4-N1#2 | 126.9(3) |
| N2-C4-C4#2 | 116.9(3) |
| N1#2-C4-C4#2 | 116.2(3) |

Symmetry transformations used to generate equivalent atoms:
#1 -x+1/2,y+1/2,-z+1/2 #2 -x,-y,-z #3 -x+1/2,y-1/2,-z+1/2

Table D-3. Hydrogen coordinates($x10^4$) and isotropic displacement parameters for **7** ($Å^2 x10^3$).

| | x | y | z | U(eq) |
|---|---|---|---|---|
| H1A | -1650 | -700 | 2740 | 20 |
| H2A | -3566 | -1823 | 1596 | 24 |
| H3A | 3507 | 2014 | 409 | 22 |

APPENDIX E
CRYSTAL STRUCTURAL DATA FOR COMPOUND **8**

Table E-1. Atomic coordinates ( x $10^4$) and equivalent isotropic displacement parameters for **8** ($Å^2$x $10^3$). U(eq) is defined as one third of the trace of the rthogonalized $U_{ij}$ tensor.

| | x | y | z | U(eq) |
|---|---|---|---|---|
| Cu | -5000 | 5000 | 5000 | 13(1) |
| O1 | -2823(2) | 4807(1) | 3040(2) | 15(1) |
| O2 | -5235(2) | 4190(1) | 5727(2) | 18(1) |
| O3 | -4009(2) | 1172(1) | 8916(2) | 23(1) |
| C1 | -5000 | 3942(1) | 7500 | 14(1) |
| C2 | -5000 | 3291(1) | 7500 | 14(1) |
| C3 | -4344(3) | 2989(1) | 9290(3) | 17(1) |
| C4 | -4303(3) | 2385(1) | 9272(3) | 18(1) |
| C5 | -5000 | 2081(1) | 7500 | 15(1) |
| C6 | -5000 | 1425(1) | 7500 | 17(1) |
| O4 | 0 | 4394(1) | 7500 | 21(1) |

Table E-2. Bond lengths [Å] and angles for **8** [°].

| | |
|---|---|
| Cu-O2#1 | 1.9245(12) |
| Cu-O2 | 1.9245(12) |
| Cu-O1 | 1.9808(13) |
| Cu-O1#1 | 1.9808(13) |
| O1-H1B | 0.83(3) |
| O1-H1A | 0.84(3) |
| O2-C1 | 1.2602(18) |
| O3-C6 | 1.2598(18) |
| C1-O2#2 | 1.2602(18) |
| C1-C2 | 1.498(3) |
| C2-C3 | 1.393(2) |
| C2-C3#2 | 1.393(2) |
| C3-C4 | 1.390(2) |
| C3-H3A | 0.95(2) |
| C4-C5 | 1.397(2) |
| C4-H4A | 0.9500 |
| C5-C4#2 | 1.397(2) |
| C5-C6 | 1.508(4) |
| C6-O3#2 | 1.2598(18) |
| O4-H4 | 0.82(3) |
| O2#1-Cu-O2 | 180.0 |
| O2#1-Cu-O1 | 90.42(6) |
| O2-Cu-O1 | 89.58(6) |
| O2#1-Cu-O1#1 | 89.58(6) |
| O2-Cu-O1#1 | 90.42(6) |
| O1-Cu-O1#1 | 180.0 |
| Cu-O1-H1B | 114(2) |
| Cu-O1-H1A | 115(2) |
| H1B-O1-H1A | 112(3) |
| C1-O2-Cu | 129.57(14) |
| O2#2-C1-O2 | 126.1(2) |
| O2#2-C1-C2 | 116.96(12) |
| O2-C1-C2 | 116.96(12) |
| C3-C2-C3#2 | 120.3(2) |
| C3-C2-C1 | 119.85(12) |
| C3#2-C2-C1 | 119.85(12) |
| C4-C3-C2 | 119.86(18) |
| C4-C3-H3A | 119.5(13) |
| C2-C3-H3A | 120.7(13) |
| C3-C4-C5 | 120.00(17) |
| C3-C4-H4A | 120.0 |
| C5-C4-H4A | 120.0 |
| C4-C5-C4#2 | 119.9(2) |
| C4-C5-C6 | 120.05(12) |
| C4#2-C5-C6 | 120.05(12) |

Table E-2. Continued

| | |
|---|---|
| O3-C6-O3#2 | 124.9(2) |
| O3-C6-C5 | 117.54(12) |
| O3#2-C6-C5 | 117.54(12) |

Symmetry transformations used to generate equivalent atoms:
#1 -x-1,-y+1,-z+1 #2 -x-1,y,-z+3/2

Table E-3. Hydrogen coordinates (x $10^4$) and isotropic displacement parameters for **8** ($Å^2x10^3$).

| | x | y | z | U(eq) |
|---|---|---|---|---|
| H1B | -2050(50) | 5079(12) | 2840(40) | 22(7) |
| H1A | -2250(50) | 4493(15) | 3310(50) | 57(9) |
| H3A | -3910(30) | 3193(9) | 10520(40) | 21(5) |
| H4A | -3801 | 2179 | 10466 | 21 |
| H4 | 260(40) | 4198(14) | 8560(50) | 51(10) |

Table E-4. Hydrogen bond lengths and angles for **8** [Å and °].

| D-H...A | d(D-H) | d(H...A) | d(D...A) | <(DHA) |
|---|---|---|---|---|
| O1-H1B...O4#3 | 0.83(3) | 1.86(3) | 2.686(2) | 171(3) |
| O1-H1A...O3#4 | 0.84(3) | 1.80(3) | 2.6345(18) | 179(3) |
| O4-H4...O3#5 | 0.82(3) | 1.87(3) | 2.6845(17) | 174(3) |

Symmetry transformations used to generate equivalent atoms:
#1 -x-1,-y+1,-z+1 #2 -x-1,y,-z+3/2 #3 -x,-y+1,-z+1
#4 -x-1/2,-y+1/2,z-1/2 #5 x+1/2,-y+1/2,-z+2

## LIST OF REFERENCES


1. Bednorz, J. G.; Müller, K. A. *Z. Phys. B*, 1986, 64, 188.

2. Dagotto, E. *Journal of Electronic Spectroscopy and Related Phenomena*, 2001, 117-118, 223.

3. Dagotto, E.; Rice, T. M. *Science*, 1996, 271, 618.

4. Maekawa, S. *Science*, 1996, 273, 1515.

5. Mott, N. F. *Proc. Phys. Soc.*, 1949, A62, 416.

6. Anderson, P. W. *Sol. State Phys.*, 1963, 14, 99.

7. Goodenough, J. B. *Magnetism and the Chemical Bond*, Interscience, New York, 1963.

8. Miller, J. S.; Calabrese, J. C.; Epstein, A. J.; Bigelow, R. W.; Zhang, J. H.; Reiff, W. M. *Chem. Commun.*, 1986, 1026.

9. Coronado, E.; Palacio, F.; Veciana, J. *Angew. Chem. Int. Ed.*, 2003, 42, 2570.

10. Coronado, E.; Delhaes, P.; Gatteschi, D.; Miller, J. S., Ed.; *Moelcular Magnetism: from Molecular Assemblies to the Devices*, Kluwer Academic Publishers, Boston, 1996.

11. Kahn, O. *Molecular Magnetism,* P 16, VCH, New York, 1993.

12. Turnbull, M. M.; Sugimoto, T.; Thompson, L. K., Ed., *Molecule-based Magnetic Materials*, ACS Symposium Series 644, Washington, DC, 1996.

13. Christou, G.; Gatteschi, D.; Hendrickson, D. N.; Sessoli, R. *MRS Bulletin*, 2000, Vol. 25, 66.

14. Mertes, K. M.; Suzuki, Y.; Sarachik, M. P.; Myasoedov, Y.; Shtrikman, H.; Zeldov, E.; Rumberger, E. M.; Hendrickson, D. N.; Christou, G. *Solid State Communications*, 2003, 127, 131.

15. Ohkoshi, S.; Hashimoto, K. *Journal of Photochemistry and Photobiology C: Photochemistry Reviews*, 2001, 2, 71.

16. Sato, O.; Iyoda, T.; Fugishima. A.; Hashimoto, K. *Science*, 1996, 272, 704.

17. Pelakovic, D. A.; Manson, J. L.; Kitamura, C.; Miller, J. S.; Epstein, A. J. *Mol. Cryst. Liq. Cryst.*, 2002, 374, 289.

18. Sato, O. *Acc. Chem. Res.*, 2003, 36, 692.

19. Bleuzen, A.; Lomenech, C.; Escax, V.; Villian, F.; Varret, F.; Cartier dit Moulin, C.; Verdaguer, M. *J. Am. Chem. Soc.*, 2000, 122, 6648.

20. Miller, J. S. *Angew. Chem. Int. Ed.*, 2003, 42, 27.

21. Sessoli, R.; Gatteschi, D.; Caneschi, A.; Novak, M. A. *Nature*, 1993, 365, 141.

22. Kahn, O.; Launay, J. P. *Chemtronics,* 1988, 3, 140.

23. Kahn, O.; Martinez, C. J. *Science*, 1998, 279, 44.

24. Fujita, W.; Awaga, K. *Journal of Solid State Chemistry*, 2001, 159, 451.

25. Delhaes, P.; Drillon, M., Ed., *Organic and Inorganic Low Dimensional Crystalline Materials*, Plenum press, New York, 1987.

26. de Jongh, L. J.; Miedema, A. R. *Experiments on Simple Magnetic Model Systems* in *Adv. Phys.*, 1974, 23, 1.

27. de Jongh, L. J., Ed., *Magnetic Properties of Layered Transition Metal Compounds*, Kluwer Academic Publishers, Boston, 1990.

28. Rouxel, J. *Acc. Chem. Res.,* 1992, 25, 328.

29. Carlin, R. L. *Magnetochemistry,* P 117, Springer-Verlag, Berlin, 1986.

30. Moulton, B.; Zaworotko, M. J. in Crystal Engineering: *From Molecules and Crystals to Materials*, Braga, D.; Grepioni, F.; Guy Orpen A., Eds., Kluwer Academic Publishers, Boston, 1999.

31. Zaworotko, M. J. in *Crystal Engineering: The Design and Application of Functional Solids*, Seddon, K. R.; Zaworotko, M. J., Eds., Kluwer Academic Publishers, Boston, 1999.

32. Moulton, B.; Zaworotko, M. J. in *Advances in Supramolecular Chemistry,* Gokel, G. W., Ed., JAI Press, Greenwich, Connecticut, 2000.

33. Moulton, B.; Zaworotko, M. J. *Chem. Rev.*, 2001, 101, 1629.

34. Maddox, J. *Nature*, 1988, 335, 201.

35. Rovira, C. *Chem. Eur. J.*, 2000, 6, 1723.

36. Hiroi, Z. *J. Solid State Chem.*, 1996, 123, 223.

37. Landee, C. P.; Turnbull, M. M.; Galeriu, C.; Giantsidis, J.; Woodward, F. M. *Phys. Rev. B*, 2001, 63, 100402-1.

38. Matsumoto, S.; Kitaoka, Y.; Ishida, K.; Asayama, K. *Phys. Rev. B,* 1996, 53, R11492.

39. Kadono, R.; Okajima, H.; Tamashita, A.; Ishii, K.; Yokoo, T.; Akimitsu, J.; Kobayashi, N.; Hiroi, Z.; Takano, M.; Nagamine, K. *Phys. Rev. B*, 1996, 54, R9628.

40. Hammer, P. R.; Reich, D. H.; Broholm, C.; Trouw, F. *Phys. Rev. B*, 1998, 57, 7846.

41. Elstner, N.; Singh, R. R. P. *Phys. Rev. B*, 1998, 58, 11484.

42. Weihong, Z.; Singh, R. R. P.; Oitmaa, J. *Phys. Rev. B*, 1997, 55, 8052.

43. Chaboussant, G.; Crowell, P. A.; Levy, L. P.; Piovesana, O.; Madouri, A.; Mailly, D. *Phys. Rev. B*, 1997, 55, 3046.

44. Watson, B. C.; Kotov, V. N.; Meisel, M. W.; Hall, D. W.; Granroth, G. E.; Montfrooij, W. T.; Nagler, S. E.; Jensen, D. A.; Backov, R.; Petruska, M. A.; Fanucci, G. E.; Talham, D. R. *Phys. Rev. Lett*., 2001, 86, 5168.

45. Patyal, B. R.; Scott, B. L.; Willett, R. D. *Phys. Rev. B*, 1990, 41, 1657.

46. Johnston, D. C.; Johnson, J. W.; Goshorn, D. P.; Jacobson, A. J. *Phys. Rev. B*, 1987, 35, 219.

47. Nagler, S. E.; Barnes, T.; Sales, B. C.; Tennant, D. A.; Garrett, A. W. *Phys. Rev. Lett.*, 1997, 79, 745.

48. Yamagushi, *et. al. Phys. Rev. B*, 1999, 60, 6731.

49. Zaworotko, M. J.; Losier, P. *Angew. Chem. Int. Ed.*, 1996, 35, 2779.

50. Evangelisti, M.; Bartolome, J.; Kahn, M. L.; Kahn, O. *Journal of Magnetism and Magnetic Materials,* 1999, 196-197, 584.

51. Cowan, D. O.; Shu, P.; Hedberg, F. L.; Rossi, M.; Kistenmacher, T. J. *J. Am. Chem. Soc*., 1979, 101, 1304.

52. Cowan, D. O. unpublished results.

53. Miller, J. S.; Calabrese, J. C.; Epstein, A. J.; Bigelow, R. W.; Zhang, J. H.; Reiff, W. M. *J. Chem. Soc., Chem. Commun*., 1986, 1026.

54. Miller, J. S.; Calabrese, J. C.; Rommelmann, H.; Chittipeddi, S. R.; Zhang, J. H.; Reiff, W. M.; Epstein, A. J. *J. Am. Chem. Soc.*, 1987, 109, 769.

55. Broderick, W. E.; Thomson, J. A.; Day, E. P.; Hoffman, B. M. *Science*, 1990, 249, 401.

56. Yee, G. T.; Manriquez, J. M.; Dixon, D. A.; McLean, R. S.; Groski, D. M.; Flippen, R. B.; Narayan, K. S.; Epstein, A. J.; Miller, J. S. *Adv. Mat.*, 1991, 3, 309.

57. Broderick, W. E.; Hoffman, B. M. *J. Am. Chem. Soc.*, 1991, 113, 6334.

58. Broderick, W. E.; Hoffman, B. M. J. *Inorg. Chem.*, 1993, 32, 491.

59. Candela, G. A.; Swartzendruber, L. J.; Miller, J. S.; Rice, M. J. *J. Am. Chem. Soc.*, 1979, 101, 2755.

60. Broderick, W. E.; Thompson, J. A.; Hoffman, B. M., *Inorg. Chem.*, 1991, 30, 2958.

61. McConnell, H. M. *J. Phys. Chem.*, 1963, 39, 1910.

62. McConnell, H. M., *Proc. R. A. Welch Found. Chem. Res.*, 11, 144 (1967)

63. Breslow, R.; Jaun, B.; Kluttz, R. Q.; Xia, Z., *Tetrahedron*, 1982, 38, 863.

64. Breslow, R. *Pure Appl. Chem.*, 1982, 54, 927.

65. Breslow, R.; Maslak, P.; Thomaides, J. *J. Am. Chem. Soc.*, 1984, 106, 6453.

66. Breslow, R. *Mol. Cryst. Liq. Cryst.*, 1985, 125, 261.

67. LePage, T. J.; Breslow, R. *J. Am. Chem. Soc.*, 1987, 109, 6412.

68. Kollmar, C.; Kahn, O. *J. Am. Chem. Soc.*, 1991, 113, 7987.

69. Kollmar, C.; Couty, M.; Kahn, O. *J. Am. Chem. Soc.*, 1991, 113, 7994.

70. de Jongh, L.T.; Miedema, A.R., *Adv. Phys.*, 1974, 23, 1.

71. Kahn, O., *Molecular Magnetism*, P 296, VCH, New York,1993.

72. Willett, R.D.; Landee, C.P.; Gaura, R.M.; Swank, D.D.; Groenendijk, H.A.; Van Duyneveldt, A.J. *J. Magn. Magn. Mater.*, 1980, 15 (8), 1055.

73. Wright, J. C.; Moos, H. W.; Colwell, J. H.; Mangum, B. W.; Thornton, D. D. *Phys. Rev. B*, 1971, 3, 843.

74. Bongaarts, A. L. M.; de Jonge, W. J. M.; *Phys. Rev. B*, 1977, 15, 3424.

75. Candela, G. A.; Swartzendruber, L. J.; Miller, J. S.; Rice, M. J. *J. Am. Chem. Soc.*, 1979, 101, 2755.

76. Han, S.J.; Manson, J.L.; Kim, J.K.; Miller, J.S. *Inorg. Chem.*, 2000, 39, 4182.

77. Fish, R. W.; Rosenblum, M. *J. Org. Chem.*, 1965, 30(4), 1253.

78. Frank, N. L.; Clerac, R.; Sutter, J. P.; Daro, N.; Kahn, O.; Coulon, C.; Green, M. T.; Golhen, S.; Ouahab, L. *J. Am. Chem. Soc.*, 2000, 122, 2053.

79. Bleaney, B.; Bowers, K. D. *Proc. Roy. Soc. (London) Ser. A*, 1952, 214, 451.

80. Kahn, O. *Molecular Magnetism*, P 103, VCH, New York, 1993.

81. Carling, R. L. *Magnetochemistry,* P 75, Springer-Verlag, Berlin, 1986.

82. Willett, R. D. in *Magneto-structural Correlations in Exchange Coupled Systems*, Willett, R. D.; Gatteschi, D.; Kahn, O., Eds., D. Reidel Publishing Company, 1985.

83. Ginsberg, A. P. *Inorg. Chim. Acta. Rev.,* 1971, 5, 45.

84. Hay, P. J.; Thibeault, J. C.; Hoffmann, R. *J. Am. Chem. Soc.*, 1975, 97:17, 4884.

85. Bencini, A.; Gatteschi, D. *Inorg. Chim. Acta.*, 1978, 31, 11.

86. Kahn, O. *Inorg. Chim. Acta.*, 1982, 62, 3.

87. Kahn, O.; Charlot, M. F. *Nouveau Journal de Chimie,* 1980, 4, 567.

88. Kahn, O. *Angew. Chem. Int. Ed.*, 1985, 24, 834.

89. Crawford, V. H.; Richardson, H. W.; Wasson, J. R.; Hodgson, D. J.; Hatfield, W. E. *Inorg. Chem.*, 1976, 15, 2107.

90. Willett, R. D.; Larsen, M. L. *Inorg. Chim. Acta.*, 1971, 5, 175.

91. Chow, C.; Chang, K.; Willett, R. D. *J. Chem. Phys.*, 1973, 59, 2629.

92. Swank, D. D.; Landee, C. P.; Willett, R. D. *Phys. Rev. B*, 1979, 20, 2154.

93. Landee, C. P.; Willett, R. D. *J. Appl. Phys.*, 1981, 52, 2240.

94. Willett, R. D.; Landee, C. P.; Waldner, F. J. *J. Appl. Phys.*, 1981, 52, 2004.

95. Landee, C. P.; Willett, R. D.; *Phys. Rev. Lett.,* 1979, 43, 463.

96. Maass, G.; Gerstein, B. C.; Willett, R. D. *J. Chem. Phys.,* 1967, 46, 401.

97. O'Bannon, G.; Willett, R. D. *Inorg. Chim. Acta*, 1981, 53, 6131.

98. Gerstein, B. C.; Gehring, F. O.; Willett, R. D. *J. Appl. Phys.*, 1972, 43, 1932.

99. Willett, R. D.; Rundle, R. E. *J. Chem. Phys.,* 1964, 40, 838.

100. Petruska, M. A.; Watson, B. C.; Meisel, M. W.; Talham, D. R. *Chem. Mater.*, 2002, 14, 2011.

101. Gavadini, N.; Heigold, G.; Henggeler, W.; Furrer, A.; Güdel, H. U.; Krämer, K.; Mutka, H. *Phys. Rev. B,* 2001, 63, 172414.

102. Grigereit, T. E.; Drumheller, J. E.; Scott, B.; Pon, G.; Willett, R. D. *J. Magn. Magn. Mater.*, 1992, 104-107, 1981.

103. Bakalbassis, E. G.; Mrozinski, J.; Perlepes, S. P.; Hadjiliadis, N.; Lianza, F.; Albinati, A. *Polyhedron,* 1994, 13, 3209.

104. Swank, D. D.; Willett, R. D. *Inorg. Chem.*, 1980, 19, 2321.

105. Rodríguez-Fortea, A.; Alemany, P.; Alvarez, A.; Ruiz, E. *Inorg. Chem.,* 2002, 41, 3769.

106. Roundhill, S. G. N.; Roundhill, D. M.; Bloomquist, D. R.; Landee, C. P.; Willett, R. D.; Dooley, D. M.; Gray, H. B. *Inorg. Chem.*, 1979, 18, 831.

107. Yaghi, O. M.; Li, H.; Groy, T. L. *Inorg. Chem.*, 1997, 36, 4292.

108. Fujita, M.; Sasaki, O.; Watanabe, K.; Ogura, K.; Yamaguchi, K. *New Journal of Chemistry*, 1998, 22, 189.

109. Vangdal, B.; Carranza, J.; Lloret, F.; Julve, M.; Sletten, J. *J. Chem. Soc., Dalton Trans.*, 2002, 566.

110. Zaworotko, M. J.; Losier, P. *Angew. Chem. Int. Ed.,* 1996, 35, 2779.

111. Carling, R. L. *Magnetochemistry*, P 30, Springer-Verlag, Berlin, 1986.

112. Ginsberg, A. P.; Martin, R. L.; Brookes, R. W.; Sherwood, R. C. *Inorg. Chem.*, 1972, 11, 2884.

113. Suarez-Varela, J.; Colacio, E.; Romerosa, A.; Hidalgo, M. A.; Romero, J. *Inorg. Chim. Acta.,* 1994, 217, 39.

114. Osio, H.; Nagashima, U. *Inorg. Chem.*, 1990, 29, 3321.

115. Meyer, F.; Ruschewitz, U.; Schober, P.; Antelmann, B.; Zsolvai, L. *J. Chem. Soc., Dalton Trans.*, 1998, 1181.

116. Kou, H. Z.; Si, S. F.; Gao, S.; Lian, D. Z.; Jiang, Z. H.; Yan, S. P.; Fan, Y. G.; Wang, G. L. *Eur. J. Inorg. Chem.*, 2002, 699.

117. Ren, X.; Chen, Y.; He, C.; Gao, S. *J. Chem. Soc., Dalton Trans.*, 2002, 3915.

118. Drago, R. S. *Physical Methods for Chemists*, Surfside Science Publisher, Gainesville, Florida, 1992.

119. Mallah, T.; Ferlay, S.; Auberger, C.; Helary, C.; L'Hermite, F.; Ouahes, R.; Wassermann, J.; Verdaguer, M.; Veillet, P. *Mol. Cryst. Liq. Cryst.*, 1995, 273, 579.

120. Mallah, T.; Thiebaut, S.; Verdaguer, M.; Veillet, P. *Science*, 1993, 262, 1554.

121. Entley, W. R.; Girolami, G. S. *Science*, 1995, 268, 5209.

122. Buser, H. J., Schwarzenbach, D.; Petter, W; Ludi, A. *Inorg. Chem.* 1977, 16, 2704.

123. Gadet, V.; Mallah, T.; Verdaguer, M. *J. Am. Chem. Soc.*, 1992, 114, 9213.

124. Ohba, M.; Okawa, H. *Coord. Chem. Rev.*, 2000, 198, 313.

125. Berseth, P. A.; Sokol, J. J.; Shores, M. P.; Heinrich, J. L.; Long, J. R. *J. Am. Chem. Soc.*, 2000, 122, 9655.

126. Berseth, P. A.; Heinrich, J. L.; Long, J. R. *Chem. Commun.*, 1998, 1231.

127. Smith, J. A.; Galan-Mascaros, J. R.; Clerac, R.; Sun, J. S.; Ouyang, X.; Dunbar, K. R. *Polyhedron*, 2001, 20, 1727.

128. Bellouard, F.; Clemente-Leon, M.; Coronado, E.; Galan-Mascaros, J. R.; Gomez-Garcia, C. J.; Romero, F.; Dunbar, K. R. Eur. J. *Inorg. Chem.*, 2002, 1603.

129. Kou, H. Z.; Liao, D. Z.; Cheng, P.; Jiang, Z. H.; Yan, S. P.; Wang, G. L.; Yao, X. K.; Wang, H. G. *J. Chem. Soc., Dalton Trans.*, 1997, 1503.

130. Kou, H. Z.; Gao, S.; Zhang, J.; Wen, G. H.; Su, G.; Zheng, R. K.; Zhang, X. X. *J. Am. Chem. Soc.,* 2001, 123, 11809.

131. Kou, H. Z.; Gao, S.; Ma, B. Q.; Liao, D. Z. *Chem. Commun.*, 2000, 713.

132. Lescouezec, R.; Vaissermann, J.; Ruiz-Perez, C.; Lloret, F.; Carrasco, R.; Julve, M.; Verdaguer, M.; Dromzee, Y.; Gatteschi, D.; Wernsdorfer, W. *Angew. Chem. Int. Ed.,* 2003, 42, 1483.

133. Mallah, T.; Auberger, M.; Verdaguer, M.; Veillet, P. *J. Chem. Soc., Chem. Commun.*, 1995, 61.

134. Okawa, H.; Ohba, M. in *Molecule-based Magnetic Materials*, Turnbull, M. M.; Sugimoto, T.; Thompson, L. K., Ed., ACS Symposium Series 644, Washington, DC, 1996.

135. Ohba, M.; Usuki, N.; Fukita, N.; Okawa, H. *Inorg. Chem.*, 1998, 37, 3349.

136. Colacio, E.; Dominguez-Vera, J. M.; Ghazi, M.; Kivekas, R.; Klinga, M.; Moreno, J. M. *Chem. Commun.*, 1998, 1071.

137. Ohba, M.; Maruono, N.; Okawa, H.; Enoki, T.; Latour, J. M. *J. Am. Chem. Soc.*, 1994, 116, 11566.

138. Ohba, M.; Fukita, N.; Okawa, H. *J. Chem. Soc., Dalton Trans.*, 1997, 1733.

139. Ferlay, S.; Mallah, T.; Vaissermann, J.; Bartolome, F.; Veillet, P.; Verdaguer, M. *Chem. Commun.*, 1996, 2482.

140. Colacio, E.; Dominguez-Vera, J. M.; Ghazi, M.; Kivekas, R.; Moreno, J.; Stoeckli-Evans, H. *Chem. Commun.*, 1999, 987.

141. Ohba, M.; Fukita, N.; Okawa, H.; Hashimoto, Y. *J. Am. Chem. Soc.*, 1997, 119, 1011.

142. Matthews, R. W.; Hamer, A. D.; Hoof, D. L.; Tisley, D. G.; Walton, R. A. *J. Chem. Soc., Dalton Trans.*, 1973, 1035.

143. Constable, E. C.; Lewis, J.; Liptrot, M. C.; Raithby, P. R. *Inorg. Chim. Acta*, 1990, 178, 47.

144. Busch, D. H. *Inorganic Synthesis*, Vol. XVIII, 1978, 2-44.

145. Watkins, D. D.; Riley, D. P.; Stone, J. A.; Busch, D. H. *Inorg. Chem.*, 1976, 15, 387.

146. Hubbard, C. D.; Moore, P.; Wilkins, R. G. in *Proceedings of The 8th Internatinal Conferece on Coordination Chemistry*, Gutmann, V. Ed., P.286-287, Vienna, 1964.

147. Bulach, V.; Duval, H.; Fischer, J.; Weiss, R. *Acta Cryst.*, 1997, C53, 543.

148. Arriortua, M. I.; Cortes, A. R.; Lezam, L.; Rojo, T.; Solans, X.; Font-Bardia, M. *Inorg. Chim. Acta.*, 1990, 174, 263.

149. Hagrman, P. J.; Zubieta, J. *Inorg. Chem.*, 2000, 39, 5218.

150. Landee, C. P.; Wicholas, M.; Willett, R. D.; Wolford, T. *Inorg. Chem.*, 1979, 18, 2317.

151. Finn, R. C.; Zubieta, J. *Inorg. Chim. Acta.*, 2002, 332, 191.

152. Claramunt, A.; Escuer, A.; Mautner, F. A.; Sanz, N.; Vicente, R. *J. Chem. Soc., Dalton Trans.*, 2000, 2627.

153. Finn, R. C.; Zubieta, J. *J. Chem. Soc., Dalton Trans.*, 2002, 856.

154. Barandika, M. G.; Cortes, R.; Lezama, L.; Urtiaga, M. K.; Arriortua, M. I.; Rojo, T. *J. Chem. Soc., Dalton Trans.*, 1999, 2971.

155. Solans, X.; Aguilo, M.; Gleizes, A.; Faus, J.; Julve, M.; Verdaguer, M. *Inorg. Chem.,* 1990, 29, 775.

156. Hagrman, P. J.; Zubieta, J. *Inorg. Chem.*, 2000, 39, 3252.

157. Catalano, V. J.; Craig, T. J. *Inorg. Chem.*, 2003, 42, 321.

158. Vangdal, B.; Carranza, J.; Lloret, F.; Julve, M.; Sletten, J. *J. Chem. Soc., Dalton Trans.*, 2002, 566.

159. Min, K. S.; Suh, M. P. *Journal of Solid State Chemistry*, 2000, 152, 183.

160. Zheng, L. M.; Fang, X.; Li, K. H.; Song, H. H.; Xin, X. Q.; Fun, H. K.; Chinnakali, K.; Razak, I. A. *J. Chem. Soc., Dalton Trans.*, 1999, 2311.

161. Kahn, O. *Molecular Magnetism,* VCH, New York, 1993.

162. Julve, M.; Verdaguer, M.; Gleizes, A.; Philoche-Levisalles, M.; Kahn, O. *Inorg. Chem.,* 1984, 23, 3808.

163. Roman, P.; Guzman-Miralles, C.; Luque, A.; Beitia, J. I.; Cano, J.; Lloret, F.; Julve, M.; Alvarez, S. *Inorg. Chem.*, 1996, 35, 3741.

164. Girerd, J. J.; Kahn, O.; Verdaguer, M. *Inorg. Chem.*, 1980, 19, 274.

165. Geiser, U.; Ramakrishna, B. L.; Willett, R. D.; Hulsbergen, F. B.; Reedijk, J. *Inorg. Chem.*, 1987, 26, 3750.

166. Bloomquist, D. R.; Hansen, J. J.; Landee, C. P.; Willett, R. D.; Buder, R. *Inorg. Chem.,* 1981, 20, 3308.

167. Armentano, D.; De Munno, G.; Faus, J.; Lloret, F.; Julve, M. *Inorg. Chem.*, 2001, 40, 655.

168. Cano, J.; Alemany, P.; Alvarez, S.; Verdaguer, M.; Ruiz, E. *Chem. Eur. J.*, 1998, 4, 476.

169. O'Connor, C. *Prog. Inorg. Chem.*, 1982, 20, 203.

170. Bonner, J. C.; Fisher, M. E. *Phys. Rev.,* 1964, A135, 640.

171. Deakin, L.; Arif, A. M.; Miller, J. S. *Inorg. Chem.*, 1999, 38, 5072.

172. Dender, D. C.; Davidovic, D.; Reich, D. H.; Broholm, C.; Lefmann, K.; Aeppli, G. *Phys. Rev. B,* 1996, 53, 2583.

173. Date, M.; Yamazaki, H.; Motokawa, M.; Tazawa, S. *Supplement of the Progress of Theoretical Physics*, 1970, 46, 194.

174. McElearney, J. N.; Losee, D. B.; Merchant, S.; Carlin, R. L. *Phys. Rev. B*, 1973, 7, 3314.

175. Watanabe, T. *J. Phys. Soc. Jpn.*, 1962, 17, 1856.

176. Swank, D. D.; Landee, C. P.; Willett, R. D. *Phys. Rev. B*, 1979, 20, 2154.

177. Cano, J.; De Munno, G.; Sanz, J. L.; Ruiz, R.; Faus, J.; Lloret, F.; Julve, M.; Caneschi, A. *J. Chem. Soc., Dalton Trans.*, 1997, 1915.

178. Sun, D.; Cao, R.; Liang, Y.; Shi, Q.; Su, W.; Hong, M. *J. Chem. Soc., Dalton Trans.*, 2001, 2335.

179. Bakalbassis, E. G.; Mrozinski, J.; Tsipis, C. A. *Inorg. Chem.*, 1986, 25, 3684.

180. Heinze, K.; Huttner, G.; Schober, P. *Eur. J. Inorg. Chem.,* 1998, 183.

## BIOGRAPHICAL SKETCH

Chen Liu was born on May 12, 1971 in the northern city of Tainjin in China. He grew up in the northwestern province of Ningxia until 1988, when his family moved back to Tianjin. In 1995, Chen obtained his Bachelor of Engineering degree in polymer engineering from Beijing University of Chemical Technology. A year later, Chen came to the United States and graduated with an M.S. in chemistry from Central Michigan University in 1998. In Spring 2000, Chen joined Professor Talham's group at the University of Florida to pursue a Ph.D. in physical chemistry. Since then, his research has focused on the synthesis and magnetism of low-dimensional molecular magnetic materials. Upon completing his doctorate, Chen plans to continue his academic training as a postdoctoral research associate and eventually to pursue an academic career.

I certify that I have read this study and that in my opinion it conforms to acceptable standards of scholarly presentation and is fully adequate, in scope and quality, as a dissertation for the degree of Doctor of Philosophy.

Daniel R. Talham, Chair
Professor of Chemistry

I certify that I have read this study and that in my opinion it conforms to acceptable standards of scholarly presentation and is fully adequate, in scope and quality, as a dissertation for the degree of Doctor of Philosophy.

Alexander Angerhofer
Associate Professor of Chemistry

I certify that I have read this study and that in my opinion it conforms to acceptable standards of scholarly presentation and is fully adequate, in scope and quality, as a dissertation for the degree of Doctor of Philosophy.

Jeffrey L. Krause
Associate Professor of Chemistry

I certify that I have read this study and that in my opinion it conforms to acceptable standards of scholarly presentation and is fully adequate, in scope and quality, as a dissertation for the degree of Doctor of Philosophy.

Robert J. Hanrahan
Professor of Chemistry

I certify that I have read this study and that in my opinion it conforms to acceptable standards of scholarly presentation and is fully adequate, in scope and quality, as a dissertation for the degree of Doctor of Philosophy.

Laurie Gower
Associate Professor of Materials Science and Engineering

This dissertation was submitted to the Graduate Faculty of the Department of Chemistry in the College of Liberal Arts and Sciences and to the Graduate School and was accepted as partial fulfillment of the requirements for the degree of Doctor of Philosophy.

May, 2004

_____

Dean, Graduate School